

Characterizing Parameter Uncertainty in Biomedical Systems for Improved Estimation,  
Prediction and Control

---

A Dissertation

Presented to  
the faculty of the School of Engineering and Applied Science  
University of Virginia

---

in partial fulfillment  
of the requirements for the degree

Doctor of Philosophy

by

Boyi Jiang

May

2015

---

---

---

Jiang, Boyi

Characterizing Parameter Uncertainty in Biomedical Systems for Improved Estimation,  
Prediction and Control

University of Virginia, PhD, 2015

Copyright © 2015 by

Boyi Jiang

All rights reserved

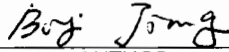
## Abstract

Recent years have witnessed the vigorous research and development of Artificial Pancreas system (AP), which attempts to “close the loop” through communications with third party devices such as continuous glucose monitoring and insulin pump aimed at dispensing the patients with diabetes from the responsibility of insulin dosing. Physiological modeling is a pragmatic methodology for explaining observed dynamic effects, interpreting the experimental data and predicting system responses under certain stimuli. Given the complexity of the insulin-glucose dynamic system, lumping the parameter set is obligatory under most circumstances. The ubiquitous inter-individual and intra-individual variability across the population requires us to consider the necessary remedial action such as characterization of the parameter uncertainties.

Insulin sensitivity (SI), is one of the critical parameters that govern the insulin-glucose dynamics. We propose and validate a Kalman Filtering based technique that is capable of tracking SI in real time based on commonly available data measurements. We then apply the developed technique to estimate SI during the menstrual cycle. The results substantiate the hypothesis that a subset of premenopausal women with T1DM will experience a decrease in insulin sensitivity during the second half of the menstrual cycle (luteal phase). With the knowledge of SI, we optimize the predictive power of a dosing algorithm; short-term (up to 45 minutes) forecasting ability of BG is studied by exploring different structural designs (full model, feed-forward, with and without SI tracking). Finally, a model based decision support system is derived for insulin dosing; long-term (4 hours) forecasting characteristics of BG influenced by individualized parameters are studied both in-silico and in-vivo.

APPROVAL SHEET

The dissertation  
is submitted in partial fulfillment of the requirements  
for the degree of  
Doctor of Philosophy

  
AUTHOR

The dissertation has been read and approved by the examining committee:

Marc D. Breton

Advisor

Stephen D. Patek

Sue A. Brown

Peter A. Beling

Barry Horowitz

Accepted for the School of Engineering and Applied Science:



Dean, School of Engineering and Applied Science

May  
2015

I would like to acknowledge the NIH NIDDK for providing the funding for this work. I would like to thank my PhD advisory committee which includes Dr. Barry Horowitz, Dr. Peter Beling and Dr. Sue Brown. I also would like to thank Dr. Boris Kovatchev and Dr. Leon Farhi for your invaluable advice. I acknowledge the thoughtful guidance of my system engineering advisor Dr. Stephen Patek. I especially acknowledge the invaluable guidance of my thesis advisor Dr. Marc Breton. Thanks to all my fellow students and colleagues for your kind help. Thank you to Xiang Li. This process has been colorful in your company. An overwhelming gratitude is for my mom and dad, whose support has provided a great encouragement.

# Table of Contents

Chapter 1. Introduction .....	1
Chapter 2. Background .....	4
2.1 Glucose Metabolism .....	4
2.2 General Physiological Models .....	5
2.3 Insulin-Glucose Models .....	8
2.4 BG Forecasting and Control .....	13
2.4.1 Short-term BG Forecasting and Closed-loop Control .....	13
2.4.2 Long-term BG Forecasting and Open-loop Control (Semi-Auto Control) .....	15
2.5 Diabetes Simulator .....	15
Chapter 3. Dynamic Parameter Uncertainties Tracking in the Insulin-Glucose System – Estimation of Insulin Sensitivity .....	20
3.1 Standard Methods and KF Method for SI Quantification .....	24
3.2 Validation of KF Method against Standards .....	29
Chapter 4. Insulin Sensitivity Extraction – Applications .....	38
4.1 Study of Insulin Sensitivity Variations during Menstrual Cycle for Diabetics .....	38
4.2 Insulin Sensitivity and Physical Exercise .....	48
Chapter 5. Enhancing Model-Based Short Term Glycemic Prediction in T1DM Using Tracking of Dynamic Parameter Uncertainties .....	53
5.1 Structural Design and SI Tracking .....	55
5.2 Performance of BG Prediction - Comparison .....	62
5.3 Validation by Simulation: SI or $\Delta$ .....	68
Chapter 6. Enhancing Model-Based Long Term Glycemic Prediction in T1DM – Application in Semi-Auto Control .....	72
6.1 Parameter Uncertainties Characterization In-silico .....	73
6.2 In-vivo Clinical Study – Application in Semi-Auto Control .....	82
6.3 Parameter Uncertainties Characterization “In-vivo” .....	89
Chapter 7. Conclusions and Future Work .....	103
References .....	107
Appendix .....	122

A. Terms in integral SI formula .....	122
B.1 KF matrices and noise covariance .....	124
B.2 Prediction matrices .....	125
C. 1 Tuned multipliers against the selected response variable (CR) by global search .....	126
C. 2 Tuned multipliers against the response variables (segments averaged) based on global search .....	129

# List of Figures

FIGURE 1: SCHEMATIC DIAGRAM OF COMPARTMENTAL MODELS OF XENOBIOTICS <sup>26</sup> . EACH COMPARTMENT IS DESCRIBED BY A DIFFERENTIAL EQUATION WITH I/O DEFINED. ....	6
FIGURE 2: STRUCTURAL SIMULATION OF BRANCHING LUNG AIR FLOW <sup>27</sup> . ....	6
FIGURE 3: MEAL MODEL DESCRIBED BY EQUATION 2.9. ....	10
FIGURE 4: MEAL MODEL DESCRIBED BY EQUATION 2.10: Q1 (FASTING ABSORPTION) AND Q2 (SLOW ABSORPTION).....	10
FIGURE 5: SUBCUTANEOUS MODEL OF INSULIN INJECTION DESCRIBED BY EQUATION 2.11. ....	13
FIGURE 6: SCHEMATIC DIAGRAM OF CLOSED-LOOP CONTROL OF DIABETES.....	14
FIGURE 7: COMPARTMENTS OF THE SIMULATOR MODELS AND SIGNAL FLOW.....	17
FIGURE 8: TYPE 1 SIMULATOR INTERFACE. ....	18
FIGURE 9: OPEN-LOOP SIMULATIONS OF 100 IN-SILICO ADULTS: ONE MEAL AND THE CORRESPONDING BOLUS PROVIDED .....	19
FIGURE 10: FEED-FORWARD DESIGN OF KALMAN FILTERING. ....	27
FIGURE 11: SI_KF_IP_RA AGAINST SI_RA (R=0.80, P<0.01). ....	31
FIGURE 12: SI_KF_SQJ_RA AGAINST SI_RA (R=0.76 , P<0.01) AND SI_MM_SQJ_RA AGAINST SI_RA (R=0.77, P<0.01). ....	32
FIGURE 13: SI_KF_IP_M AGAINST SI_RA (R=0.81 , P<0.01) AND SI_MM_IP_M AGAINST SI_RA (R=0.84, P<0.01). ....	32
FIGURE 14: SI_KF_SQJ_M AGAINST SI_RA (R=0.80 , P<0.01) AND SI_MM_SQJ_M AGAINST SI_RA (R=0.77, P<0.01). ....	33
FIGURE 15: SI VALIDATION USING CGM: A) SI_KF AND SI_SP AGAINST SI_RA (R=0.91, P<0.05 AND R=0.81, P<0.05), B) SI_KF AND SI_SP AGAINST SI_MM (R=0.89, P<0.05 AND R=0.87, P<0.05).....	34
FIGURE 16: SI (MEAN±SE) BY KALMAN FILTER AND MINIMAL MODEL METHODS. ....	36
FIGURE 17: MENSTRUAL CYCLE AND ASSOCIATED HORMONES <sup>97</sup> .....	39

FIGURE 18: STUDY SPANNED THREE CONSECUTIVE MENSTRUAL CYCLES WITH VISITING DAYS FOR EACH CYCLE DESIGNATED.....	40
FIGURE 19: TRACKING OF G, X AND SI FROM 1 AM TO 6 AM THE NEXT DAY (60 TO 1800 MINUTES). ....	41
FIGURE 20: EARLY FOLLICULAR DAYS COMBINED AS PHASE 1, EARLY LUTEAL AND MID LUTEAL DAYS AS PHASE 4, MID LATE FOLLICULAR, OVULATION AND LATE LUTEAL DAYS AS PHASE 2, 3, 5.....	42
FIGURE 21: SI (MEAN±SE) OF EARLY FOLLICULAR PHASE, EARLY MIDDLE LUTEAL PHASE, LATE LUTEAL PHASE AND MIDDLE LATE LUTEAL PHASE: A) SI_KF, B) SI_SP. ....	44
FIGURE 22: HISTOGRAM OF SI CHANGES BEFORE AND AFTER OVULATION.....	45
FIGURE 23: SI IN LUTEAL PHASE AGAINST SI IN FOLLICULAR PHASE.....	46
FIGURE 24: CYCLE-AVERAGED SI FOR EACH SUBJECT. PHASE 1 TO 7 CORRESPONDS TO EARLY FOLLICULAR 3, EARLY FOLLICULAR 5, MIDDLE LATE FOLLICULAR, OVULATION, EARLY LUTEAL, MIDDLE LUTEAL AND LATE LUTEAL RESPECTIVELY. ....	46
FIGURE 25: THE THREE PATTERNS OF SI VARIATIONS: A) 15 OUT OF 36 CYCLES EXPERIENCED DECREASED SI IN LUTEAL PHASE, B) 13OUT OF 36 CYCLES EXPERIENCED UNCHANGED SI, C) 8 OUT OF 36 CYCLES EXPERIENCED INCREASED SI. ....	47
FIGURE 26: TIMELINE OF THE STUDY: 1-H RECOVERY SESSION TAKEN AFTER 1-H PHYSICAL EXERCISE WITH A 3H-OGTT TEST FOLLOWED <sup>101</sup> .....	49
FIGURE 27: SI (MEAN±SE) DERIVED BY MINIMAL MODEL IN CONTROL, MIE AND HIE.....	51
FIGURE 28: BG FITTING BY OGTT MODEL OF SUBJECT008: A) CONTROL GROUP, B) MIE AND C) HIE.....	52
FIGURE 29: 3X2 MODEL IMPLEMENTATIONS: I) SOGMM-FULL MODEL, II) SOGMM-CORE+Δ, III) SOGMM-CORE MODEL WITH SI, IV) LOG-FULL MODEL, V) LOG-CORE MODEL+Δ, VI) LOG-CORE MODEL WITH SI AND STRUCTURES OF PREDICTION VECTOR XI.....	58
FIGURE 30: BG PREDICTION MARDS (MEAN±SE) BY 6 IMPLEMENTATIONS FOR PH=30, 45MIN. SOGMM AND LOG MODELS WERE COMPARED FOR EACH IMPLEMENTATION. RAW CGM WAS USED FOR MEASUREMENT INPUT. ....	63

FIGURE 31: BG PREDICTION MARDS (MEAN±SE) BY 6 IMPLEMENTATIONS FOR PH=30, 45MIN. SOGMM AND LOG MODELS WERE COMPARED FOR EACH IMPLEMENTATION. NON-CAUSAL SMOOTHED CGM WAS USED FOR MEASUREMENT INPUT. ....	65
FIGURE 32: BG PREDICTION MARDS (MEAN±SE) BY 6 IMPLEMENTATIONS FOR PH=30, 45MIN. SOGMM AND LOG MODELS WERE COMPARED FOR EACH IMPLEMENTATION. CAUSAL SMOOTHED CGM WAS USED FOR MEASUREMENT INPUT. ....	66
FIGURE 33: SIMULATION OF ONE MEAL IN OPEN LOOP (ADULT #005). ....	71
FIGURE 34: 27-HOUR CLOSED-LOOP SIMULATION WITH INTRA-DAY VARIATIONS AND DAWN PHENOMENON (ADULT #005). ....	71
FIGURE 35: THE TWO-LAYER ARCHITECTURE OF SAIA <sup>114</sup> . ....	73
FIGURE 36: “LOG-CORE MODEL+Δ” STRUCTURE FOR STATE ESTIMATION AND PREDICTION <sup>114</sup> . ....	76
FIGURE 37: 2X2 TUNING DESIGN: (TOP) A MEAL AND BOLUS SERVED WITHOUT OPTIMAL CORRECTION 1 HOUR AFTERWARDS, (BOTTOM) A MEAL AND BOLUS SERVED WITH OPTIMAL CORRECTION 1 HOUR AFTERWARDS. FOUR PREDICTION WINDOWS A0, B0, A1, B1 WERE CHOSEN. ....	77
FIGURE 38: LINEAR PIECE-WISE COST WEIGHTS FOR TWO DIFFERENT PREDICTION WINDOWS: WA STARTS AT 1 HOUR AFTER THE MEAL, WB STARTS AT 4 HOUR AFTER THE MEAL. ....	78
FIGURE 39: REGRESSIONS OF PARAMETER MULTIPLIERS TO CR.....	81
FIGURE 40: TIME IN RANGE: CONVENTIONAL THERAPY VS. ADVISORY SYSTEM. ....	82
FIGURE 41: EXPERIMENTAL AND CONTROL SESSIONS OF A TEST DAY. ....	83
FIGURE 42: HYPERGLYCEMIC GRID.....	85
FIGURE 43: CLINICAL STUDY (TOP) AND RECONSTRUCTION OF BG PREDICTION AROUND THE FIRST MEAL IN THE SIMULATOR (BOTTOM) OF SUB28101. ....	86
FIGURE 44: CLINICAL STUDY (TOP) AND RECONSTRUCTION OF BG PREDICTION AT DECISION TIME IN THE SIMULATOR (BOTTOM) OF SUB28102. ....	87
FIGURE 45: PREDICTED (BLUE) AND SIMULATED (RED) BG TRACES STARTING FROM 200 MG/DL WITH BASAL INSULIN DELIVERED (SUBJECT ADULT #025). ....	88

FIGURE 46: SIMULATION OF 100 SUBJECTS STARTING FROM 200 MG/DL WITH BASAL INSULIN DELIVERED: LIGHT BLUE) SIMULATED BG ENVELOP WITH MEAN, BLUE) PREDICTED BG ENVELOP WITH MEAN BY LOG MODEL. ....	88
FIGURE 47: PREDICTION STARTED FROM 1 HOUR AFTER THE MEAL AND LASTED 4 HOURS. ....	90
FIGURE 48: TUNED MULTIPLIERS AGAINST THE SELECTED PREDICTORS. ....	96
FIGURE 49: DISTRIBUTION OF MARD IN 4 PREDICTION HORIZON ACROSS ALL SUBJECTS. ....	97
FIGURE 50: INTERQUARTILE RANGE OF MRD FOR EACH PREDICTION HORIZON. ....	97
FIGURE 51: DISTRIBUTION OF MRD OF DIFFERENT PREDICTION HORIZON: (A)PH=[0 1]H, (B)PH=[1 2]H, (C)PH=[2 3]H, (D)PH=[3 4]H USING THE NEW REGRESSION MODEL. ....	98
FIGURE 52: DISTRIBUTION OF MARD IN 4 PREDICTION HORIZON ACROSS ALL SUBJECTS. BLUE USES THE NEW REGRESSION MODEL AND RED USES THE OLD REGRESSION MODEL. ....	99
FIGURE 53: DISTRIBUTION OF MRD OF DIFFERENT PREDICTION HORIZON: (A)PH=[0 1]H, (B)PH=[1 2]H, (C)PH=[2 3]H, (D)PH=[3 4]H USING OLD REGRESSION MODEL. ....	100
FIGURE 54: A. MEAL RATE OF APPEARANCE F(T) AND B. CARBOHYDRATES ON BOARD COB(T). ....	122
FIGURE 55: INSULIN ON BOARD AS FUNCTION OF TIME. ....	123
FIGURE 56: TUNED MULTIPLIERS AGAINST THE SELECTED RESPONSE VARIABLE (CR) BY GLOBAL SEARCH. .....	128
FIGURE 57: TUNED MULTIPLIERS AGAINST THE RESPONSE VARIABLES (SEGMENTS AVERAGED) BASED ON GLOBAL SEARCH. ....	133

# List of Tables

TABLE 1: IN-SILICO SUBJECT DESCRIBED BY 13 DIFFERENTIAL EQUATIONS.....	16
TABLE 2: PHYSIOLOGICAL PARAMETERS OF THE IN-SILICO PATIENTS .....	17
TABLE 3: NOISE COVARIANCE SETTING OF KF .....	29
TABLE 4: MEAN AND STANDARD ERROR OF SI_KF IN DIFFERENT PHASES AND THE PAIR T-TESTS .....	43
TABLE 5: MEAN AND STANDARD ERROR OF SI_SP IN DIFFERENT PHASES AND THE PAIR T-TESTS .....	43
TABLE 6: AVERAGED SI BEFORE AND AFTER OVULATION FOR EACH SUBJECT ACROSS 3 CYCLES .....	45
TABLE 7: SOGMM AND LOG MODEL DISCRETIZED IN 5 MINUTE INTERVAL. THE STATES AND INPUTS OF SOGMM ARE DEVIATIONS FROM THE OPERATING POINT .....	56
TABLE 8: PREDICTION VECTOR XI OF EACH IMPLEMENTATION .....	58
TABLE 9: MARDS ( $\pm$ SE) OF 6 MODEL IMPLEMENTATIONS FOR PH=30, 45MIN.....	62
TABLE 10: MARDS OF 6 MODEL IMPLEMENTATIONS USING NON-CAUSAL SMOOTHED CGM.....	65
TABLE 11: MARDS OF 6 MODEL IMPLEMENTATIONS USING CAUSAL SMOOTHED CGM.....	66
TABLE 12: PREDICTION MARDS BY TWO IMPLEMENTATIONS USING FIVE SIMULATION SCENARIOS.....	70
TABLE 13: THE MODEL IN ON-DEMAND BOLUS ADVISOR IS COMPOSED OF LOG CORE, FEED-FORWARD INSULIN AND MEAL COMPARTMENTS. FOUR MULTIPLIERS ARE CHOSEN TO ADJUST THE CORRESPONDING PARAMETERS.....	75
TABLE 14: POPULATION AVERAGED PARAMETERS AND TUNING MULTIPLIERS.....	75
TABLE 15: STEP-WISE SELECTION OF REGRESSION MODEL .....	80
TABLE 16: INTERQUARTILE RANGE OF MRD FOR EACH PREDICTION HORIZON .....	99
TABLE 17: COMPARISON OF MARD USING TWO DIFFERENT REGRESSION MODELS.....	99
TABLE 18: KF STATES AND NOISE SETTINGS .....	124
TABLE 19: PREDICTION STATES AND MATRICES.....	125

# Chapter 1. Introduction

Diabetes, or diabetes mellitus, is a group of metabolic diseases arising from gene defect and environmental stimuli. It is usually characterized by chronic high blood glucose (hyperglycemia). Long time exposure to hyperglycemia may cause irreversible complications, such as blurred vision, cardiovascular diseases, neuropathy, renal disease and loss of limb<sup>1-5</sup>. There are two main diabetes: type 1 diabetes (T1DM) and type 2 diabetes (T2DM). Type 1 Diabetes is a disorder of the endocrine system mainly diagnosed in children and young adults whose insulin secreting cells ( $\beta$ -cells of the Langerhans islets in the pancreas) are destroyed by the body's immune system. The only treatment is the administration of exogenous insulin. Dosing insulin also brings in the risk of low blood glucose (hypoglycemia) which can cause hunger, seizures, unconsciousness and even death<sup>6-9</sup>. Type 2 diabetes is a progressive condition. At early stages, a patient's body does not produce enough insulin to compensate the elevated blood glucose. Without receiving proper treatment, it gradually gets worse and exogenous insulin becomes a necessity. The risk of developing type 2 diabetes increases with the aging process and is higher for overweight and obese people. Early treatment includes physical exercise, healthy diet, weight control and glucose monitoring<sup>10-13</sup>. Prediabetes is an intermediate condition in the transition between health and type 2 diabetes, characterized by impaired fasting glucose (IFG) and impaired glucose tolerance (IGT)<sup>14</sup> and is associated with increased risk for developing cardiovascular disease<sup>15,16</sup>. Gestational diabetes is a temporary condition diagnosed in female

whose blood sugar level is elevated abnormally during pregnancy<sup>17</sup>. One of the consequences is that a “big baby” (much more weight than normal newborn) may be delivered. With proper physical exercise and healthy diet, blood sugar can be well controlled and most patients will recover after the delivery.

In 2012, the United States had 21.98 million people (8.3% of the population) that were diagnosed with diabetes and an estimated 8.1 million remaining undiagnosed<sup>18</sup>. In 2007, the estimated total cost of diagnosed diabetes was \$174 billion<sup>19</sup>. The cost rose to \$245 billion in 2012 that was composed of \$176 billion in medical costs and \$69 in lower productivity<sup>20</sup>. The cost increase from 2007 to 2012 was ascribed to two main aspects: growth of the diagnosis of diabetes and elevated average cost for each case. Among the diabetes population, 5% are diagnosed with type 1 diabetes<sup>21</sup>, 90%-95% with type 2 diabetes<sup>22</sup> and gestational diabetes affects 1%-14% of pregnancies<sup>23</sup>.

The management of diabetes is an interdisciplinary subject worldwide. This dissertation is focused on improving the accuracy of state estimation and forecasting by physiological modeling and the subsequent enhancement in the control performance of insulin dosing. We start from the modeling of general physiological systems by giving two illustrative examples. Then we introduce the insulin-glucose system and point out the challenges of characterizing time-varying parameters in such a system. Insulin sensitivity (SI), or coarsely the gain of insulin-glucose dynamic is one of those critical parameters. In chapter 3, we propose a Kalman Filtering (KF) based technique that is capable of tracking SI in real time and the validation against the gold standard method shows significantly positive correlation. A posterior application of the established technique to a clinical study is then reported in chapter 4. The results substantiate the hypothesis that a subset of premenopausal women with T1DM will experience a decrease in

insulin sensitivity during the second half of the menstrual cycle (luteal phase). And in another study, we confirm with the publications that a bout of physical exercise increases insulin sensitivity. In chapter 5, we explore the short-term (up to 45 minutes) forecasting of blood glucose (BG) of by physiological modeling methodology and compare the different structural designs (full model, feed-forward, with and without SI tracking) to better understand the impact of these design choices on BG forecasting. Finally in chapter 6, we discuss how to provide a robust and predictive model by characterizing the uncertainties of the individualized parameters for the On-Demand Bolus Advisor system in artificial pancreas (AP).

The contribution of this research is the formalization of a series of techniques developed for characterizing the physiological parameter uncertainties of an insulin-glucose system aimed at enhancing model based insulin dosing strategies in diabetes. We present an innovative method that enables the online tracking of insulin sensitivity. It provides us with a relatively convenient and less obtrusive way to extract SI compared to the traditional clinical methodologies. In addition, with the knowledge of real time SI, short-term forecasting of blood glucose can be improved, which is of importance to the dosing decision considering the kinetics of modern insulin analogs. Discussions over how the uncertainties in physiological parameters affect the insulin-glucose system in a long-term time scale and a formalization of the model refinement process for applications, i.e. bolus advisory system (semi-auto control) are covered in this dissertation.

# Chapter 2. Background

## 2.1 Glucose Metabolism

Carbohydrate, digested and absorbed through the gastrointestinal system, is the principle source of energy (calories). It can be broken down into several sugars: glucose, galactose and fructose. As the central molecule in carbohydrate metabolism, glucose initializes the pathway by transport across the cell membrane. Several glucose transport proteins are involved in the diffusion process: the Glut-1 transporter is present in all cells, responsible for the basal level glucose uptake as is a necessity to provide the sustaining energy generation; Glut-2 is expressed by tubular cells in kidney and liver, in charge of transporting glucose across the membrane and into the interstitial fluid and plasma and Glut-4 transporter is responsible for the glucose utilization spurred by the insulin exclusively in cardiac, skeletal muscle and adipose tissue.

Part of the transported glucose is stored as a polymer in the human body. One of such polymer is glycogen, which is critical for providing energy to the central nervous system metabolism and to short bouts of intense physical work, is stored in two major sites: liver (~25%) and skeletal muscle (~75%). When the blood glucose level is low, liver converts the glycogen to glucose through the process known as glycogenolysis and muscle glycogen is also broken down, releasing glucose to the blood stream. Different from the liver site, the muscle glycogen can be used only by muscle. When the level of blood glucose is high, some of the glucose is converted

to liver and muscle glycogen. This push-pull mechanism helps to maintain a constant blood glucose level. Refer to <sup>24</sup> for more fundamentals about the glucose metabolism.

Hormone insulin, secreted and produced in the beta cells in the islets of Langerhans is one of most important stimulus of glucose utilization. When abundant substrate (glucose) supply is given, insulin is produced and secreted to prompt the use of exogenous nutrients and in parallel inhibit the endogenous production. When the exogenous substrate goes low, insulin secretion is attenuated, mediating the glucose utilization. This substrate-hormone pair acts like a feedback system for the plasma glucose regulation. In type 1 diabetes, the beta-cells are destroyed by the immune system. Without the essential feedback signal, insulin, the level of plasma glucose becomes susceptible to the exogenous as well as the endogenous disturbances.

## 2.2 General Physiological Models

Models, as a representation usually smaller than the real subject, facilitate the analyzing process in four general aspects: describing quantitative relations between stakeholders, interpreting experimental data, predicting system's responses under specific stimuli and explaining the observed dynamic effects <sup>25</sup>. For the physiological systems, mathematical models have been extensively used in both academy and industry. An illustrative example is the application of physiological pharmacokinetic models in the assessment of carcinogenic risk <sup>26</sup>: the dynamic of carcinogenic xenobiotics' the reactive metabolites is described by a differential equation for each part of the body (plasma, skin, fat tissue, liver and kidney) known as "compartments". Figure 1 shows the inputs and outputs of each compartment. The dynamic of the dose as a function of time can be obtained by solving equation 2.1.

$$\dot{C}_i(t) = \frac{Q_i}{U_i} (C_b(t) - V_i(t)) + \frac{1}{U_i} (\dot{Y}_i(t) - \dot{Z}_i(t)) \quad (2.1)$$

$C_i(t)$  is the concentration of xenobiotic in tissue  $i$ ,  $Q_i$  is the blood flow rate,  $U_i$  is the tissue volume,  $Y_i$  is the entering xenobiotic and  $Z_i$  is the removed xenobiotic <sup>26</sup>.

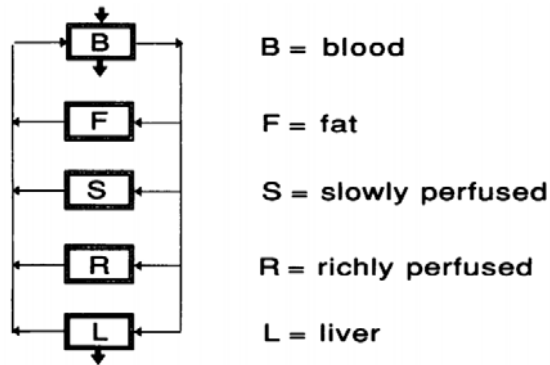


Figure 1: Schematic diagram of compartmental models of xenobiotics <sup>26</sup>. Each compartment is described by a differential equation with i/o defined.

Another classic example is the modeling of the branching lung airway <sup>27</sup>. By expressing the motion of micron-size particles as differential equations 2.2, the air flow fields can be simulated to better interpret the human respiratory system. Figure 2 shows the segmentations of the branching lung airway.

$$\dot{V}(t) = -\frac{1}{\rho}\nabla p + \nu \left[ \nabla^2 V(t) + (\nabla V(t))^{tr} \right] - (V(t) \cdot \nabla)V(t) \quad (2.2)$$

$V$  is the velocity vector,  $\rho$  is the density,  $p$  stands for the pressure and  $\nu$  is the kinematic viscosity.

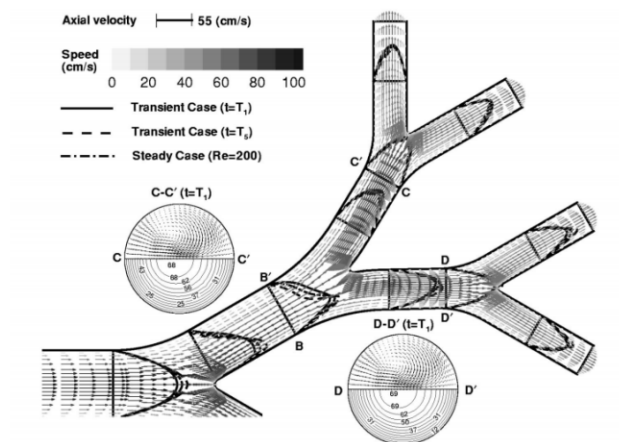


Figure 2: Structural simulation of branching lung air flow <sup>27</sup>.

Refer to <sup>28</sup> : with a selected model structure,  $\mathcal{M}$ , for the physiological system, the critical step is to identify the parameters,  $\theta$ , based on the experimental data. A typical method is to minimize the prediction error (equation 2.3) of the model by searching the optimal set of the parameters.

$$\varepsilon(t, \theta^*) = y(t) - \hat{y}(t|\theta^*) \quad (2.3)$$

We can also limit the freedom of the error by assigning weights to the error sequence (equation 2.4). With cost function defined as  $C(\theta) = \frac{1}{N} \sum_{t=1}^N l(\varepsilon_L(t, \theta))$ , the parameters are obtained by solving equation 2.5. According to different designs and implementations of the error function and the optimization technique, the advocated parameter estimation methods include: linear regression and the least-square method, maximum likelihood method, correlating prediction errors with past data, instrumental-variable method and model fitting using frequency domain data <sup>25,29-31</sup>.

$$\varepsilon_L(t, \theta) = L(q)\varepsilon(t, \theta) \quad (2.4)$$

$$\hat{\theta} = \underset{\theta}{\operatorname{argmin}} C(\theta) \quad (2.5)$$

For general linear, time-invariant systems, these methods can be expected to render desirable results. However, the approaches for non-linear, time-varying systems are still limited. The use of Maximum likelihood method, Extended Kalman Filter (EKF) and a feedback control-analog method have been reported <sup>30,32,33</sup>.

For physiological systems, non-linearity and dynamic parameters are practically ubiquitous. Albeit time-invariant linear models can be useful in representing certain physiological systems; the characterization of the dynamic parameters are inevitable when we need a more robust and

rigorous model to represent the real subject. The approach will be discussed surrounding the insulin-glucose system in this dissertation.

## 2.3 Insulin-Glucose Models

In a healthy subject, the blood glucose concentration is regulated by feedback hormonal signals. The most important one is insulin, secreted and produced by beta cells in the islets of Langerhans. When the blood glucose is perturbed, for example increasing postprandial, more insulin is produced to compensate the glucose entering the plasma from the gastrointestinal system. A counterregulatory mechanism involving glucagon, cortisol, epinephrine, and growth hormone<sup>34-37</sup> is present to prevent overcompensation that can cause hypoglycemia. The minimal model, as indicated by the name, that comprises minimum numbers of identifiable parameters, is a pragmatic tool to describe the core kinetic of the insulin-glucose interaction. Equations 2.6-7 delineate one form of such model:  $G$  and  $X$  represent the blood glucose concentration and the insulin action respectively. The equations facilitate the interpretation of the dynamic effect by observing the physiological parameters:  $S_G$  is in part the glucose effectiveness,  $p_2$  describes the rate of the insulin action,  $p_3$  is a scale factor of insulin action,  $G_b$  is the fasting glucose given the plasma insulin concentration equal to a baseline value ( $I_b$ ),  $R_a$  describes the rate of glucose appearance in plasma, and  $V$  its distribution volume.

$$G\dot{(t)} = -[S_G + X(t)] \cdot G(t) + S_G \cdot G_b + \frac{R_a(t)}{V}, \quad G(0) = G_b \quad (2.6)$$

$$X\dot{(t)} = -p_2 \cdot X(t) + p_3 \cdot [I(t) - I_b], \quad X(0) = 0 \quad (2.7)$$

One of the critical parameters is insulin resistance (insulin sensitivity). The human body responds to insulin with different effectiveness. An insulin sensitivity index is usually used to describe this effect quantitatively. Having low insulin sensitivity (high resistance) means the

subject needs more insulin to regulate the blood glucose than one having high insulin sensitivity if other metabolic states stay identical. In type 2 diabetes, insulin resistance (low insulin sensitivity) can cause the body to compensate by secreting more insulin. Chronic elevated insulin on board leads to a variety of symptoms such as obesity, high blood pressure and lower urinary tract symptoms<sup>38-40</sup>. High insulin sensitivity is generally taken as a good sign. But under certain circumstances, for example, exogenous insulin treatment for type 1 diabetes, high insulin sensitivity can cause over-corrected blood glucose (hypoglycemia) by miscalculated insulin dosing.

Over the decades, extensive studies have been conducted surrounding the quantification and qualification of insulin sensitivity. The gold standard for measuring the whole-body insulin sensitivity is the hyperinsulinemic-euglycemic clamp<sup>41</sup> in which the plasma insulin concentration is raised to a plateau and maintained at that level while the glucose plasma concentration is maintained at euglycemic level. The insulin sensitivity is calculated based on the historical insulin infusion and blood glucose concentration measurements. Intravenous glucose tolerance tests (IVGTT)<sup>42</sup> and oral glucose tolerance tests (OGTT)<sup>43</sup> are two alternative methods. In IVGTT, a single IV injection of glucose is given to the subject and the plasma glucose and insulin concentrations are measured and recorded during the test; in OGTT, the IV injection of glucose is replaced by an oral glucose dose. For IVGTT, the insulin sensitivity is obtained by fitting the minimal model (equation 2.6-7) to the collected data:

$$SI = \frac{p_3}{p_2} V \quad (2.8)$$

While for OGTT, additional models (gastrointestinal compartments, equation 2.9 for instance) are needed to account for the glucose flow from oral to the plasma. The expanded parameter set will add complexity to the identification process.

$$\begin{aligned} \dot{Q}_1(t) &= -k_\tau \cdot Q_1(t) + meal \\ \dot{Q}_2(t) &= k_\tau \cdot Q_1(t) - k_{abs} \cdot Q_2(t) \end{aligned} \quad (2.9)$$

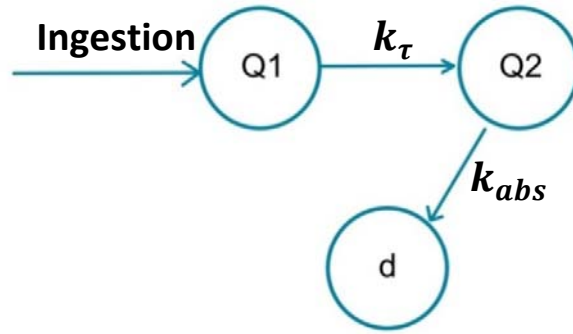


Figure 3: Meal model described by equation 2.9.

Figure 4 shows another form of meal model which contains two compartments ( $Q_1$  and  $Q_2$ ) corresponding to fast absorption and slow absorption respectively. The rate of plasma glucose appearance is the combination of the two absorptions.

$$\begin{aligned} \dot{Q}_1(t) &= -a_1 \cdot Q_1(t) - a_d \cdot Q_1(t) + M(t) \\ \dot{Q}_2(t) &= -a_2 \cdot Q_2(t) + a_d \cdot Q_1(t) \\ R_a(t) &= a_1 \cdot Q_1(t) + a_2 \cdot Q_2(t) \end{aligned} \quad (2.10)$$

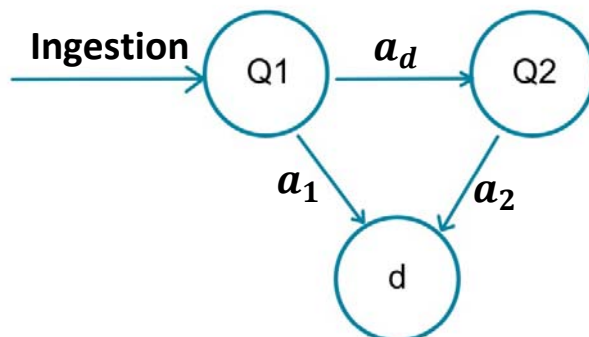


Figure 4: Meal model described by equation 2.10: Q1 (fasting absorption) and Q2 (slow absorption).

The assumption of constant SI during these tests is coarse and non-physiological (to a lesser extent in OGTT and IVGTT compared to the clamp). SI actually varies with time subject to a variety of factors. We will discuss in detail how to characterize this time varying parameter in chapter 3.

## **Glucose Observation and Insulin Intervention**

### *Glucose Sensing*

Blood glucose self-monitoring (SMBG) is a traditional approach used to measure the blood glucose level by fingerstick episodically each day. It helps diabetic patients to form a better perception of the individualized blood glucose profile and to adjust the treatment strategies effectively<sup>44,45</sup>. The advent of continuous glucose monitoring (CGM), which generates equally spaced readings (every 5 minutes), has further pushed the boundaries of glucose observation and the treatment of diabetes. It has to be pointed out that the present CGM technique is still confronted with multiple challenges. Since the sensor measures the interstitial fluid glucose (IG) instead of capillary blood glucose, a device calibration has to be taken to compensate the gradient between the two sites. Also, there is a time lag for glucose to diffuse from BG to IG and the effect is associated with the direction of BG change. It is generally accepted that the delay is about 4-10 minutes<sup>46</sup>. On top of that, non-white additive noise further confounds the CGM time series. Extensive researches have been conducted regarding the described challenges: device calibration to account for the gradient between capillary blood glucose and interstitial fluid glucose<sup>47-49</sup>, exploration in the BG-IG time lag<sup>50-53</sup> and application of denoising techniques<sup>54-56</sup>.

CGM generates much more complex data than SMBG. Not surprisingly, it brings in valuable information that SMBG is incapable of, such as change rate of BG and the direction of change.

This is particularly critical for development of intensive BG control system, i.e. closed-loop control, also known as artificial pancreas. Kovatchev et al. reported that using CGM as a substitute of SMBG for insulin dosing is feasible given the sensor error is below a certain level <sup>46</sup>.

### *Insulin Delivery*

Multiple daily insulin (MDI) therapy is a widely accepted treatment of insulin dependent diabetes. The dosing involves long-acting insulin once or twice a day and episodic fast-acting insulin to compensate the meal perturbation. Continuous subcutaneous insulin infusion (CSII), also known as pump therapy, has been advocated since its first clinical trial <sup>57</sup>. Rapid-acting insulin is delivered precisely by a portable device called an insulin pump. The dosing involves two kinds: basal, active continuously, injecting small amount of insulin at short time interval (5 minutes) and bolus, additional large amount of insulin to compensate the meal carbohydrate. The pump users in the United States have grown from 70,000 since 1998 to 350,000 <sup>58</sup>. MDI and CSII have been compared in multiple studies <sup>59-61</sup>.

Subcutaneous model of insulin injection is applied (if necessary) to account for the insulin transportation as an extension of the minimal model. Figure 5 shows an example of insulin model composed of three compartments.

$$\begin{aligned}
 \dot{I}_{SC1}(t) &= -k_d \cdot I_{SC1}(t) + J(t) \\
 \dot{I}_{SC2}(t) &= -k_d \cdot I_{SC2}(t) + k_d \cdot I_{SC1}(t) \\
 \dot{I}_p(t) &= -k_{cl} \cdot I_p(t) + k_d \cdot I_{SC2}(t)
 \end{aligned}
 \tag{2.11}$$

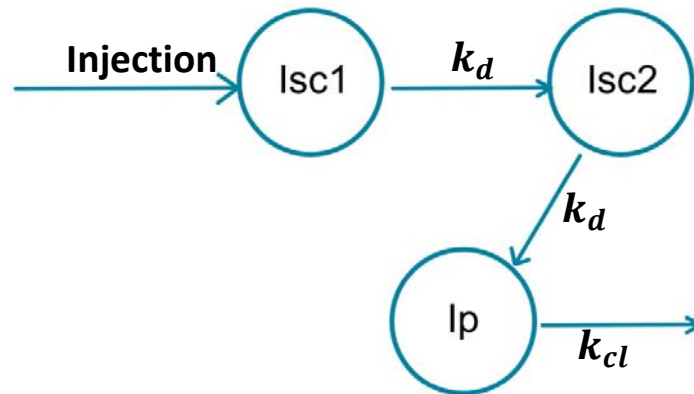


Figure 5: Subcutaneous model of insulin injection described by equation 2.11.

## 2.4 BG Forecasting and Control

The advent of continuous glucose monitoring opens a door to more advanced treatment of diabetes. It has been pushing forward the intensive treatment of type 1 diabetes and thanks to it, here approaches artificial pancreas, an integrated system which attempts to “close the loop” through connections to third party devices (continuous glucose monitoring and insulin pump) aimed at dispensing the diabetics patients from cognitive concern of insulin dosing (Figure 6). The development of artificial pancreas is an interdisciplinary subject that spans fields such as physiological modeling, signal processing, control theory and health care. This dissertation is focused on the how to characterize the parameter uncertainties in the insulin-glucose system for improving state estimation, prediction and control.

### 2.4.1 Short-term BG Forecasting and Closed-loop Control

As we discussed in section 2.3, the advancing CGM and pump technologies have unleashed the development of closed-loop control for insulin dependent diabetes. In the regime of artificial pancreas, the intensive control signal (dosing insulin) is adjusted every 5 minutes. For a healthy body, the blood glucose responds to pulsatile secretion of insulin in 5 to 15 minutes<sup>62</sup>. However,

for pump users, the latency of insulin action ascribed to the subcutaneous transportation is non-negligible. It takes the rapid-acting insulins approximately 15 minutes to reach the bloodstream and 30 to 90 minutes to peak the action <sup>63</sup>. Therefore, the projection of the blood glucose concentration for an accurate dosing at decision time is obligatory. It is essential for the bottom-layer controller in the AP architecture, namely “Safety Module” which is capable of attenuating insulin injection or shutting off the pump when short-term (up to 45 minutes) hypoglycemic events are forecasted.

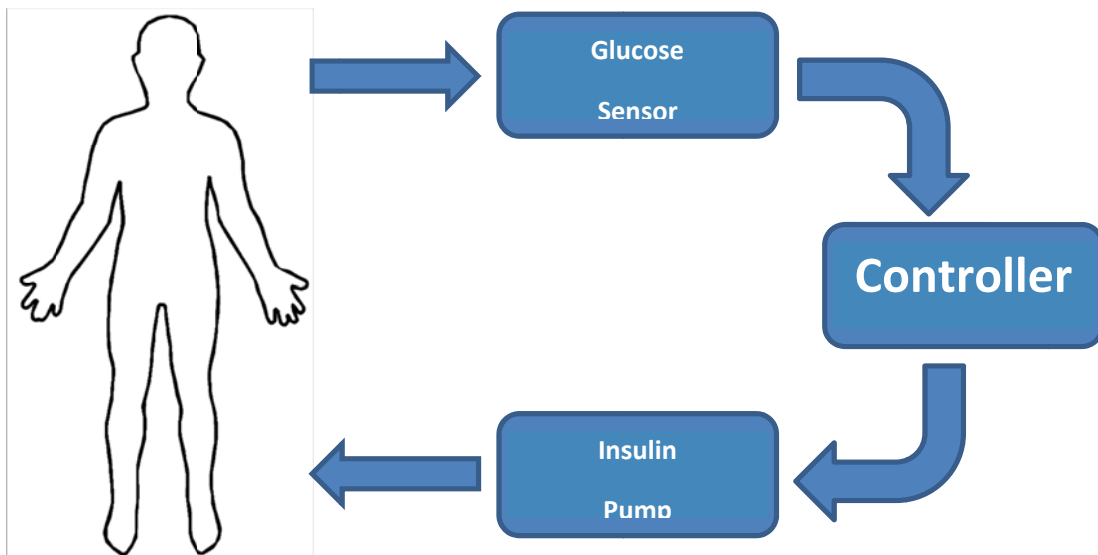


Figure 6: Schematic diagram of closed-loop control of diabetes.

Recent years have witnessed a variety of methods applied in the short-term forecasting of BG. We are particularly interested in how to improve the BG forecasting by characterizing the parameter uncertainties of the physiological model. The insulin sensitivity (coarse gain of the insulin-glucose kinetic) is our focus. The details will be discussed in chapter 5.

#### **2.4.2 Long-term BG Forecasting and Open-loop Control (Semi-Auto Control)**

The other side of the coin is the open-loop control (or semi-auto control) which is built above the safety layer. The algorithms that have been tested and reported are Proportional Integral Derivative (PID) or Model Predictive Control (MPC). The controller in this level usually computes the bolus insulin delivery that is supposed to compensate the blood glucose for a long time scale depending on the length of the control window. Considering the pronounced inter-individual variability reflected in this scale, the leverage of the average model is minimized. Therefore, development of a robust individual specific model that is capable of projecting long-term blood glucose concentration becomes one of our priorities. The details of how to improve the parameter estimation as well as the process of the individual controller calibration will be discussed in chapter 6.

### **2.5 Diabetes Simulator**

Compared to the minimal model, maximal models are composed of a large number of equations and parameters, useful for investigating insulin-glucose dynamics as well as evaluating the treatment strategies in preclinical studies. In 2008, a type 1 diabetes simulator<sup>64</sup> co-developed by University of Virginia and University of Padova, Italy was accepted by the Food and Drug Administration (FDA) as a substitute to animal trials for the preclinical testing of open-loop and closed-loop control strategies of diabetes. The simulator is equipped with 100 adults, 100 children and 100 adolescents (Table 2). The in-silico cohort spans the observed variability of the general T1DM population. Each subject is a complex entity of 26 individual parameters that govern 13 first-order differential equations (Table 1 and Figure 7)<sup>65</sup>.

Table 1: In-silico subject described by 13 differential equations

$$\begin{aligned} \dot{G}_p &= -k_2 \cdot G_p + k_1 \cdot G_t - U_{ii} - E_t + k_{p1} - k_{p2} \cdot G_p - k_{p3} \cdot I_d + \frac{f \cdot k_{abs} \cdot Q_{gut}}{BW} \\ \dot{G}_t &= -k_1 \cdot G_t + k_2 \cdot G_p - \frac{(V_{m0} + V_{mx} \cdot X)G_t}{K_{m0} + G_t} \\ \dot{G}_{sc} &= -k_{sc}(G_{sc} - \frac{G_p}{V_g}) \\ \dot{I}_p &= -(m_2 + m_4) \cdot I_p + m_1 \cdot I_l + k_{a1} \cdot I_{sc1} + k_{a2} \cdot I_{sc2} \\ \dot{I}_l &= -(m_1 + m_3) \cdot I_l + m_2 \cdot I_p \\ \dot{I}_1 &= -k_i(I_1 - \frac{I_p}{V_i}) \\ \dot{I}_d &= -k_i(I_d - I_1) \\ \dot{X} &= -p_{2h}(X - (\frac{I_p}{V_i} - I_b)) \\ \dot{I}_{sc1} &= -k_d \cdot I_{sc1} - k_{a1} \cdot I_{sc1} + \frac{J(t)}{BW} \\ \dot{I}_{sc2} &= k_d \cdot I_{sc1} - k_{a2} \cdot I_{sc2} \\ \dot{Q}_{sto1} &= -k_{gri} \cdot Q_{sto1} + M(t) \\ \dot{Q}_{sto2} &= -k_{empt} \cdot Q_{sto2} + k_{gri} \cdot Q_{sto1} \\ \dot{Q}_{gut} &= k_{abs} \cdot Q_{gut} + k_{empt} \cdot Q_{sto2} \end{aligned}$$

In addition, virtual Continuous Glucose Monitoring (CGM) sensor and insulin pump were modeled and implemented in the simulation platform that enabled the testing with subcutaneous insulin delivery with or without the sensor data. The simulator was designed in a way that different combinations of meal pattern and insulin dosing plan can be pre-defined in a “scenario” file. Such a platform helps to test the stability of control algorithms in extreme circumstances. A new version of the simulator (S2013) was submitted to FDA with improved glucose kinetic in hypoglycemia as well as glucagon kinetics being incorporated <sup>66</sup>.

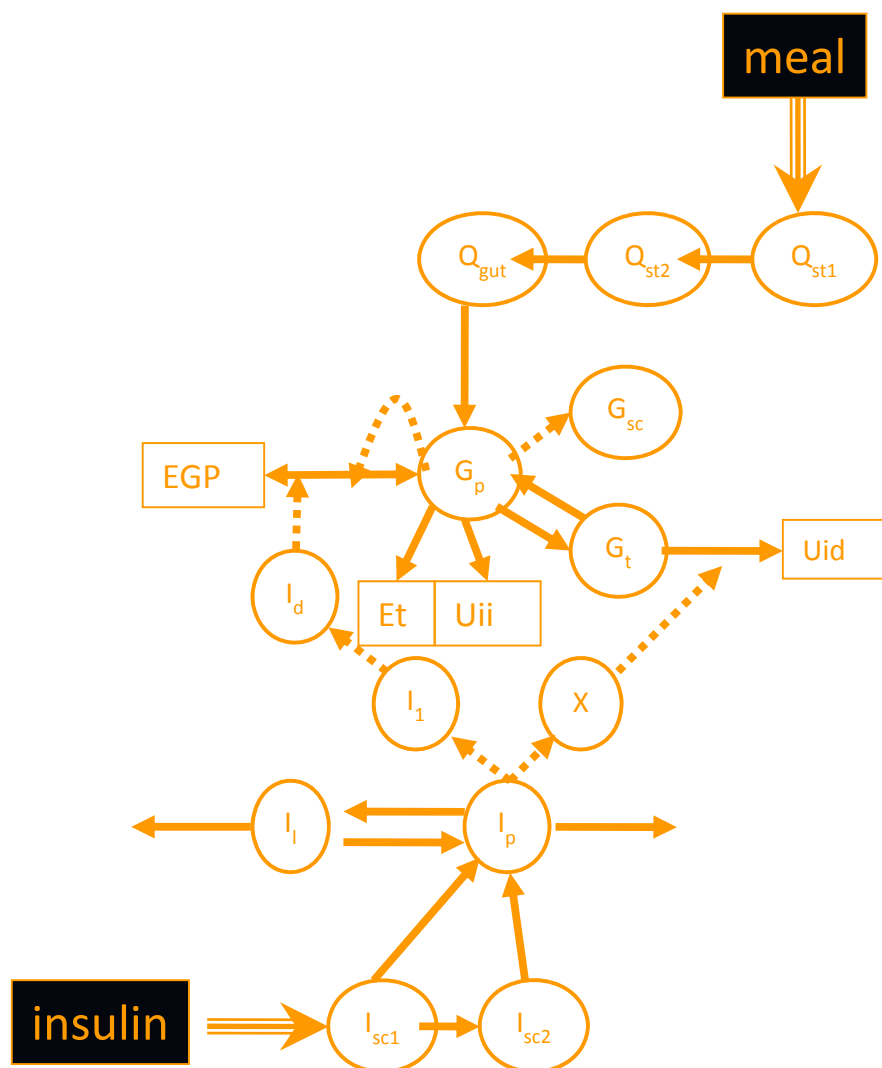


Figure 7: Compartments of the simulator models and signal flow

Table 2: Physiological parameters of the in-silico patients

Parameter	Adults			Adolescents			Children		
	Mean(SD)	Min	Max	Mean(SD)	Min	Max	Mean(SD)	Min	Max
Weight(kg)	79.7(12.8)	52.3	118.7	54.7(9.0)	37.0	88.7	39.8(6.8)	27.6	60.6
Insulin(U/day)	47.2(15.2)	21.3	98.4	53.1(18.2)	22.6	141.5	34.6(9.1)	17.6	56.1
Carb ratio (g/U)	10.5(3.3)	4.6	21.1	9.3(2.9)	3.2	19.9	14.0(3.8)	8.0	25.5

The simulator is developed in Simulink@Matlab. Figure 8 shows the interface of the latest version. “Load Scenario” block is for users to pick a pre-defined test scenario or create a new scenario through GUI. “Select Subject” block provides handy functionalities to select in-silico patient(s) among 3 groups: adults, adolescents and children. “Hardware” block is designed for testing control algorithms using third party devices (insulin pump or/and CGM). “Pre-test/screening” block provides quick access to simulations of standard clinical test and “Outcomes” block is where users choose the output form of the simulated results.

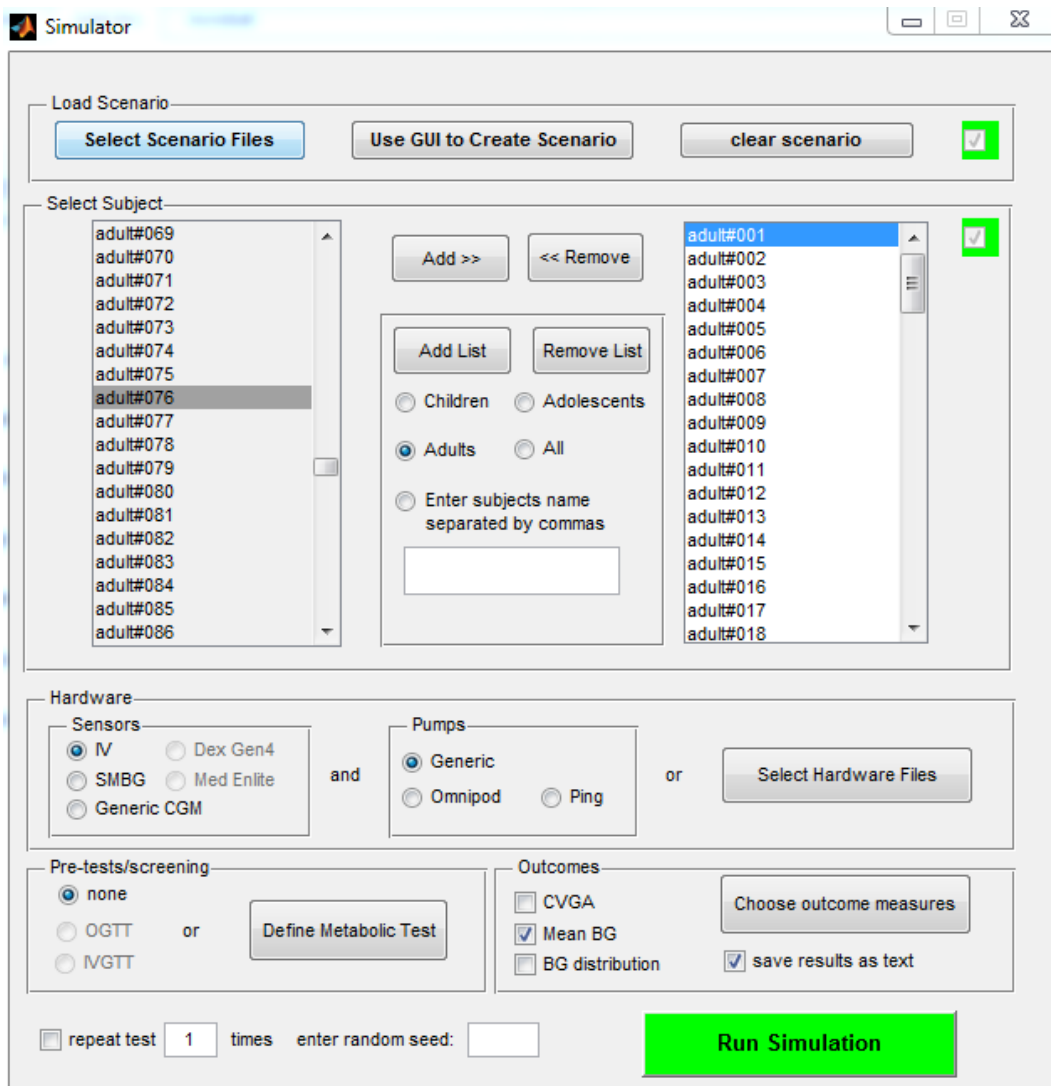


Figure 8: Type 1 simulator interface.

### A Simulation Example

As an illustration of the use of the simulation environment, one simple simulation example is given here. 100 in-silico adults were chosen and for each subject, a meal with 0.8 gram/kg amount of carbohydrates was served 1 hour after the beginning of the simulation. Corresponding bolus computed based on subject's "carbohydrates: insulin" ratio was also provided. The entire simulation lasted 16 hours. Figure 9 shows the simulated BG traces of all in-silico adults.

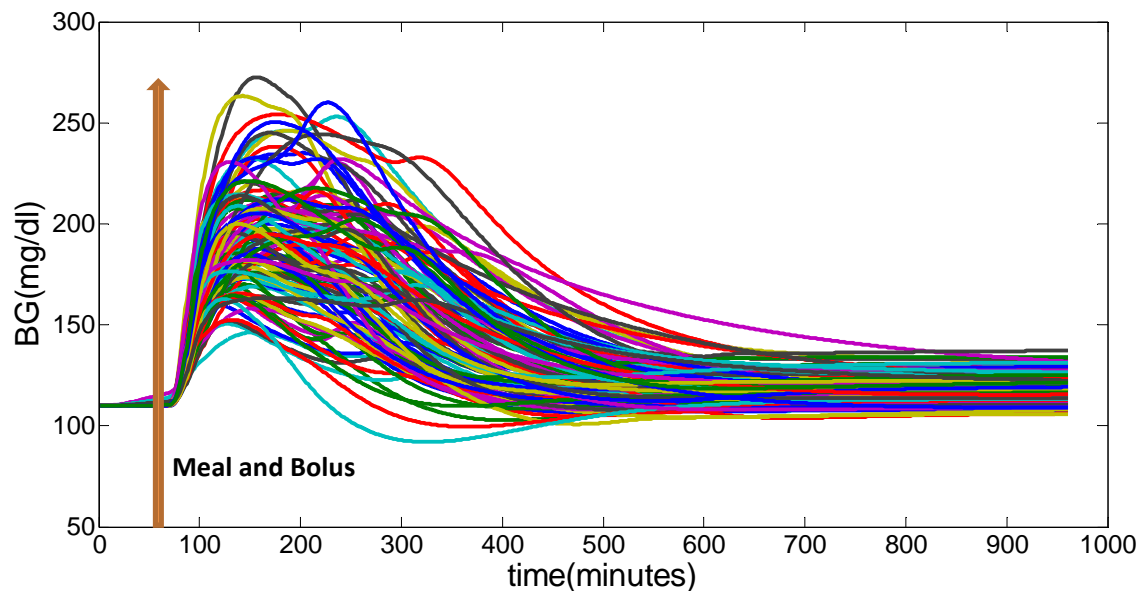


Figure 9: Open-loop simulations of 100 in-silico adults: one meal and the corresponding bolus provided

In this dissertation, both in-vivo and in-silico data were exploited. Arguably, either cannot be replaced completely by the other. The simulation approach provides a fast way to test extremes and rule out inappropriate scenarios but it can never guarantees the consistency of performance from in-silico to in-vivo.

# Chapter 3. Dynamic Parameter Uncertainties Tracking in the Insulin- Glucose System – Estimation of Insulin Sensitivity

Considering the fact that it is impossible to match every single parameter to the in-vivo biomedical data, lumping the parameter set has become a necessity. Simple first-order time-invariant model is beneficial under certain circumstances, however, if a substantial amount of systematic residuals cannot be accounted for, introducing nonlinearity or/and time-varying parameters is indispensable. A consequence it brings then is the difficulty of parameter tracking. One coping solution is recursive least-square algorithm.

Refer equation 3.1-5 to <sup>28</sup>: if a system can be described as follows

$$\begin{aligned} X(t) &= H(t, X(t-1), y(t), u(t)) \\ \hat{\theta}(t) &= h(X(t)) \end{aligned} \tag{3.1}$$

a recursive expression of parameter set  $\hat{\theta}(t)$  is of form:

$$\begin{aligned} \hat{\theta}(t) &= \hat{\theta}(t-1) + \gamma_t Q_\theta(X(t), y(t), u(t)) \\ X(t) &= X(t-1) + \mu_t Q_X(X(t-1), y(t), u(t)) \end{aligned} \tag{3.2}$$

The recursive least-square algorithm tries to obtain  $\hat{\theta}(t)$  by solving the minimization problem (equation 3.3) which assigns weight  $(\beta(t, k))$  to the residuals.

$$\hat{\theta}(t) = \underset{\theta}{\operatorname{argmin}} \sum_{k=1}^t \beta(t, k) [y(k) - \varphi^T(k)\theta]^2 \quad (3.3)$$

A time-varying system then can be formalized by a treatment of  $\beta(t, k)$  such as equation 3.4 which means the older a measurement is taken, the less a weight is assigned.

$$\beta(t, k) = \lambda^{t-k} \quad (3.4)$$

The tracking of  $\hat{\theta}(t)$  becomes:

$$\begin{aligned} \hat{\theta}(t) &= \hat{\theta}(t-1) + \frac{P(t-1)\varphi(t)}{\lambda + \varphi^T(t)P(t-1)\varphi(t)} [y(t) - \varphi^T\hat{\theta}(t-1)] \\ P(t) &= \frac{1}{\lambda} \left[ P(t-1) - \frac{P(t-1)\varphi(t)\varphi^T(t)P(t-1)}{\lambda + \varphi^T(t)P(t-1)\varphi(t)} \right] \end{aligned} \quad (3.5)$$

The term  $\lambda$  is usually called “forgetting factor”. The larger it is, the more difficult to track the parameter, because the corresponding time constant gets larger. The choice of the magnitude of  $\lambda$  plays an important role in balancing the parameter tracking and the noise sensitivity.

The archetypal described above have been further developed to adapt to different biomedical system. We use Avanzolini’s publication in 1997 as an illustrative example<sup>67</sup>. He and his colleagues developed a new approach for on-line tracking of respiratory mechanical parameters. The respiratory system in artificial ventilation was expressed by a first-order lumped parameter model (equation 3.6).

$$P_{tp}(t) = R(t)f(t) + E(t)v(t) + K \quad (3.6)$$

$P_{tp}(t)$  was transpulmonary pressure,  $f(t)$  was ventilatory flow,  $v(t)$  was the lung volume change,  $K$  was the calibration point,  $R(t)$  and  $E(t)$  were time-varying parameters corresponding to tissue viscosity and lung elastance respectively. By incorporating the recursive

analysis of mean and standard deviation of the parameters, a common characteristic constant for the forgetting factor ( $\lambda$ ) was obtained and therefore a good compromise between meaningful parameter estimates and model robustness had been achieved.

As we discussed in section 2.3, the dynamic of the insulin-glucose system is often described by a highly lumped parameter model. Some of the time-varying parameters play a critical role in the insulin-glucose interaction. An online parameter tracking technique is therefore particularly desirable.

Insulin Sensitivity, the index that describes the effectiveness of insulin reacting to glucose, is one of the most important parameters. It has been the focus of many studies over the last four decades. In the late 1970's, DeFronzo proposed a hyperinsulinemic-euglycemic clamp technique for measuring the whole-body insulin sensitivity, which turned into the gold standard for SI quantification in the hospital setting <sup>41</sup>. Intravenous glucose tolerance tests (IVGTT) <sup>42</sup> and oral glucose tolerance tests (OGTT) are two alternatives in which a predetermined amount of designated of glucose is dosed intravenously (IV) or orally. The oral minimal model is a useful tool for SI estimation based on OGTT data <sup>43,68-70</sup>. Albeit effective and robust, these traditional techniques do require subjects to be in the inpatient clinical setting either with IV lines attached or enduring multiple venipunctures. They are invasive to the patients and are also disruptive to T1DM patients' daily insulin treatment in the home setting.

The advancement of Continuous Glucose Monitors (CGM) and insulin pumps has significantly changed glucose management in T1DM. It also shed light onto the study of SI quantification. Schiavon proposed a method to estimate insulin sensitivity using the pump and CGM data <sup>71</sup>. The liberation from mandatory measurements of plasma glucose and insulin concentration has opened the door to convenient access to SI for Type 1 diabetics in daily life.

One difficulty with the traditional techniques is that SI is treated as a time invariant physiological parameter (at least during the test process: about 2 hours for hyperinsulinemic-euglycemic clamp and about 4-7 hours for IVGTT and OGTT). However, studies have shown that SI does vary significantly in response to many factors; among the most common are circadian rhythm<sup>72</sup>, physical activity<sup>73</sup>, dietary habits<sup>74</sup>, and illness or stress. Pilonetto et al. proposed a new dynamic insulin sensitivity index to tackle this issue, reporting that the dynamic SI was more precise than the regular SI in patients who had slow insulin action<sup>75</sup>. Lin and her collaborators showed that the first order estimate of insulin sensitivity could be obtained through stochastic modeling<sup>76</sup>.

The purpose of this study is to propose a new method to track insulin sensitivity utilizing CGM and pump data and validate it against the gold standard.

## **Data**

After signed informed consent, thirty-two subjects (17 females, 15 males) with type 1 diabetes (Mean±SD: age=44±11 yr, body weight=78.4±17.5 kg, BMI=26.6±4.7 kg/m<sup>2</sup>, A1c=7.3±1.1) completed the phase 2 (IRB-HSR#15131) study designed to investigate the insulin sensitivity and counterregulatory function. The subjects had been using an insulin pump for at least six months prior to the study. Rapid-acting insulin (lispro) was provided for the subjects who did not use such insulin before. Aside from a screening visit, females were required to pay two visits to the hospital and males were required one visit. On the visiting days, the subject was admitted to the research center at approximately 1600 hours. Dinner and insulin bolus were provided around 1700 hours. A meal test (mixed nutrition drink, 41 gram) started at 0800 hours. Blood samples were collected at -120, -60, -30, -20, -10, 0, 5, 10, 15, 20, 30, 40, 50, 60, 75, 90, 120, 150, 180, 210

and 240 minutes for C-peptide, insulin and glucose. The patients were required to wear CGM during at least one visit.

### 3.1 Standard Methods and KF Method for SI Quantification

Including the new insulin index  $SI_{KF}$  proposed in this manuscript, we computed four SI indices based on the mixed meal test: a)  $SI_{Ra}$ , published by Dalla Man et al<sup>70</sup> served as the control group, b)  $SI_{mm}$ , by oral glucose minimal model, referring to Dalla Man<sup>77</sup>, c)  $SI_{sp}$ , published by Schiavon [4] and d)  $SI_{KF}$ . Different treatments of blood glucose appearance ( $R_a$ ) and plasma insulin concentration ( $I$ ) would be taken as the inputs.

#### Standard Methods

##### a) Insulin Sensitivity from Oral Glucose Minimal Model ( $SI_{Ra}$ )

Referring to Dalla Man<sup>70</sup>, the insulin sensitivity as well as blood glucose appearance,  $R_{a\ ogtt}$  was derived by oral glucose minimal model.  $R_{a\ ogtt}$  was defined as a piece-wise linear function:

$$\dot{G}(t) = -[S_G + X(t)] \cdot G(t) + S_G \cdot G_b + \frac{R_{a\ ogtt}(\alpha, t)}{V}, \quad G(0) = G_b \quad (3.7)$$

$$\dot{X}(t) = -p_2 \cdot X(t) + p_3 \cdot [I(t) - I_b], \quad X(0) = 0 \quad (3.8)$$

$$R_{a\ ogtt}(\alpha, t) = \begin{cases} \alpha_{i-1} + \frac{\alpha_i - \alpha_{i-1}}{t_i - t_{i-1}}(t - t_{i-1}), & \text{per } t_{i-1} \leq t \leq t_i \quad i = 1 \dots 7 \\ 0, & \text{Otherwise} \end{cases} \quad (3.9)$$

$$SI_{Ra} = \frac{p_3}{p_2} \cdot V \quad (3.10)$$

The parameter set to be estimated was  $[p_2, p_3, \alpha]$ .  $G_b$  and  $I_b$  were set to the values at the beginning of the tolerance test ( $t=0$ ).  $S_G = 0.02$ .

b) Insulin Sensitivity from Extended Minimal Model ( $SI_{mm}$ )

An alternative to the piece-wise linear  $R_{\alpha_{ogtt}}(\alpha, t)$  was a derived  $R_{\alpha}(t)$  from a meal transport model which was composed of two (fast and slow) glucose absorption compartments ( $Q_1$  and  $Q_2$ ), referring to Dalla Man <sup>77</sup>.

$$\dot{G}(t) = -[S_G + X(t)] \cdot G(t) + S_G \cdot G_b + \frac{R_{\alpha}(t)}{V}, \quad G(0) = G_b \quad (3.11)$$

$$\dot{X}(t) = -p_2 \cdot X(t) + p_3 \cdot [I(t) - I_b], \quad X(0) = 0 \quad (3.12)$$

$$\dot{Q}_1(t) = -(a_1 + a_d) \cdot Q_1(t) + M(t) \quad (3.13)$$

$$\dot{Q}_2(t) = a_d \cdot Q_1(t) - a_2 \cdot Q_2(t) \quad (3.14)$$

$$R_{\alpha}(t) = a_1 \cdot Q_1(t) + a_2 \cdot Q_2(t) \quad (3.15)$$

The parameter set to be estimated was  $[p_2, p_3]$ .  $G_b$  and  $I_b$  were set to the values at the beginning of the tolerance test ( $t=0$ ).  $S_G = 0.02$ .

$$SI_{mm} = \frac{p_3}{p_2} \cdot V \quad (3.16)$$

c) Insulin Sensitivity from Integration of the Minimal Model ( $SI_{sp}$ )

Referring to Schiavon [4], by integration of the minimal model and with appropriate computational approximation of blood glucose and insulin concentration from CGM and pump data, the insulin sensitivity was

$$SI_{sp}(meal) = \frac{\frac{AoC(meal)}{BW} - GEZI \cdot AUC(\Delta CGM) - V_G \cdot [CGM(t_{end}) - CGM(t_{meal})]}{\left[ \frac{1}{CL} \int_{t_{basal}}^{t_{end}} basal(t) dt + \sum_{t_k=t_{meal}}^{t_{end}} \frac{bolus(t_k)}{CL} + IOB(t_{meal}) - IOB(t_{end}) \right] \cdot \left[ \frac{AUC(|\Delta CGM|)}{t_{end} - t_{meal}} \right]} \quad (3.17)$$

## Kalman Filtering Method

### d) Insulin Sensitivity by Kalman Filtering ( $SI_{KF}$ )

Kalman Filtering possesses a favorable feature of state tracking by tunable noise filtration. It is generally accepted that SI is considered a time-invariant constant during clamp, IVGTT and OGTT. Through transforming the time-invariant physiological parameter SI into a time-varying state, online SI estimation by KF computation became applicable. The transformation was accomplished by adding an extra first order SI dynamic to the nominal minimal model. The feature of the dynamic was to drive the SI state to the equilibrium value  $SI_b$  in a finite time period (characteristic time = 60 minutes).

A preliminary application of this approach produced occasional incidences of negative SI, inspiring the logarithmic transformation of blood glucose state ( $\log(\frac{G}{G_b})$ ), remote insulin action ( $\log(\frac{X}{X_b})$ ) and insulin sensitivity ( $\log(\frac{SI}{SI_b})$ ) influenced by the nonlinear structure of the minimal model. It is worthwhile to point out that the multiplicative term  $G \cdot X$  turned into an additive component. The insulin-glucose model embedded in KF therefore became:

$$\begin{bmatrix} \ln\left(\frac{G(k+1)}{G_b}\right) \\ \ln\left(\frac{X(k+1)}{X_b}\right) \\ \ln\left(\frac{SI(k+1)}{SI_b}\right) \end{bmatrix} = \begin{bmatrix} -p_1 & -p_2 & -p_3 \\ 0 & -p_4 & 0 \\ 0 & 0 & -1/\tau_{SI} \end{bmatrix} \begin{bmatrix} \ln\left(\frac{G(k)}{G_b}\right) \\ \ln\left(\frac{X(k)}{X_b}\right) \\ \ln\left(\frac{SI(k)}{SI_b}\right) \end{bmatrix} + \begin{bmatrix} p_6 & 0 \\ 0 & p_4 \\ 0 & 0 \end{bmatrix} \begin{bmatrix} R_a(k) \\ I(k) \end{bmatrix} \quad (3.18)$$

$R_a(k)$  and  $I(k)$  represented blood glucose appearance and plasma insulin respectively, this plus the measurement were taken as inputs into the KF. Without direct access,  $R_a(k)$  and  $I(k)$  were computed by meal and insulin transport compartments separately. This “feed-forward

modules" idea was inspired by Grossman <sup>78</sup>. Figure 10 shows the structure of the KF implementation.

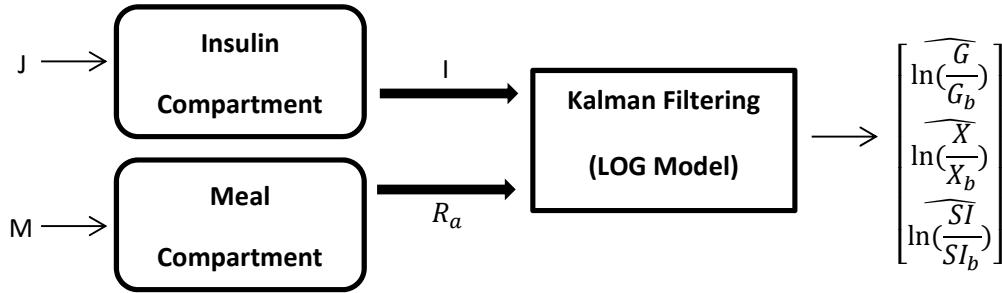


Figure 10: Feed-forward design of Kalman Filtering.

*meal compartment:*

$$\begin{bmatrix} Q_1(k+1) \\ Q_2(k+1) \end{bmatrix} = \begin{bmatrix} -(a_1 + a_d) & 0 \\ a_d & -a_2 \end{bmatrix} \begin{bmatrix} Q_1(k) \\ Q_2(k) \end{bmatrix} + \begin{bmatrix} 1 \\ 0 \end{bmatrix} M(k) \quad (3.19)$$

$$R_a(k) = a_1 \cdot Q_1(k) + a_2 \cdot Q_2(k) \quad (3.20)$$

The model had two compartments representing the fast ( $Q_1$ ) and slow ( $Q_2$ ) meal absorption respectively. The blood glucose appearance was the sum of the two.

*insulin compartment:*

$$\begin{bmatrix} I_{sc1}(k+1) \\ I_{sc2}(k+1) \\ I_p(k+1) \end{bmatrix} = \begin{bmatrix} -k_d & 0 & 0 \\ k_d & -k_d & 0 \\ 0 & k_d & -k_{cl} \end{bmatrix} \begin{bmatrix} I_{sc1}(k) \\ I_{sc2}(k) \\ I_p(k) \end{bmatrix} + \begin{bmatrix} 1 \\ 0 \\ 0 \end{bmatrix} J(k) \quad (3.21)$$

$$I(k) = \frac{I_p(k)}{VI \cdot BW} - I_b \quad (3.22)$$

VI was the insulin volume of distribution.

The model was discretized in 5-minute intervals to match the frequency of CGM collection. We started the KF at the beginning of the admission day at 1600 hours and kept it active until 1300 hours the next day. SIs during the test (0800-1200 hours) were collected and averaged as the  $SI_{KF}$ . The initial values of KF states were set to  $[0 \ 0 \ 0]'$ .

*Kalman Filtering setting:*

The model embedded in KF was discretized as a 5-minute discrete system in state-space:

$$\begin{bmatrix} \ln\left(\frac{G(k+1)}{G_b}\right) \\ \ln\left(\frac{X(k+1)}{X_b}\right) \\ \ln\left(\frac{SI(k+1)}{SI_b}\right) \end{bmatrix} = \begin{bmatrix} -p_1 & -p_2 & -p_3 \\ 0 & -p_4 & 0 \\ 0 & 0 & -\frac{1}{\tau_{SI}} \end{bmatrix} \begin{bmatrix} \ln\left(\frac{G(k)}{G_b}\right) \\ \ln\left(\frac{X(k)}{X_b}\right) \\ \ln\left(\frac{SI(k)}{SI_b}\right) \end{bmatrix} + \begin{bmatrix} p_6 & 0 \\ 0 & \frac{p_4}{VI \cdot BW} \\ 0 & 0 \end{bmatrix} \begin{bmatrix} R_a(k) \\ I_p(k) \end{bmatrix} + Gw[k] \quad (3.23)$$

$$\begin{bmatrix} \ln\left(\frac{G(k)}{G_b}\right) \\ \ln\left(\frac{X(k)}{X_b}\right) \\ \ln\left(\frac{SI(k)}{SI_b}\right) \end{bmatrix} = [1 \ 0 \ 0] \begin{bmatrix} \ln\left(\frac{G(k)}{G_b}\right) \\ \ln\left(\frac{X(k)}{X_b}\right) \\ \ln\left(\frac{SI(k)}{SI_b}\right) \end{bmatrix} + Du[n] + Hw[n] + v[k] \quad (3.24)$$

in which  $w[n]$  and  $v[n]$  stand for processing noise and measurement noise respectively. The tuning factors were defined as noise covariance as:  $E(w[n]w[n]^T) = Q$ ,  $E(v[n]v[n]^T) = R$ ,  $E(w[n]v[n]^T) = N$ .

By solving the discrete Riccati equation, the gain =  $(APC^T + \bar{N})(CPC^T + \bar{R})^{-1}$ , where

$$\bar{R} = R + HN + N^T H^T + HQH^T \quad (3.25)$$

$$\bar{N} = G(QH^T + N) \quad (3.26)$$

Details of matrices and covariance are listed in Table 3. We assumed that the analogous insulin action  $\ln(\frac{X}{X_b})$  possessed no process noise. The choices of Q/R were made considering the expected magnitude of variation in the estimation of physiological states (G from 40 to 600 mg/dl and SI from 1e-4 to 1e-2 1/min per mU/l). We allowed that  $\ln(\frac{SI}{SI_b})$  could vary by 100 percent.

Table 3: Noise covariance setting of KF

$G$	$H$	$Q$	$R$	$N$
$\begin{bmatrix} 0.05 & 0 & 0 \\ 0 & 0 & 0 \\ 0 & 0 & 1 \end{bmatrix}$	$[0 \ 0 \ 0]$	$\begin{bmatrix} 1 & 0 & 0 \\ 0 & 1 & 0 \\ 0 & 0 & 1 \end{bmatrix}$	0.5	$[0 \ 0 \ 0]'$

### 3.2 Validation of KF Method against Standards

The validation has two components:

#### Validation using YSI

41 test traces were available for analysis (17 females with 2 visits and 7 males with 1 visit). We used  $SI_{Ra}$  as the baseline group and the obtained  $R_{a\ ogtt}$  was applied to several implementations by other methods. The YSI were interpolated in 5-minute intervals as the measurement input of KF. Based on different combinations of feed-forward inputs, we obtained four  $SI_{KF}$ : i)  $SI_{KF\_Ip\_Ra}$ , using plasma insulin concentration and  $R_{a\ ogtt}$  as the inputs of KF, ii)  $SI_{KF\_SQJ\_Ra}$ , applying subcutaneous insulin compartment and using  $R_{a\ ogtt}$ , iii)  $SI_{KF\_Ip\_M}$ , using

plasma insulin concentration and applying meal compartment, iv)  $SI_{KF\_SQJ\_M}$ , applying both subcutaneous insulin compartment and meal compartment.

For comparison, three  $SI_{mm}$  were obtained: i)  $SI_{mm\_SQJ\_Ra}$ , ii)  $SI_{mm\_Ip\_M}$ , iii)  $SI_{mm\_SQJ\_M}$ . We computed the correlation of these 7 SIs to  $SI_{Ra}$ .

#### Validation using CGM

Because of missing data, we ended up with 6 test traces with complete CGM as well as other recordings.  $SI_{KF\_SQJ\_M\_CGM}$  was computed applying both subcutaneous insulin compartment and meal compartment and using 5-minute CGM sampling data as the measurement input of KF. For comparison,  $SI_{sp}$  was also computed. We validated  $SI_{KF\_SQJ\_M\_CGM}$  and  $SI_{sp}$  against  $SI_{Ra}$  and  $SI_{mm}$  respectively.

#### **Statistical Analysis**

Data are presented as Mean $\pm$ SE unless otherwise noted. Comparison between implementations was conducted using standard T-tests with a significance level of 5%.

## Results and Discussions

### Validation using YSI

The correlations of  $SI_{KF\_Ip\_Ra}$ ,  $SI_{KF\_SQJ\_Ra}$ ,  $SI_{KF\_Ip\_M}$  and  $SI_{KF\_SQJ\_M}$  to  $SI_{Ra}$  were 0.80 ( $p < 0.01$ ), 0.76 ( $p < 0.01$ ), 0.81 ( $p < 0.01$ ) and 0.80 ( $p < 0.01$ ); the correlations of  $SI_{mm\_SQJ\_Ra}$ ,  $SI_{mm\_Ip\_M}$ , and  $SI_{mm\_SQJ\_M}$  to  $SI_{Ra}$  were 0.77 ( $p < 0.01$ ), 0.84 ( $p < 0.01$ ), and 0.77 ( $p < 0.01$ ). Refer to Figure 11, Figure 12, Figure 13, Figure 14.

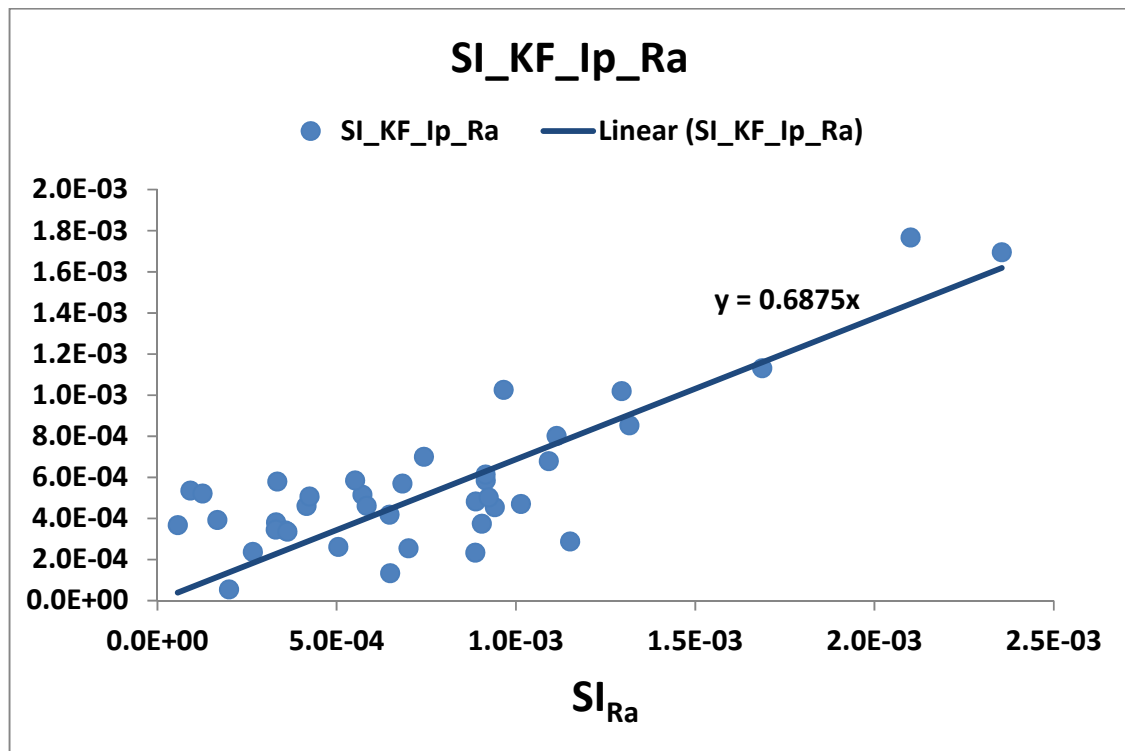


Figure 11:  $SI_{KF\_Ip\_Ra}$  against  $SI_{Ra}$  ( $R=0.80$ ,  $p < 0.01$ ).

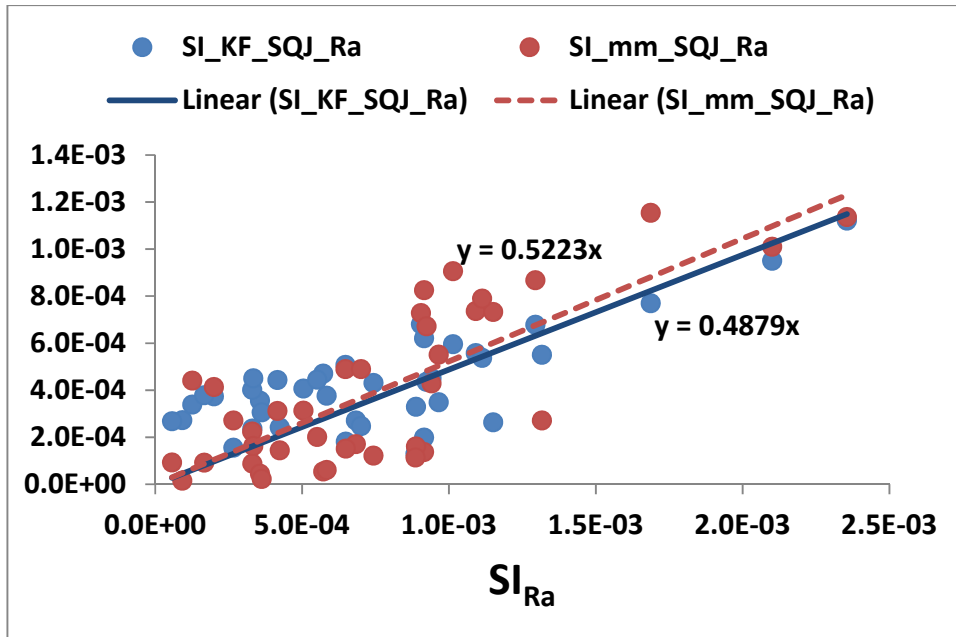


Figure 12:  $SI_{KF\_SQJ\_Ra}$  against  $SI_{Ra}$  ( $R=0.76$ ,  $p<0.01$ ) and  $SI_{mm\_SQJ\_Ra}$  against  $SI_{Ra}$  ( $R=0.77$ ,  $p<0.01$ ).

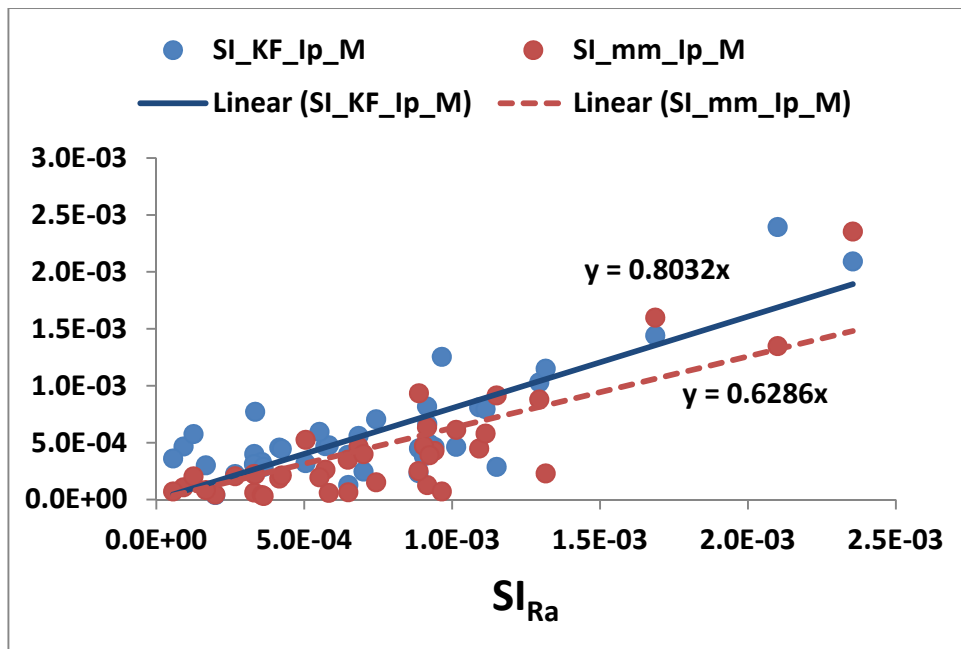


Figure 13:  $SI_{KF\_Ip\_M}$  against  $SI_{Ra}$  ( $R=0.81$ ,  $p<0.01$ ) and  $SI_{mm\_Ip\_M}$  against  $SI_{Ra}$  ( $R=0.84$ ,  $p<0.01$ ).

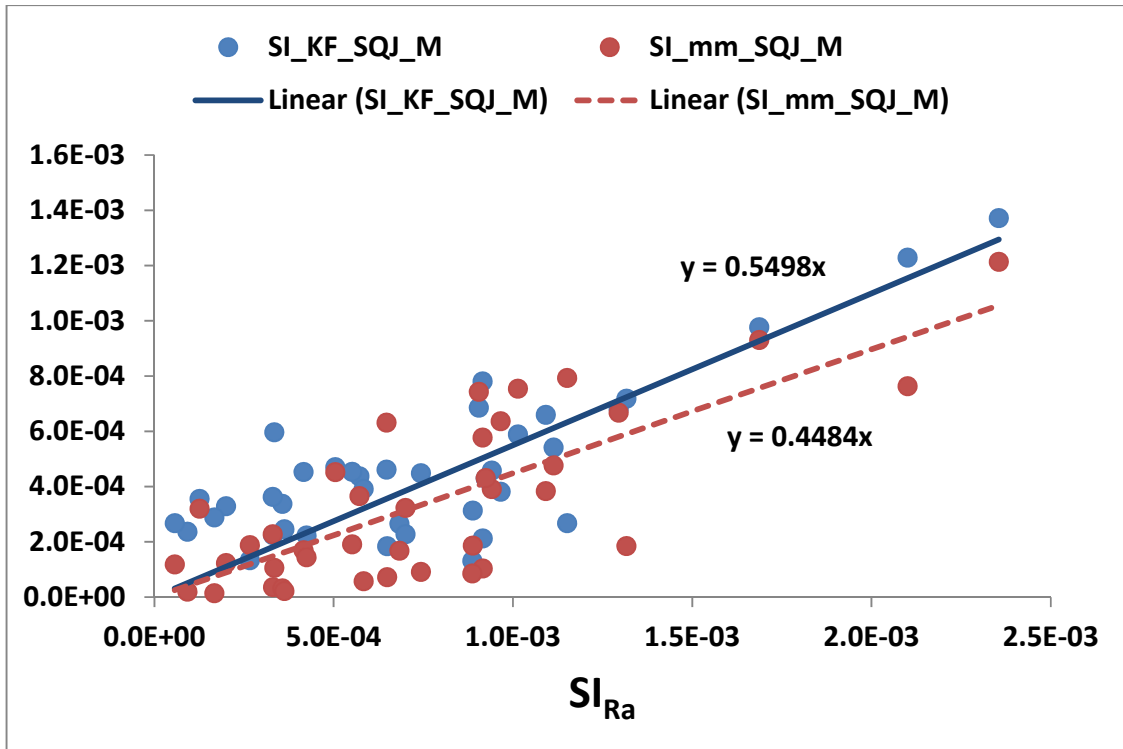


Figure 14:  $SI_{KF\_SQJ\_M}$  against  $SI_{Ra}$  ( $R=0.80$ ,  $p<0.01$ ) and  $SI_{mm\_SQJ\_M}$  against  $SI_{Ra}$  ( $R=0.77$ ,  $p<0.01$ ).

#### Validation using CGM

The correlations of  $SI_{KF\_CGM}$ ,  $SI_{sp\_CGM}$  to  $SI_{Ra}$  were 0.91 ( $p<0.05$ ) and 0.81 ( $p<0.05$ ); The correlations of  $SI_{KF\_CGM}$ ,  $SI_{sp\_CGM}$  to  $SI_{mm}$  were 0.89 ( $p<0.05$ ) and 0.87 ( $p<0.05$ ). The correlation of  $SI_{KF\_CGM}$  and  $SI_{sp\_CGM}$  was 0.84 ( $p<0.05$ ). Refer to Figure 15.

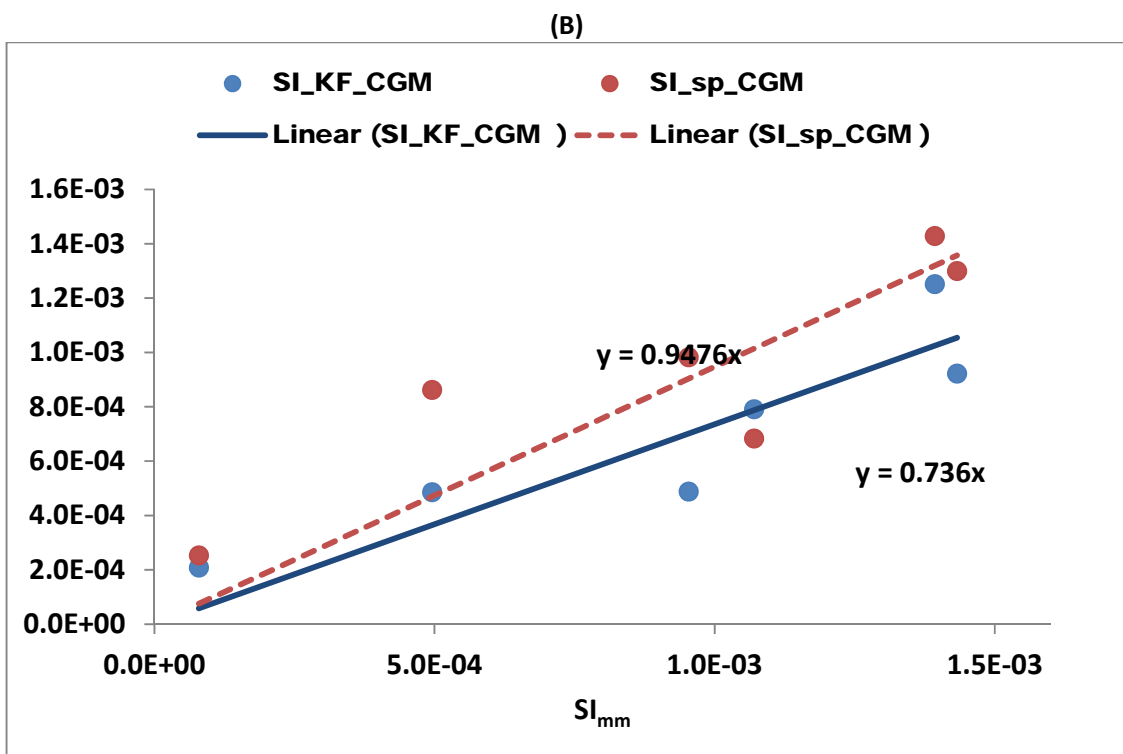
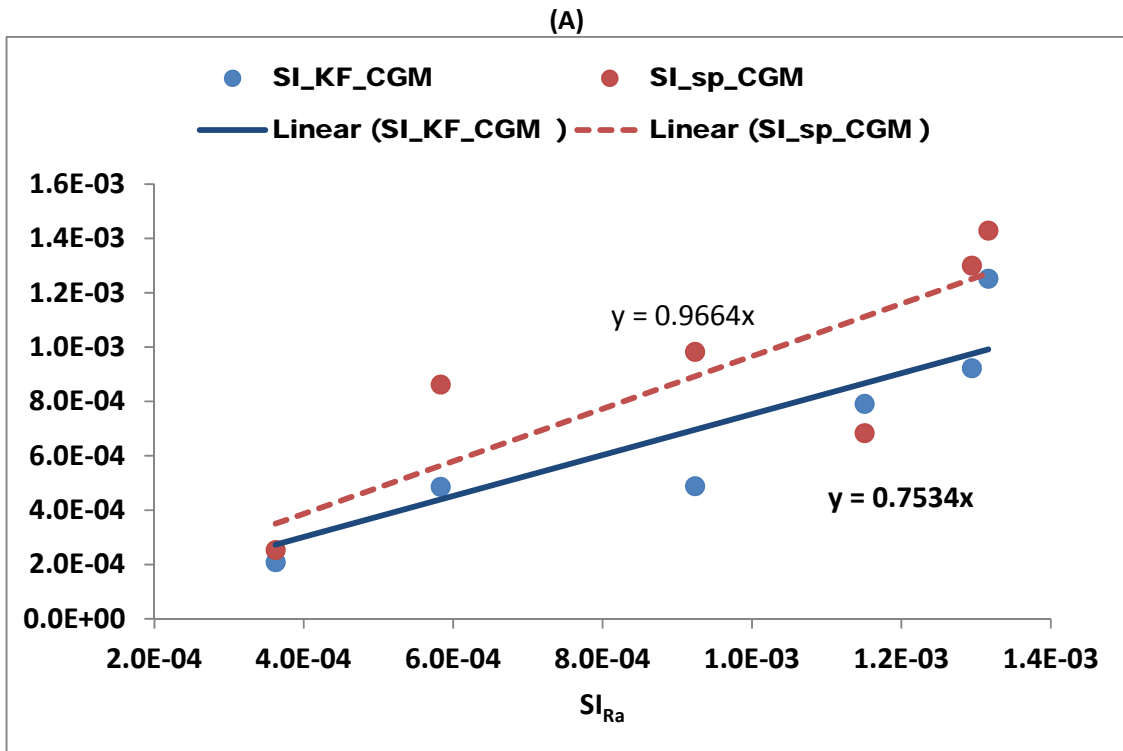


Figure 15: SI validation using CGM: A) SI<sub>KF</sub> and SI<sub>sp</sub> against SI<sub>Ra</sub> (R=0.91, p<0.05 and R=0.81, p<0.05), B) SI<sub>KF</sub> and SI<sub>sp</sub> against SI<sub>mm</sub> (R=0.89, p<0.05 and R=0.87, p<0.05).

The KF's iteration frequency was determined by the sampling rate of CGM (Dexcom SEVEN® PLUS). In order to match the validation process using CGM, the interpolated YSI with 5-minute intervals was taken as the measurement input of the KF. The validation process of KF method using the blood glucose concentration had four components: as shown in Figure 11, validation of the core model residing in KF structure; Figure 12 validated the subcutaneous insulin model; Figure 13 validated the gut model; Figure 14 validated the comprehensive structure. All four of these were well correlated with the counterparts ( $SI_{Ra}$ ) obtained by applying Dalla Man<sup>70</sup>. For comparison, the corresponding  $SI_{mm}$  was computed by applying a similar treatment of  $R_a(k)$  and  $I(k)$ . The correlation of  $SI_{mm}$  with  $SI_{Ra}$  was also satisfactory. On average,  $SI_{mm}$  had smaller values than  $SI_{KF}$  and both  $SI_{mm}$  and  $SI_{KF}$  were lower than  $SI_{Ra}$ , referring to Figure 16. Interestingly, the application of subcutaneous insulin model imposed an impact on  $SI_{KF}$  and  $SI_{mm}$  (Figure 16) such that the magnitudes of both indices were decreased on average. We found that the measurement of plasma insulin concentration in some subjects was underestimated. The model-derived component had greater value, which led to the decreased insulin sensitivity.

The emergence of continuous glucose monitoring has changed blood glucose management for diabetics. It has been proved that CGM can improve glycemic control in T1D adults<sup>79</sup>. The closed loop control of diabetes has been pushing the boundaries of CGM applications<sup>80,81</sup>. In this study, we further took advantage of CGM, proposing a technique that enables quick access to a dynamic physiological parameter, SI. The validation showed a significant correlation of  $SI_{KF}$  with  $SI_{Ra}$  and  $SI_{mm}$  respectively (Figure 15). The  $SI_{sp}$  proposed by Schiavon [4] also correlated well with  $SI_{Ra}$  and  $SI_{mm}$ . On average,  $SI_{sp}$  was 45% higher than  $SI_{KF}$  ( $p < 0.05$ ). It should be pointed out that we did not include the interstitial compartment to account for the time lag from plasma for glucose. The CGM readings were taken as the direct measure of blood glucose

concentration. Research has been intense on the time lag issue<sup>82-84</sup>. A recent study by Basu et al<sup>51</sup> found that the time lag of glucose appearance from the intravascular to the interstitial compartment was less than 10 minutes. It should not be a considerable barrier to our technique. However, considering the limited population size in our analysis, further studies with larger cohort are necessary.

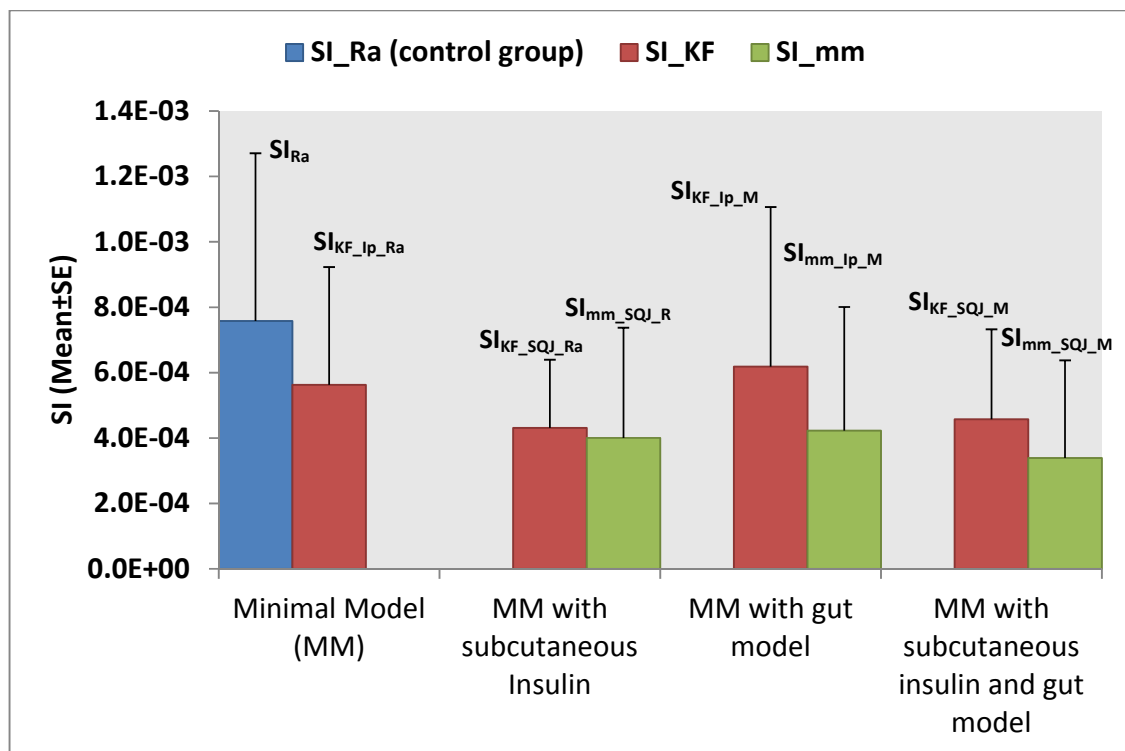


Figure 16: SI (Mean±SE) by Kalman Filter and minimal model methods.

A negative SI implies that increased insulin elevates the blood glucose concentration which should be avoided. The original impetus for introduction of the LOG model was to tackle this issue. It is worth noting that the logarithmic blood glucose actually possesses some preferred properties in constructing the glucose control objective function in risk space instead of the one derived from the seminal work of Kovatchev et al<sup>85</sup>. This application is further described in Patek et al.<sup>81</sup>: the objective function in risk space allows for appropriate balance between hypo

and hyperglycemic risk. A dynamic insulin sensitivity also gives us the opportunity to explore the insulin-glucose dynamic in some special cases, for example, physical exercise. The association of insulin sensitivity with physical exercise has been discussed in many studies<sup>86,87</sup>. McMahon et al found that the glucose requirements were increased in a biphasic manner after a moderate-intensity afternoon exercise for T1D<sup>88</sup>. We are interested in applying our new technique to study the patterns of insulin sensitivity influenced by physical exercise.

Traditional methods of insulin sensitivity quantification usually require frequent and extra blood sampling to measure the plasma insulin and glucose concentration. In this paper, we propose an innovative technique, which enables online SI tracking using CGM and pump data. The validation of KF-generated SI against the minimal-model fitted SI showed a significantly high correlation. We believe this technique can push the boundaries of fast and easy access to SI as an auxiliary to the treatment of Type 1 diabetics in the daily life.

# Chapter 4. Insulin Sensitivity Extraction – Applications

## 4.1 Study of Insulin Sensitivity Variations during Menstrual Cycle for Diabetics

The menstrual cycle plays an essential role in the sexual reproduction. It occurs in the uterus and ovary for the possible fertilization and implantation. The cycle length varies among females. An average number is 28 days<sup>89</sup>. Under the influence of the endocrine system, each cycle can be divided into three main phases: follicular phase, ovulation and luteal phase<sup>90</sup>. In the follicular phase, the amount of estradiol hormone builds up gradually and plummets before the ovulation while the Luteinizing Hormone (LH) surges which triggers the dominant follicle to release an egg. After ovulation, the progesterone concentration starts to increase, preparing the body for the potential implantation. Without implantation occurrence or egg being fertilized, the drop of progesterone and estrogen causes the uterus to shed its lining. This is what we call - the menstruation.

There have been studies on the insulin sensitivity variation during menstrual cycle in T1DM patients. Goldner found that two of the four subjects consistently demonstrated hyperglycemia in the luteal phase<sup>91</sup> and the work by Trout showed that three of the five subjects experienced decline in SI but no statistical significance was found<sup>92</sup> by using frequently sampled intravenous

glucose tolerance test (FSIGT). Pulido and his colleague reported that the mean insulin sensitivity decreased in the luteal phase of 12 healthy regularly menstruating women<sup>93</sup>. More debate on the mechanism of how the associating hormones impose impact to the insulin-glucose metabolism can be found in<sup>94-96</sup>.

The purpose of this study was to analyze the SI in different menstrual cycle phases and to find a potential SI variation pattern. The hypothesis of Launchpad trial was that a subset of premenopausal women with T1DM would experience a decrease in insulin sensitivity during the second half of the menstrual cycle (luteal phase).

### Study Design

12 T1D subjects (Mean±SD: age=33±7 yr, TDI per kg=0.5±0.1 unit/kg, duration of T1D=21.1±8.2 yr, Total Daily Insulin=32.8±7.4 unit, BMI=25.7±2.9 kg/m<sup>2</sup>, HbA1c=6.8%±0.7) completed the study (Launchpad). The inclusion criteria was women 18 years old or older with T1D on an insulin pump with regular cycles (20-40 days) and HbA1c<10%. The study included three consecutive menstrual cycles and the visit days for each cycle were designated in different cycle phases

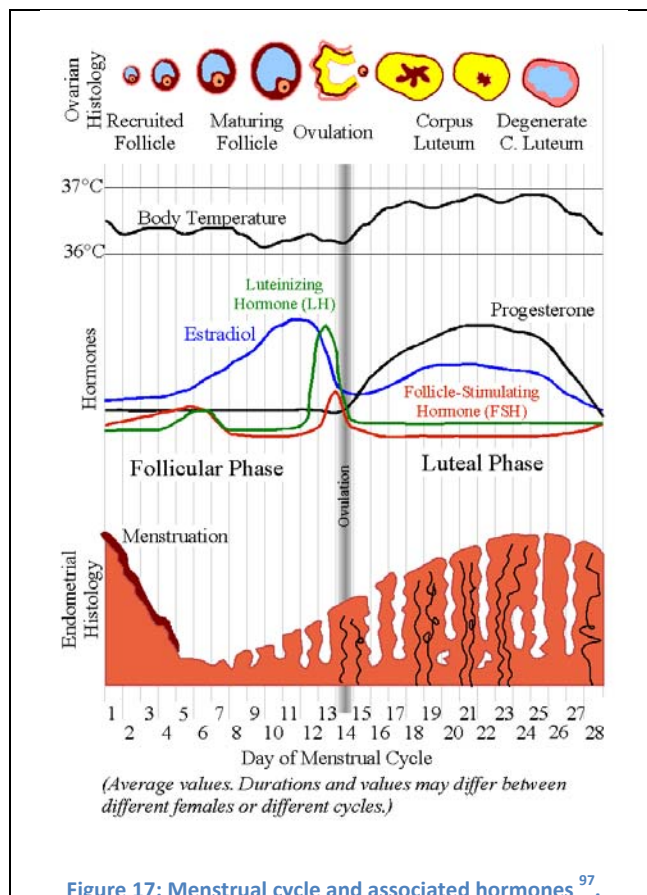


Figure 17: Menstrual cycle and associated hormones<sup>97</sup>.

(Figure 18): subjects paid visit to hospital during early follicular, middle luteal phase and late

luteal phase for the first and the third menstrual cycle; during early and middle follicular phase, ovulation, middle and late luteal phase for the second menstrual cycle. On the visiting days, subjects' sex steroid assays (estradiol, progesterone, LH, follicle-stimulating hormone (FSH), total testosterone and sex-hormone binding globulin (SHBG)) were collected.

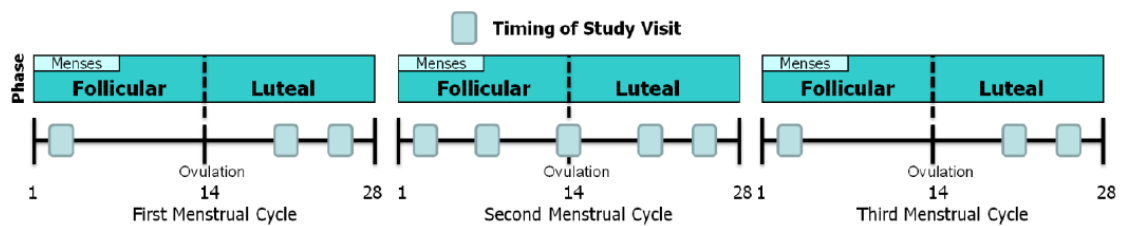


Figure 18: Study spanned three consecutive menstrual cycles with visiting days for each cycle designated.

The determination of the menstrual cycle phase was based on recorded dates of menses, ovulation prediction kits and serum assays of sex steroids. As shown in Figure 18, the start of menses was tagged as day 1 and the cycle ended on day 28. The estrogen peak and the LH spike were captured by validating the ovulation prediction kit. Insulin administration was downloaded from the pump and continuous glucose monitoring values were recorded throughout the three cycles.

## SI Quantifications and Comparison

### SI by KF method ( $SI_{KF}$ )

The technique introduced in section 3.1 d) was applied to inform SI estimation every 5 minutes. The KF was turned on at 10 PM and kept active for 32 hours, which spanned the whole visiting day. The data points of the first 3 hours (10 PM to 1 AM) were excluded from the final analysis for eliminating the potential error brought by the initial condition's impact.

Nocturnal SI was extracted from the obtained SI time series: 1 AM-6 AM and 1AM-6AM the next day (60-360 minutes and 1500-1800 minutes in Figure 19) and the average was taken as the SI value of that day. SI during the day was excluded to avoid the errors introduced by discrepancies of our model matching to meals.

### Subject 22102 on visiting day 8

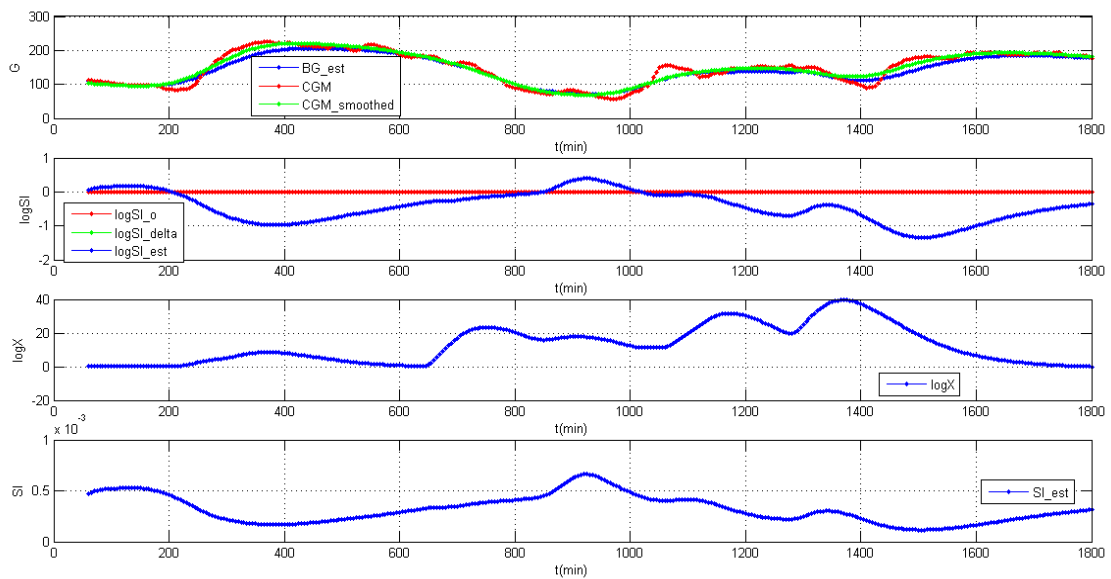


Figure 19: Tracking of G, X and SI from 1 AM to 6 AM the next day (60 to 1800 minutes).

### SI by integral method ( $SI_{sp}$ )

Invented by Schiavon [4], the  $SI_{sp}$  indexing was an integral form of the minimal model (equation 4.1). The inputs included historical insulin administration, meal consumption and CGM values. This index was a proper tool to quantify the insulin sensitivity on patient's visiting days. The explanation of AoC and IOB term can be found in appendix A.



**Insulin sensitivity variations on visiting days (meal recorded)**

**a) Nocturnal SI by KF method**

The standard T-test showed SI was decreased significantly ( $p=0.01$ ) from early follicular to middle late luteal phase ( $4.6\pm 0.5$  vs.  $3.9\pm 0.9$  \* $e-4$ /min per mU/l). Other pair comparisons can be found in Table 4.

**Table 4: Mean and standard error of SI\_KF in different phases and the pair t-Tests**

phases	EarlyFoll	EarlyMidLut	LateLut	MidLateLut
mean $\pm$ sd ( $e-4$ *1/min per mU/l)	4.6 $\pm$ 0.5	4.0 $\pm$ 0.9	4.0 $\pm$ 1.0	3.9 $\pm$ 0.9
t-Test		EarlyFoll vs. EarlyMidLut	EarlyFoll vs. LateLut	EarlyFoll vs. MidLateLut
		P=0.05	P=0.03	P=0.01

**b) SI by integration method**

The standard T-test showed SI was decreased significantly from early follicular to middle late luteal phase ( $28\pm 19$  vs.  $15\pm 6$  \* $e-4$ /min per mU/l,  $p=0.04$ ) and from early follicular to early middle luteal phase ( $28\pm 19$  vs.  $14\pm 7$  \* $e-4$ /min per mU/l,  $p=0.03$ ). The difference between the early follicular phase and the late luteal phase was not significant.

**Table 5: Mean and standard error of SI\_sp in different phases and the pair t-Tests**

phases	EarlyFoll	EarlyMidLut	LateLut	MidLateLut
mean $\pm$ sd ( $e-4$ *1/min per mU/l)	28 $\pm$ 19	14 $\pm$ 7	17 $\pm$ 9	15 $\pm$ 6
t-Test		EarlyFoll vs. EarlyMidLut	EarlyFoll vs. LateLut	EarlyFoll vs. MidLateLut
		P=0.03	P=0.1	P=0.04

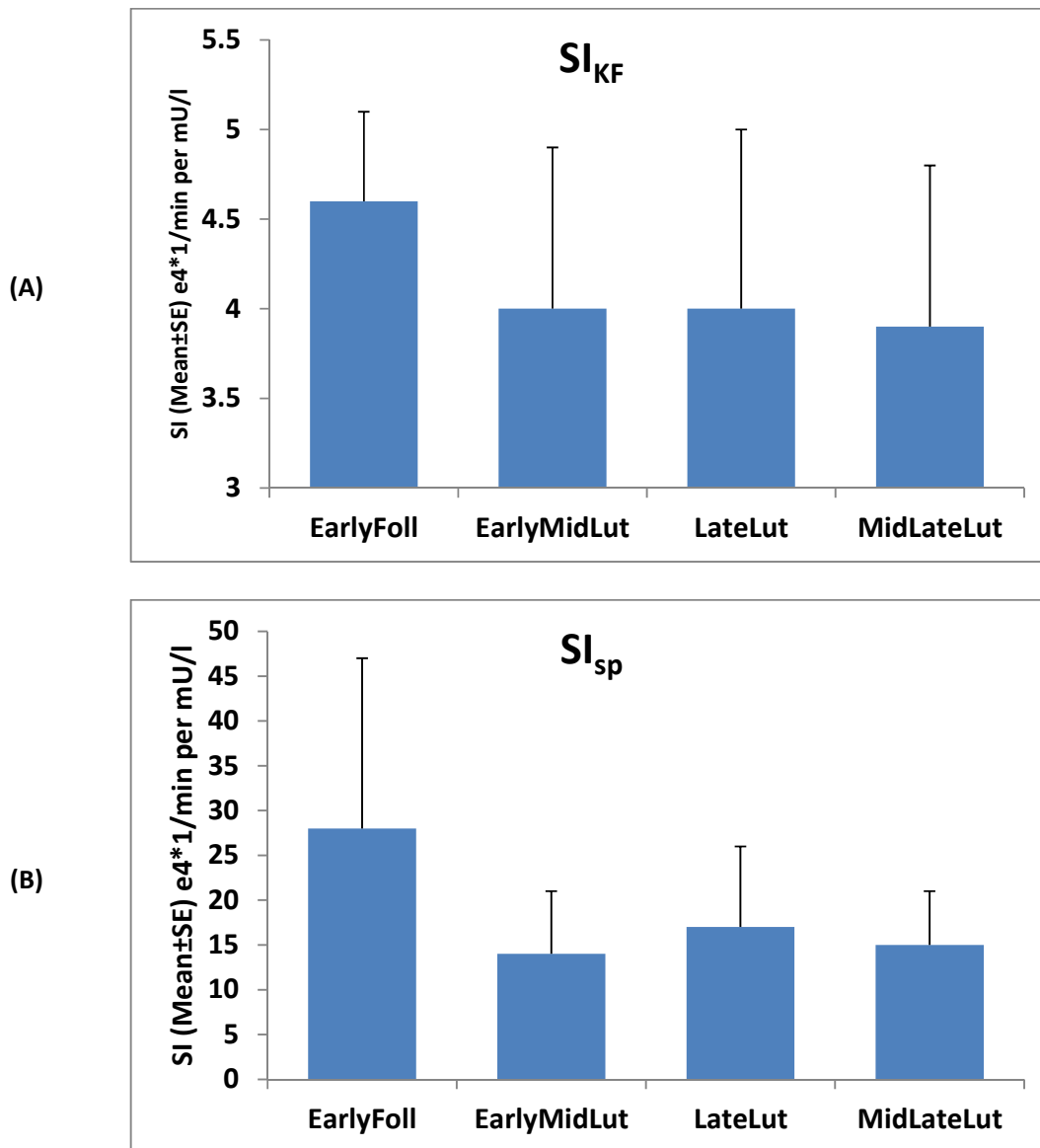


Figure 21:  $SI$  (mean $\pm$ SE) of early follicular phase, early middle luteal phase, late luteal phase and middle late luteal phase: A)  $SI_{KF}$ , B)  $SI_{sp}$ .

### Insulin sensitivity variations across 3 cycles

The historical CGM and insulin data of each day across the three cycles was accessible. For those days without meal recordings,  $SI_{KF}$  served as an appropriate index to quantify the insulin

sensitivity. We ran the KF from 10 PM to 6 AM and considered the mean value of SI estimations as the insulin sensitivity for that day.

**Table 6: Averaged SI before and after ovulation for each subject across 3 cycles**

1 <sup>st</sup> Cycle			2 <sup>nd</sup> Cycle			3 <sup>rd</sup> Cycle		
$SI_{bef\_0}$	$SI_{aft\_0}$	$\Delta(\%)$	$SI_{bef\_0}$	$SI_{aft\_0}$	$\Delta(\%)$	$SI_{bef\_0}$	$SI_{aft\_0}$	$\Delta(\%)$
4.2E-04	3.5E-04	-17.5	3.5E-04	3.4E-04	-3.9	3.9E-04	3.1E-04	-22.8
3.7E-04	3.2E-04	-15.7	3.3E-04	3.2E-04	-2.8	3.6E-04	2.6E-04	-34.8
4.1E-04	4.2E-04	3.0	4.3E-04	4.1E-04	-4.1	3.8E-04	4.0E-04	6.6
3.6E-04	3.4E-04	-5.0	3.5E-04	3.5E-04	-0.5	4.2E-04	3.4E-04	-25.1
4.2E-04	3.6E-04	-17.6	3.7E-04	3.6E-04	-2.3	3.4E-04	3.2E-04	-6.2
3.4E-04	3.7E-04	7.4	3.8E-04	4.7E-04	18.9	4.0E-04	3.6E-04	-12.1
3.1E-04	2.2E-04	-37.7	2.5E-04	3.6E-04	29.6	4.5E-04	4.5E-04	0.0
5.3E-04	4.9E-04	-9.1	4.9E-04	4.7E-04	-3.8	5.0E-04	4.7E-04	-6.2
3.9E-04	3.9E-04	1.4	5.4E-04	5.0E-04	-7.3	4.1E-04	5.2E-04	21.0
4.3E-04	5.3E-04	19.2	5.0E-04	4.9E-04	-0.2	4.9E-04	4.5E-04	-7.8
5.0E-04	4.9E-04	-1.3	4.0E-04	4.6E-04	12.2	4.4E-04	4.7E-04	7.6
5.5E-04	4.1E-04	-35.2	3.8E-04	3.6E-04	-5.3	3.7E-04	3.7E-04	-1.5

The analysis generated 12 (subjects) by 3 (cycles) SI traces. For each trace, we computed the average SI before (follicular) and after (luteal) the ovulation. Table 6 lists the SI of across 3 cycles: 26 out of 36 traces experienced decreased SI, 13 traces had absolute differences within 5% among which 11 underwent decreased SI, 15 traces and 8 traces had decreased SI and increased SI greater than 5% respectively. Figure 22 shows the histogram of SI changes before and after ovulation and Figure 23 plots the three groups of SI.

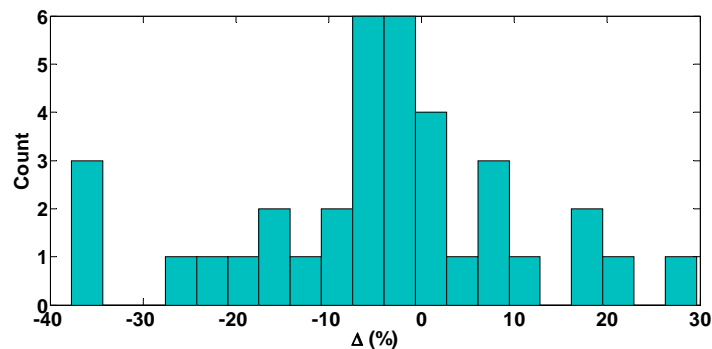


**Figure 22: Histogram of SI changes before and after ovulation.**

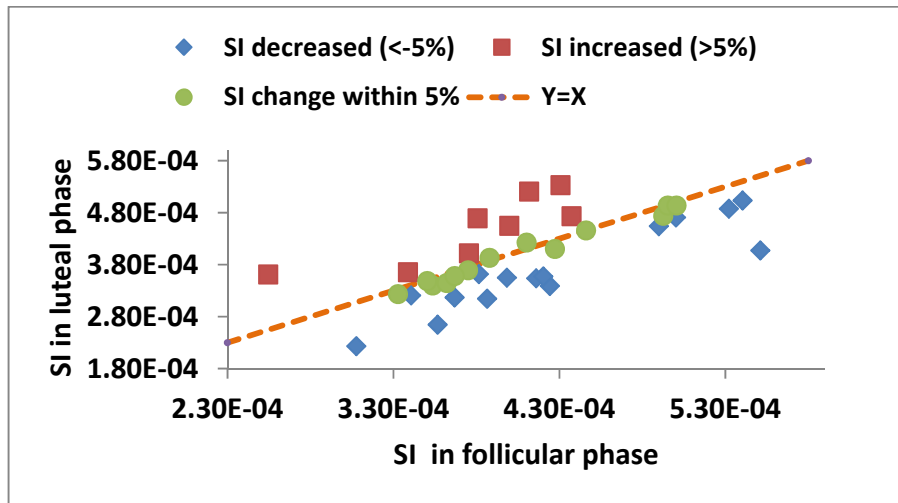


Figure 23: SI in luteal phase against SI in follicular phase.

We also computed the phase-average SI across 3 cycles for each subject (refer to Figure 24). And the average SI variations across cycle for each group was obtained (refer to Figure 25).

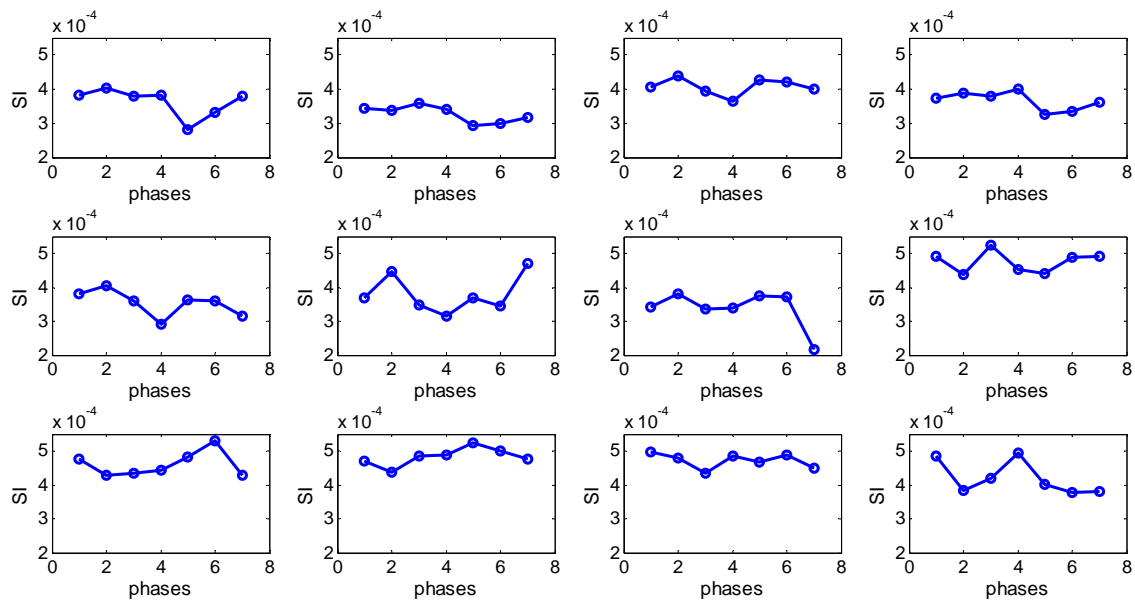


Figure 24: Cycle-averaged SI for each subject. Phase 1 to 7 corresponds to early follicular 3, early follicular 5, middle late follicular, ovulation, early luteal, middle luteal and late luteal respectively.

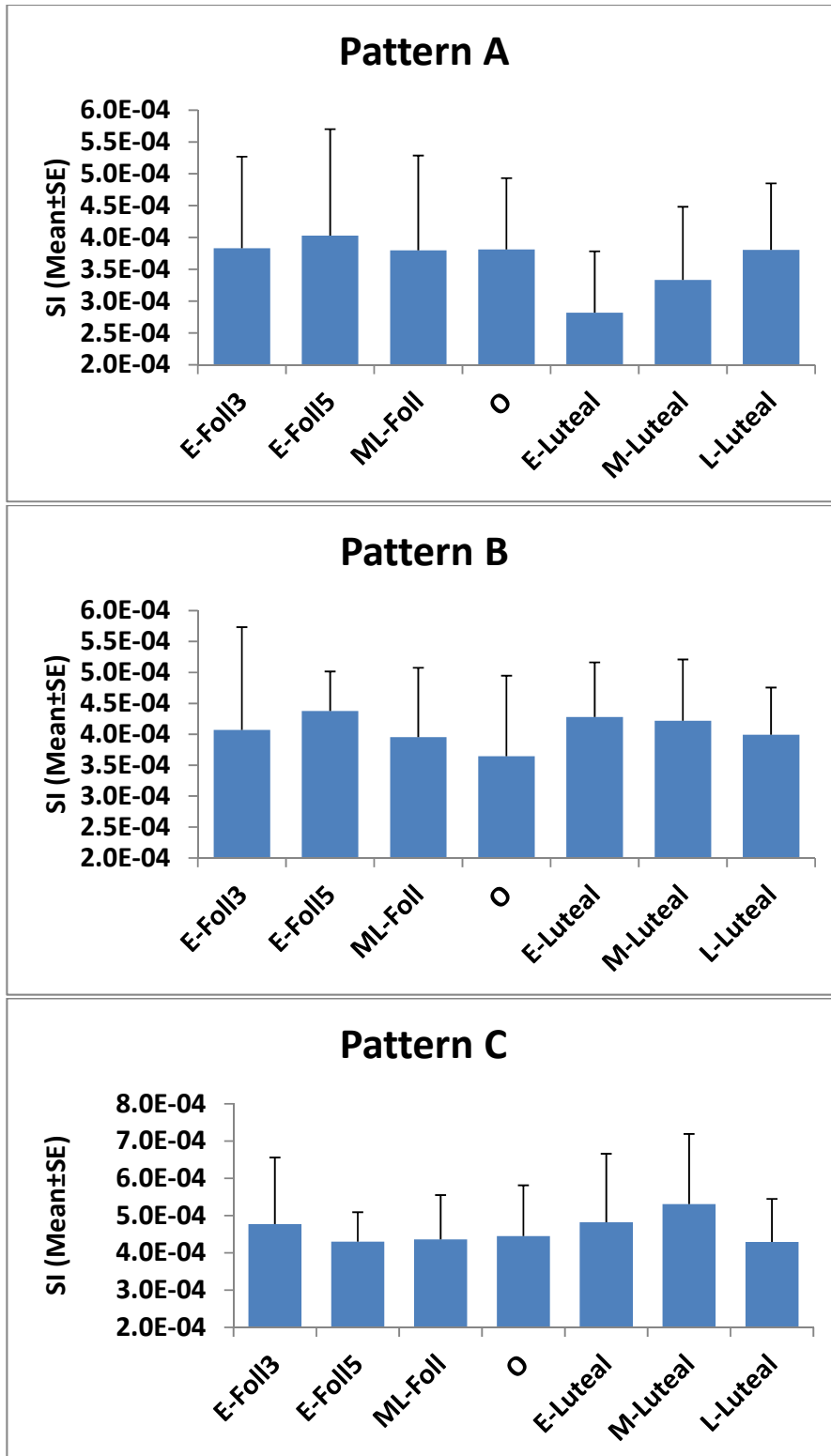


Figure 25: The three patterns of SI variations: A) 15 out of 36 cycles experienced decreased SI in luteal phase, B) 13 out of 36 cycles experienced unchanged SI, C) 8 out of 36 cycles experienced increased SI.

We substantiated the hypothesis that a subset of premenopausal women with T1DM would experience a decrease in insulin sensitivity during the second half of the menstrual cycle (luteal phase).

Our ultimate goal is to develop an advisory system aimed at improving the diabetes control in younger women experiencing BG variation related to menstrual cycle. The future work includes: 1) develop detection algorithms to inform the patients of abnormal BG fluctuations related to menstrual cycle, 2) train a model to project the BG based on the historical data and the menstrual cycle parameters (date of menses, average length of cycle and timing of ovulation), 3) design a user-friendly interface for patients to better interact with the device.

## **4.2 Insulin Sensitivity and Physical Exercise**

The association between physical activity and insulin resistance has been vigorously investigated for many years. It is confirmed that trained subjects have more insulin resistance than untrained subjects<sup>98,99</sup>. Devlin et al. reported that a bout of physical exercise improved the insulin sensitivity<sup>100</sup>. The mechanism behind this has been discussed in<sup>86,87</sup>. In 2006, McMahon et al. found an biphasic glucose requirement to maintain euglycemia following moderate intensity in adolescents with T1D<sup>88</sup>. The impact of exercise intensity to the postprandial insulin sensitivity remains unclear to the society.

### **Hypothesis**

In prediabetic adults, acute exercise has an effect on improving postprandial glycaemia and insulin sensitivity.

## Data

18 subjects (age  $49 \pm 14$ ; weight  $94.6 \pm 21$  kg; HbA1c  $5.7 \pm 0.4$  %; fasting BG  $105 \pm 11$  mg/dl; 2h glucose  $170 \pm 32$  mg/dl) completed the clinical study designed to investigate the impact of exercise intensity to the postprandial insulin sensitivity in prediabetes. Two levels of exercise were assigned: moderate-intensity exercise (MIE) and high-intensity exercise (HIE) distinguished by the peak  $O_2$  consumption and lactate threshold (LT). MIE was characterized at LT and HIE was 75% difference between LT and peak  $O_2$  consumption. As shown in Figure 26, after 30 minutes from the initialization, the subject completed a 60-minute exercise (MIE or HIE). A 3-h OGTT (75 gram) test was followed post the 60-minute recovery time period. For the control group, the subject was seated for 60 minutes instead of any exercise. Blood was sampled frequently to measure the blood glucose value (YSI 2700), plasma insulin concentration and C-peptide level.

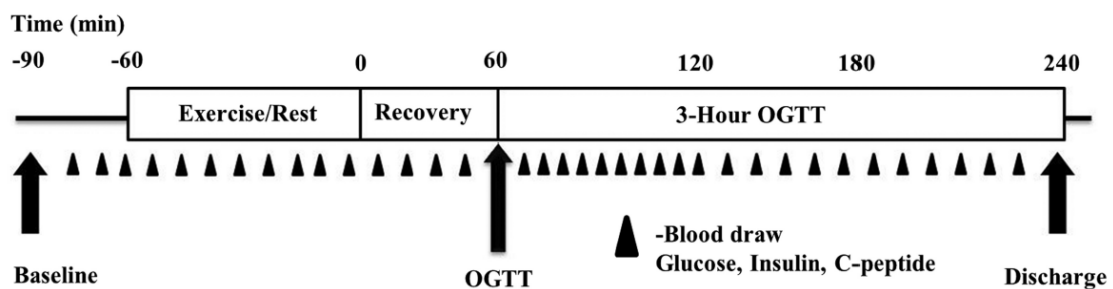


Figure 26: Timeline of the study: 1-h recovery session taken after 1-h physical exercise with a 3h-OGTT test followed<sup>101</sup>.

## Method

In 2005, Dalla Man<sup>70</sup> reported the validation process of an oral glucose minimal model based insulin sensitivity ( $SI$ ) against clamp ( $SI^{clamp}$ ). The results showed that the correlation of  $SI$  and  $SI^{clamp}$  was satisfactory ( $r=0.81$ ,  $p<0.001$ ). We decided to apply this validated index to extract  $SI$  from our clinical data. In this model,  $R_{\alpha_{ogtt}}$  was defined as a piece-wise linear

function and the insulin sensitivity as well as blood glucose appearance  $R_{a\ ogtt}$  was derived by matching the oral glucose minimal model to the collected BG and insulin data. The parameter set to be estimated was  $[p_2, p_3, \alpha]$ .

$$\dot{G}(t) = -[S_G + X(t)] \cdot G(t) + S_G \cdot G_b + \frac{R_{a\ ogtt}(\alpha, t)}{V}, \quad G(0) = G_b \quad (4.2)$$

$$\dot{X}(t) = -p_2 \cdot X(t) + p_3 \cdot [I(t) - I_b], \quad X(0) = 0 \quad (4.3)$$

$$R_{a\ ogtt}(\alpha, t) = \begin{cases} \alpha_{i-1} + \frac{\alpha_i - \alpha_{i-1}}{t_i - t_{i-1}}(t - t_{i-1}), & \text{per } t_{i-1} \leq t \leq t_i \quad i = 1 \dots 7 \\ 0, & \text{Otherwise} \end{cases} \quad (4.4)$$

$$SI = \frac{p_3}{p_2} \cdot V \quad (4.5)$$

$p_2$  was the rate describing the dynamic of insulin action,  $p_3$  was the parameter governing the magnitude of insulin action,  $G$  was plasma glucose concentration,  $X$  was the insulin action,  $S_G$  represented the glucose effectiveness that measured the glucose disposal,  $G_b$  and  $I_b$  were set to the values at the beginning of the tolerance test ( $t=0$ ).

## Results and Discussion

Figure 28 shows an example of the BG fitting. Across the cohort, SI was improved by 47% on the MIE ( $1.55 \pm 1.00$  vs.  $2.30 \pm 1.71$   $e4^*1/\text{min per mU/l}$ ,  $p < 0.05$ ) and 61% HIE ( $1.55 \pm 1.00$  vs.  $2.51 \pm 1.37$   $e4^*1/\text{min per mU/l}$ ,  $p < 0.05$ ) compared to the control group, respectively (Figure 27).

The results substantiated the hypothesis that after moderate intensity exercise and high intensity exercise, whole-body insulin sensitivity derived by the oral minimal model was improved. Acute physical exercise has been advocated for its effect on improving insulin action.

The timing of exercise and meal also plays a role here in affecting the post-prandial glycaemia. Consuming meals near the end of exercise was shown to inflect the insulin action

whereas in the 30 minutes to 3 hours' time scale, studies have shown contradicting results<sup>102,103</sup>.

This work was focused on the post-prandial BG variations shortly (1 hour) after the physical exercise. It should be pointed out that acute physical exercise also has a prolonged impact to the insulin sensitivity. OGTT is a pragmatic tool for measuring insulin sensitivity in the early phase of exercise effect; however,  $SI_{KF}$  is considered a more appropriate tool for measuring SI in both early and late phase of exercise effect. One of our future works is to extract SI from clinical data involving physical activity and identify patterns that can be exploited to help in improving glycemic control.

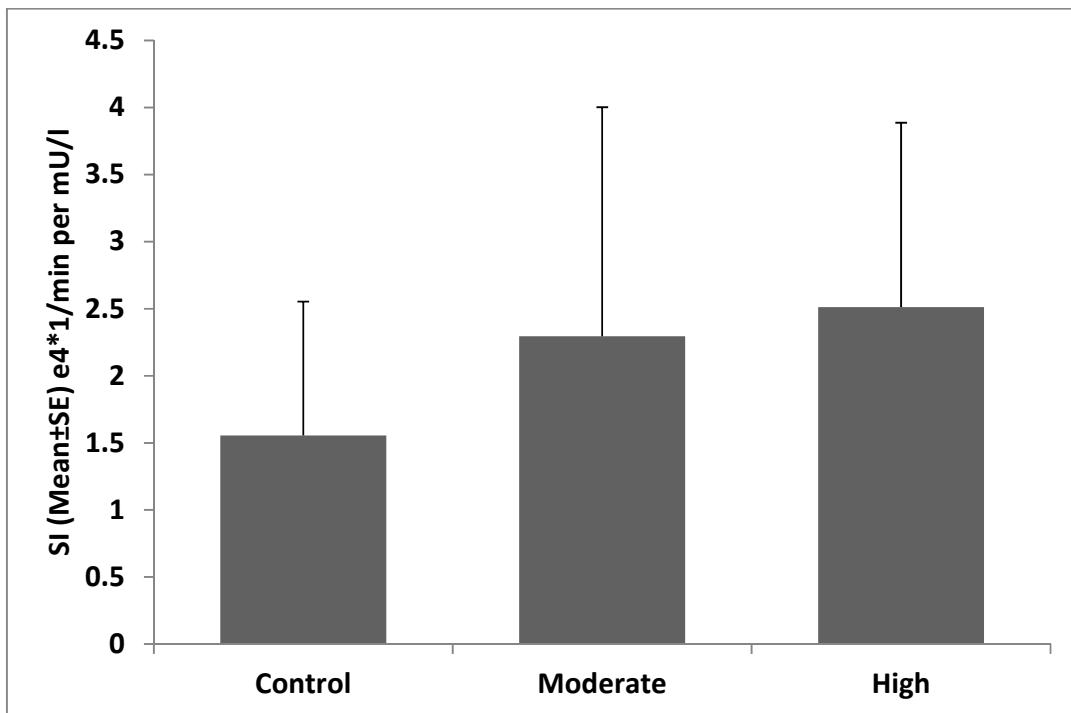


Figure 27: SI (Mean±SE) derived by minimal model in Control, MIE and HIE.

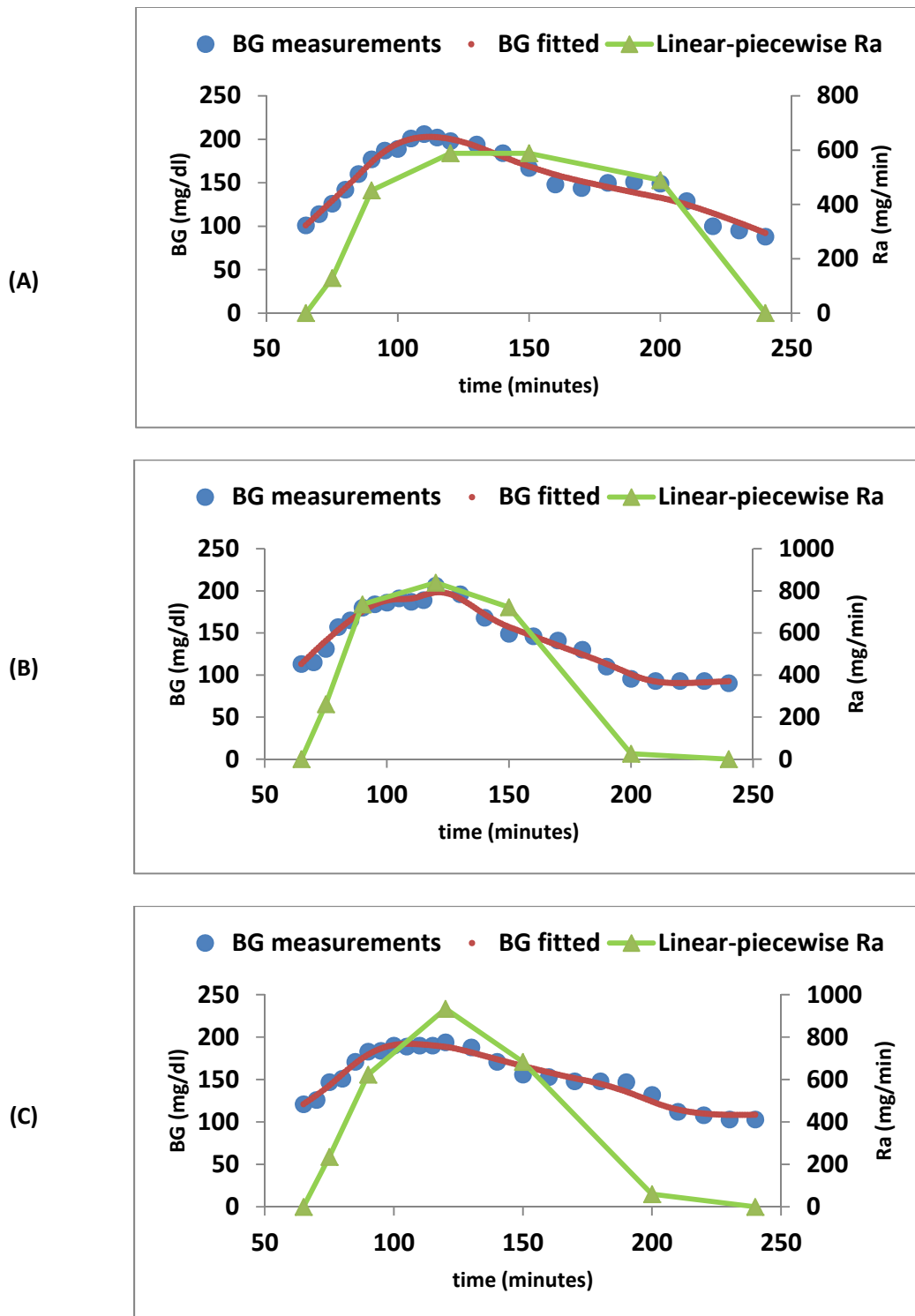


Figure 28: BG fitting by OGTT model of subject008: A) control group, B) MIE and C) HIE.

# Chapter 5. Enhancing Model-Based Short Term Glycemic Prediction in T1DM Using Tracking of Dynamic Parameter Uncertainties

While the kinetics of insulin to reach the bloodstream vary with each formulation, it is generally accepted that modern rapid-acting insulins reach the bloodstream in approximately 15 minutes, peak at around 30 to 90 minutes and linger for 3 to 5 hours. As a consequence, dosing decisions must be taken not only on the current glucose concentration, but accounting for what glucose levels will be when insulin is truly active. Such forecasting of glucose levels has been made possible by the appearance in the early 2000s of Continuous Glucose Monitors (CGM) which provide frequent BG measurements, compared to Self-Monitoring of Blood Glucose (SMBG, on average 3-4 per day). In this manuscript, we focus on improving the performance of short term glucose prediction. (Of note, “prediction” will be used interchangeably with “forecasting” in the remainder of chapter.)

Most published BG prediction methods utilize CGM-based time-series techniques. Cameron et al. showed that a multiple statistical linear prediction algorithm rendered a mean lead prediction time of 23 minutes without missed hypoglycemic bouts<sup>104</sup>. Sparacino et al. reported that BG could be predicted 30 minutes in advance by using either a first-order polynomial or an autoregressive (AR) model<sup>105</sup>. Neural network methods have been used to

predict BG for longer time horizons (50 to 180 minutes) and also for the short terms (15 to 45 minutes) <sup>106,107</sup>. Those methods rely heavily on the accuracy of CGM measurements although they do not need any historical knowledge on meal, insulin on board, exercise, etc. In contrast, methods using physiological models often use these additional inputs to palliate erroneous sensors and provide intrinsic interpretation of BG variation rate as well as the direction of change. Buckingham et al. and Kuure-Kinsey et al. discussed the application of Kalman filter (KF) technique to CGM denoising <sup>56,108</sup> whereas Palerm et al. discussed the trade-off between the missed hypoglycemic incidences and the false alarm rate influenced by the parameter tuning of the optimal estimator <sup>109</sup>. Finally, Hughes et al. developed a model based 30-minute glucose prediction as the core of an insulin attenuation technique which reduced the upcoming hypoglycemia events significantly <sup>110</sup>.

Intra-individual and inter-individual variability in insulin-glucose dynamics has long been identified as a critical challenge in physiological modeling <sup>111-113</sup>, and is one of the causes cited for degraded prediction performances. In this chapter, we propose to explore the use of physiologically based model in conjunction with Kalman Filtering (KF) to track one of the key variable parameters, insulin sensitivity (SI), which corresponds coarsely to the gain of the insulin/glucose system. We hope to demonstrate that BG prediction performance then can be bolstered by adding SI tracking into the prediction process.

For that purpose we study the short-term (up to 45 minutes) BG prediction performance of such systems and explore different implementations (full model, feed-forward, with and without SI tracking) to better understand the impact of these design choices on glucose prediction.

## 5.1 Structural Design and SI Tracking

The structure of KF is determined by the embedded physiological model. We use in this chapter two models: the SOGMM model<sup>110</sup> derived from the seminal minimal model of glucose kinetic<sup>42</sup> and extended by adding subcutaneous insulin compartment and gut/intestinal compartment, and the “LOG” model, a newly designed mathematical description of glucose homeostasis in logarithm space ( $\log(\frac{G}{G_b})$ ), influenced by the nonlinear structure of the MMGK<sup>114</sup>. Refer to Table 7 for the equations and parameters.

For each model, we optionally add a first order SI dynamic. The feature of the dynamic is to drive SI state to the equilibrium value,  $SI_b$ , in a limited time (characteristic time = 60 minutes). By integration into the KF, we are capable of tracking SI online. One advantage of LOG model over SOGMM in terms of SI tracking is that the logarithm form of SI guarantees that the SI estimation is positive.

SOGMM is linearized around the operating point which is obtained by solving the continuous model in equilibrium state:

$$[G_{op}, X_{op}, Ip_{op}, Isc1_{op}, Isc2_{op}, Q1_{op}, Q2_{op}, SI_{op}, J_{op}, M_{op}] = [112.5, 8.4e - 3, 257.7, 3.2e + 3, 3.2e + 3, 0, 0, 4.5e - 3, J_{basal}, 0]$$

Both models are discretized with 5 minute time interval to pertain to the CGM measurement.  $SI_b$  is set to  $4.46e-4$  (1/min per mU/l) , the population averaged insulin sensitivity value<sup>115</sup>, and  $G_b$  is equal to 112.5 mg/dl.  $X_b$  corresponds to the subjects basal rate.

Table 7: SOGMM and LOG model discretized in 5 minute interval. The states and inputs of SOGMM are deviations from the operating point

<b>SOGMM</b>			
<b>Feed-Forward</b>	<b>Meal Model</b>	$\begin{bmatrix} Q_1(k+1) \\ Q_2(k+1) \end{bmatrix} = \begin{bmatrix} 0.6270 & 0 \\ 0.3617 & 0.9445 \end{bmatrix} \begin{bmatrix} Q_1(k) \\ Q_2(k) \end{bmatrix} + \begin{bmatrix} 3.9953 \\ 0.9851 \end{bmatrix} M(k)$	(5.1)
	<b>Insulin Model</b>	$\begin{bmatrix} I_{sc1}(k+1) \\ I_{sc2}(k+1) \\ I_p(k+1) \end{bmatrix} = \begin{bmatrix} 0.9029 & 0 & 0 \\ 0.0922 & 0.9029 & 0 \\ 0.0033 & 0.0544 & 0.2811 \end{bmatrix} \begin{bmatrix} I_{sc1}(k) \\ I_{sc2}(k) \\ I_p(k) \end{bmatrix} + \begin{bmatrix} 4.7531 \\ 0.2387 \\ 0.0062 \end{bmatrix} J(k)$	(5.2)
<b>Core Model</b>	$\begin{bmatrix} G(k+1) \\ X(k+1) \end{bmatrix} = \begin{bmatrix} 0.8753 & -381.2051 \\ 0 & 0.5123 \end{bmatrix} \begin{bmatrix} G(k) \\ X(k) \end{bmatrix} + \begin{bmatrix} \frac{0.0190}{BW} & -0.6667 \\ 0 & \frac{0.0022}{BW} \end{bmatrix} \begin{bmatrix} Q_2(k) \\ I_p(k) \end{bmatrix}$		(5.3)
<b>SI</b>	$SI(k+1) = 0.9200 \cdot SI(k) + 0.0800 \cdot SI_b$		(5.4)
<b>LOG</b>			
<b>Feed-Forward</b>	<b>Meal Model</b>	$\begin{bmatrix} Q_1(k+1) \\ Q_2(k+1) \end{bmatrix} = \begin{bmatrix} 0.9048 & 0 \\ 0.0452 & 0.9048 \end{bmatrix} \begin{bmatrix} Q_1(k) \\ Q_2(k) \end{bmatrix} + \begin{bmatrix} 4.7581 \\ 0.1170 \end{bmatrix} M(k)$	(5.5)
	<b>Insulin Model</b>	$\begin{bmatrix} I_{sc1}(k+1) \\ I_{sc2}(k+1) \\ I_p(k+1) \end{bmatrix} = \begin{bmatrix} 0.9029 & 0 & 0 \\ 0.0922 & 0.9029 & 0 \\ 0.0033 & 0.0544 & 0.2811 \end{bmatrix} \begin{bmatrix} I_{sc1}(k) \\ I_{sc2}(k) \\ I_p(k) \end{bmatrix} + \begin{bmatrix} 4.7531 \\ 0.2387 \\ 0.0062 \end{bmatrix} J(k)$	(5.7)
<b>Core Model</b>	$\begin{bmatrix} \ln\left(\frac{G(k+1)}{G_b}\right) \\ \ln\left(\frac{X(k+1)}{X_b}\right) \end{bmatrix} = \begin{bmatrix} 0.9662 & -0.0023 \\ 0 & 0.9253 \end{bmatrix} \begin{bmatrix} \ln\left(\frac{G(k)}{G_b}\right) \\ \ln\left(\frac{X(k)}{X_b}\right) \end{bmatrix} + \begin{bmatrix} -0.1113 & \frac{0.0001}{BW} & -0.0015 \\ 0 & 0 & \frac{1.2440}{BW} \end{bmatrix} \begin{bmatrix} \ln\left(\frac{SI(k)}{SI_b}\right) \\ R_a(k) \\ I_p(k) \end{bmatrix}$		(5.8)
<b>SI</b>	$\ln\left(\frac{SI(k+1)}{SI_b}\right) = 0.9200 \cdot \ln\left(\frac{SI(k)}{SI_b}\right)$		(5.9)

## Model Implementations

The most straightforward way of implementing our KF based prediction plant is to integrate all equations into the KF and take CGM, pump data and meal as the inputs. “SOGMM-Full model” and “LOG-Full model” implementations adopt this strategy. Alternative implementations “SOGMM-Core model+ $\Delta$ ” and “LOG-Core model+ $\Delta$ ”, inspired by the idea of “feed-forward modules” described by Grossman <sup>78</sup>, separate insulin and meal transport compartments from the KF core model as feed-forward compartments leaving only blood glucose  $G$  (or  $\ln(\frac{G}{G_b})$ ) and remote insulin  $X$  (or  $\ln(\frac{X}{X_b})$ ) compartments embedded in the main filter. In this case, computed plasma insulin concentration and glucose rate of appearance as well as CGM (or  $\ln(\frac{CGM}{G_b})$ ) are taken as the inputs into the KF. In these implementations, we introduce the  $\Delta$  term:  $\Delta = \hat{X} - X$  (or  $\ln(\frac{\hat{X}}{X_b}) - \ln(\frac{X}{X_b})$ ). By appropriate process noise setting of  $X$  (or  $\ln(\frac{X}{X_b})$ ) in KF, the model discrepancy could be extracted and embedded in  $\Delta$  through  $\hat{X}$  (or  $\ln(\frac{\hat{X}}{X_b})$ ).  $\Delta$  is then associated with a 1000 min characteristic time in the prediction, so as to ensure a quasi constant value across the prediction horizon, i.e. model discrepancies are stable across the prediction horizon. Finally, by adding SI dynamic equations, two more implementations “SOGMM-Core model with SI” and “LOG-Core model with SI” are obtained. The role of SI is similar to  $\Delta$ . (Refer to Figure 29)

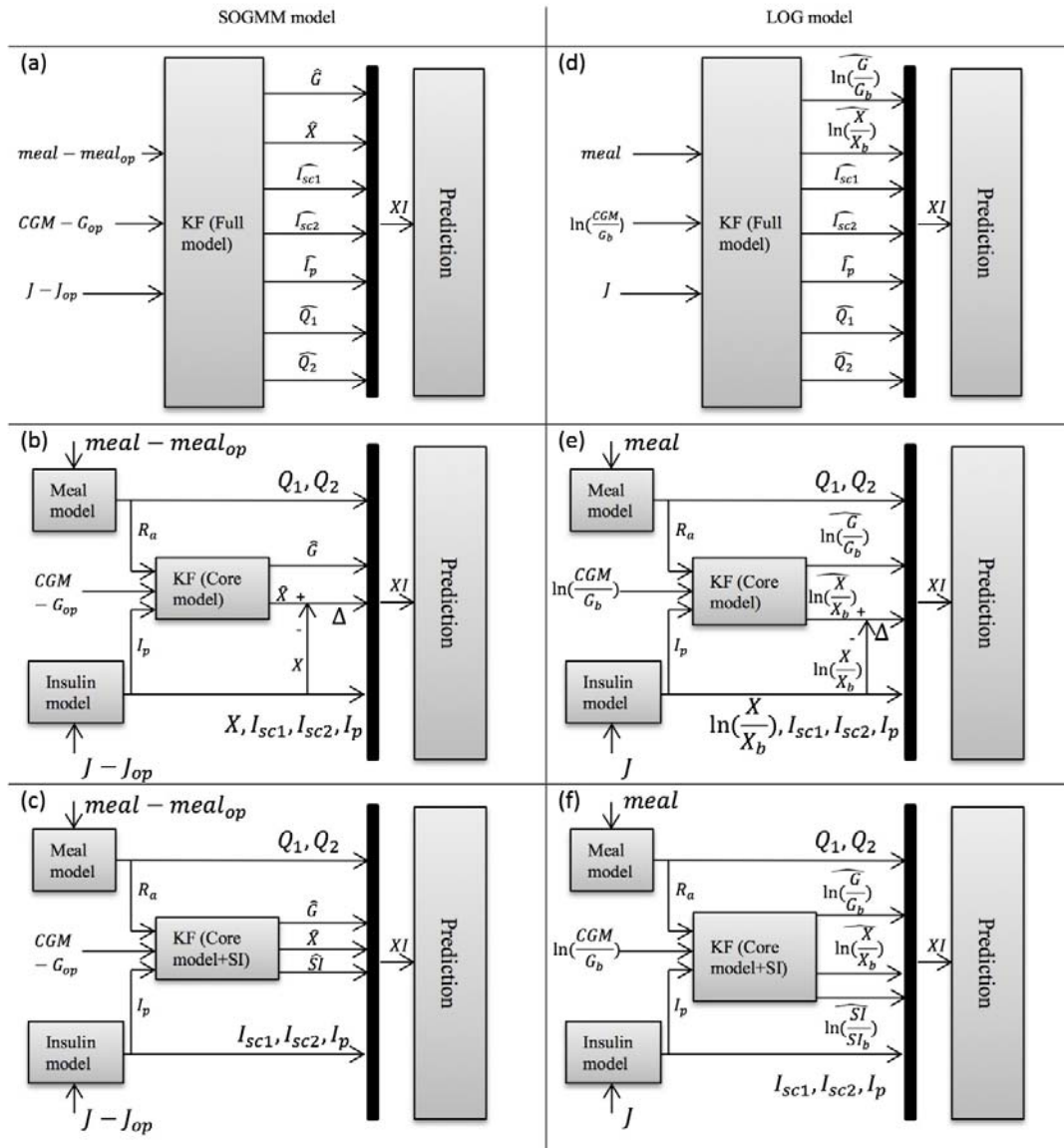


Figure 29: 3x2 model implementations: i) SOGMM-Full model, ii) SOGMM-Core+ $\Delta$ , iii) SOGMM-Core model with SI, iv) LOG-Full model, v) LOG-Core model+ $\Delta$ , vi) LOG-Core model with SI and structures of prediction vector XI.

Table 8: Prediction vector XI of each implementation

XI	SOMM model	LOG model
Full model	$[\hat{G} \quad \hat{X} \quad \hat{I}_{sc1} \quad \hat{I}_{sc2} \quad \hat{I}_p \quad \hat{Q}_1 \quad \hat{Q}_2]$	$[\ln(\frac{\hat{G}}{G_b}) \quad \ln(\frac{\hat{X}}{X_b}) \quad \hat{I}_{sc1} \quad \hat{I}_{sc2} \quad \hat{I}_p \quad \hat{Q}_1 \quad \hat{Q}_2]$
Core model + $\Delta$	$[\hat{G} \quad X + \Delta \quad I_{sc1} \quad I_{sc2} \quad I_p \quad Q_1 \quad Q_2]$	$[\ln(\frac{\hat{G}}{G_b}) \quad \ln(\frac{X}{X_b}) + \Delta \quad I_{sc1} \quad I_{sc2} \quad I_p \quad Q_1 \quad Q_2]$
Core model With SI	$[\hat{G} \quad \hat{X} \quad I_{sc1} \quad I_{sc2} \quad I_p \quad Q_1 \quad Q_2 \quad \hat{SI}]$	$[\ln(\frac{\hat{G}}{G_b}) \quad \ln(\frac{\hat{X}}{X_b}) \quad I_{sc1} \quad I_{sc2} \quad I_p \quad Q_1 \quad Q_2 \quad \ln(\frac{\hat{SI}}{SI_b})]$

## Kalman Filter Setting

The model embedded in KF is linearized as 5 minute discrete equations in state-space:

$$x[n + 1] = Ax[n] + Bu[n] + Gw[n] \quad (5.10)$$

$$y[n] = Cx[n] + Du[n] + Hw[n] + v[n] \quad (5.11)$$

in which  $w[n]$  and  $v[n]$  stand for processing noise and measurement noise respectively. The tuning factors are defined as noise covariance as:  $E(w[n]w[n]^T) = Q$ ,  $E(v[n]v[n]^T) = R$ ,  $E(w[n]v[n]^T) = N$ .

By solving the discrete Riccati equation, we obtain the gain  $= (APC^T + \bar{N})(CPC^T + \bar{R})^{-1}$ , where

$$\bar{R} = R + HN + N^T H^T + HQH^T \quad (5.12)$$

$$\bar{N} = G(QH^T + N) \quad (5.13)$$

Refer to Stengel for more fundamentals about the KF <sup>116</sup>. For the “SOGMM-Full model” implementation, process noise is added to  $I_{sc1}, Q_1, Q_2$ . This is in line with the setting that Hughes deployed in her publication <sup>110</sup>, while for “LOG-Full model” implementation the process noise is involved with  $\ln(\frac{G}{G_b})$  and  $\ln(\frac{X}{X_b})$  since we found that the setting from <sup>110</sup> would generate a substantial prediction error. For “Core+ $\Delta$ ” implementations, process noise is added to G and X (or  $\ln(\frac{G}{G_b})$  and  $\ln(\frac{X}{X_b})$ ) and for “Core with SI” implementations, process noise is added to G and SI (or  $\ln(\frac{G}{G_b})$  and  $\ln(\frac{SI}{SI_b})$ ) based on the assumption that the role of  $\Delta$  and SI is similar. The choices of Q/R were made considering the expected magnitude of variation in the estimation of physiological states (G from 40 to 600 mg/dl and and SI from 1e-4 to 1e-2 1/min per mU/l). The details of matrices and covariance for all six implementations are listed in appendix B.1.

## CGM Assessment

The incidences of anomalies, errors and missing values in CGM are believed to have a non-negligible impact on the states tracking and prediction, therefore, in addition to the actual CGM signal, we generated a smoothed-out CGM trace applying a cubic smoothing spline for each run. The predictions based on raw CGM and treated CGM were compared (see below).

## Prediction

Predictions are computed using the appropriate full, linearized and discretized (5min) models. 2 different prediction horizons are used: 30 and 45 min. The initial states vector  $XI$  for prediction is composed of KF outputs and feed-forward outputs if used. In the prediction calculation, basal insulin input is assumed. For SOGMM model implementations,  $u = J_{basal} - J_{op} = 0$  and for LOG model implementations,  $u = J_{op}$ . The calculations of  $N$  step (5 min interval) prediction are:

SOGMM model implementations:

$$G_{pred} = C_p \cdot A_p^N \cdot XI \quad (5.14)$$

LOG model implementations:

$$i) x = XI; \quad (5.15)$$

ii) for  $i = 1:N - 1$

$$x = A_p \cdot x + B_p \cdot u; \quad (5.16)$$

end

$$iii) \ln\left(\frac{G_{pred}}{G_b}\right) = C_p \cdot x \quad (5.17)$$

The prediction model matrices are listed in appendix B.2 and the structures of  $XI$  vector can be found in Table 8.

## Data

Twelve subjects (5 females, 7 males) with type 1 diabetes (mean±SD: age=40±13 yr, body weight=70.8±9.6 kg, BMI= 24.3±3.1 kg/m<sup>2</sup>, HbA1c=7.1%±1.0) underwent clinical trials designed to test an Artificial Pancreas control algorithm (NCT01418703). Each subject was admitted to the hospital twice to complete the “closed loop” and “open loop” studies, which correspond to CGM-based insulin management therapy vs. conventional therapy. Patients were required to wear the CGM and an insulin pump from 09:00 AM to 08:00 AM next day. Subcutaneous blood glucose concentration was measured every 5 minutes by CGM. Every half an hour, the blood glucose concentration was collected using YSI 2300 Stat Plus<sup>TM</sup> analyzer. Lunch was served at 11:15 AM, dinner at 19:15 PM and snack at 22:40 PM. A physical exercise was from 16:00 PM to 16:30 PM.

## Data Analysis

Four subjects were excluded from the analysis for data missing. We will compare prediction performance for 2 different prediction horizons: 30 and 45 minutes. Predictions are made every 5 minutes for both horizons, and predicted glucose is compared to CGM values 30 and 45 minutes afterward, respectively, using Mean Relative Absolute Difference (MARD, see equation 5.18). Prediction horizons including a meal are removed from the analysis as causal predictions cannot be expected to be accurate in this case (as the meal input is assumed to be 0 across the horizon).

$$MARD = \frac{1}{n} \sum_{i=1}^n \frac{|G_{pred}(i) - G(i)|}{G(i)} \quad (5.18)$$

Data are presented as Mean±SE unless otherwise noted, comparison between implementation is conducted using standard T-tests with a significance level of 5%.

## 5.2 Performance of BG Prediction - Comparison

MARDs for both prediction horizons are shown in Table 9. At PH=30min, LOG model-based predictions performed similarly to SOGMM-based predictions all implementations. “Core model +  $\Delta$ ” implementation consistently outperformed “Full model” implementation (SOGMM: 6.1%±2.6 vs. 6.9%±2.9,  $p<0.01$ , LOG: 6.0%±2.5 vs. 6.8%±2.5,  $p<0.01$ ), and were in turn outperformed by “Core model with SI” implementations with SOGMM (6.1%±2.6 vs. 5.6%±2.1,  $p=0.05$ ), but not using the LOG model. Similar results held for PH=45min (see Table 9) except that it was not significant different between “Core model+ $\Delta$ ” and “Core model with SI” implementations (8.7%±3.5 vs. 8.2%±2.7  $p=0.2$ ).

Table 9: MARDs (±SE) of 6 model implementations for PH=30, 45min

Prediction Horizon (min) \ Implementation	30	45
SOGMM-Full model	6.9%±2.9	9.3%±3.6
SOGMM-Core model+ $\Delta$	6.1%±2.6	8.7%±3.5
SOGMM-Core model with SI	5.6%±2.1	8.2%±2.7
LOG-Full model	6.8%±2.5	10.1%±3.5
LOG-Core model+ $\Delta$	6.0%±2.5	8.3%±3.4
LOG-Core model with SI	6.1%±2.4	9.2%±3.4

Seven pair of hypothesis (PH=30min) were set and the results of standard T-test for each pair were: “SOGMM-Full model” vs. “SOGMM-Core model+ $\Delta$ ”:  $p<0.01$ ; “SOGMM-Core model+ $\Delta$ ” vs. “SOGMM-Core model with SI”:  $p=0.05$ ; “LOG-Full model” vs. “LOG-Core model+ $\Delta$ ”:  $p<0.01$ ; “LOG-Core model+ $\Delta$ ” vs. “LOG-Core model with SI”:  $p=0.5$ ; “SOGMM-Full model” vs. “LOG-Full model”:  $p=0.76$ ; “SOGMM-Core model+ $\Delta$ ” vs. “LOG-Core model+ $\Delta$ ”:  $p=0.59$ ; “SOGMM-Core model with SI” vs. “LOG-Core model with SI”:  $p=0.11$ .

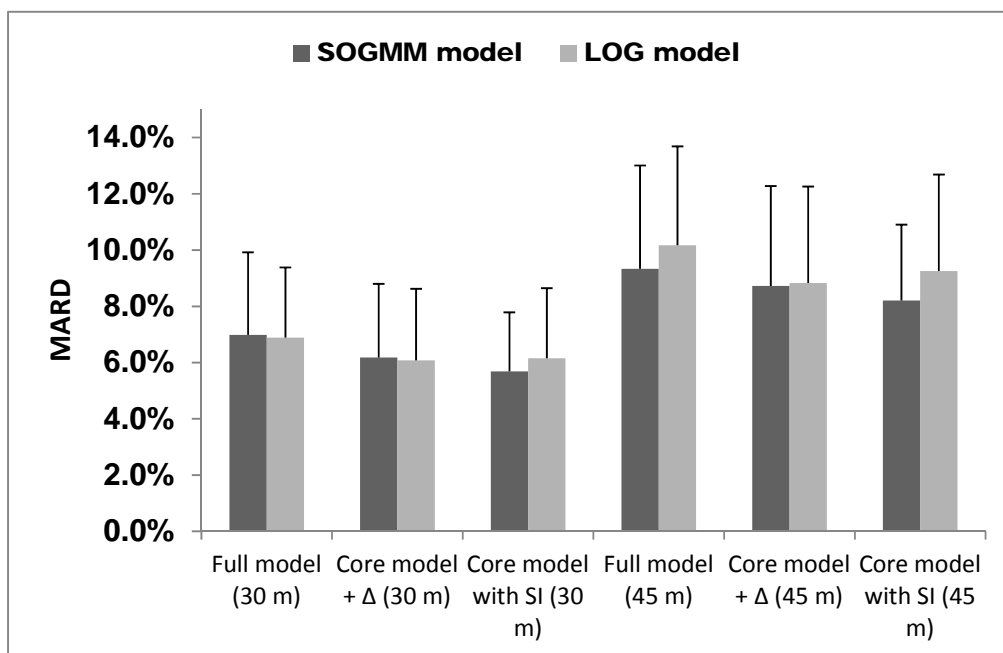


Figure 30: BG Prediction MARDs (Mean±SE) by 6 implementations for PH=30, 45min. SOGMM and LOG models were compared for each implementation. Raw CGM was used for measurement input.

In “Core model with SI” implementation, SOGMM model had better prediction performance than LOG model for PH=30,45min (5.6%±2.1 vs. 6.1%±2.4 p=0.01 and 8.2%±2.7 vs. 9.2%±3.4 p=0.01). By feeding smoothed CGM into KF instead of raw CGM data, LOG model seemed outperforming SOGMM model for PH=30min and having a close result to SOGMM model for PH=45min. However, the results were insignificant (3.5%±1.1 vs. 3.8%±1.0 p=0.14) and (6.2%±2.1 vs. 6.2%±1.7 p=0.3).

Wang *et al.* reported the relative error of 30-minute BG prediction by extreme learning machine, support vector regression, autoregressive model, and a newly proposed frame ranged from 7.3% to 9.5%<sup>117</sup>. Our results showed that methods using physiological models could provide more accurate BG forecasting (MARD<7%) for PH=30min. The “SOGMM-Full model” implementation presented in this manuscript was in accordance with the structure that Hughes

deployed in her hypoglycemia prevention technique<sup>110</sup>. We proved by simplifying the Kalman Filter models through extracting parts of the models as feed-forward models and by adding dynamic SI tracking technique, the 30 minutes BG prediction was improved for SOGMM (6.9%±2.9 vs. 6.1%±2.6 p<0.01; 6.9%±2.9 vs. 5.6%±2.1 p<0.01).

By splitting “Full model” into feed-forward compartments and core model, the KF process noise setting was limited inside the core model. The KF therefore only focused on the insulin-glucose interaction without considering the meal and insulin transportations. The  $\Delta$  and SI techniques were then developed then based on this structure.

The application of  $\Delta$  improved the BG prediction performance of both SOGMM and LOG model compared to full model implementations (PH=30, 45min). The characteristic time of  $X$  and  $\ln(\frac{X}{X_b})$  could be approximated as  $1/0.13=7$  minutes and  $1/0.01=100$  minutes for SOGMM and LOG model respectively. The  $\Delta$ 's 1000-min characteristic time was significantly larger than the PHs that it imposed different dynamics on model discrepancy vs. insulin action in the whole prediction horizon.

Incidences of large excursions of SI estimations were spotted by LOG model using raw CGM. One of the likely causes was the non-white nature of sensor noise<sup>53</sup>, especially when there were artifacts possibly caused by accidentally pressing the sensor. The exponential transformation of  $\ln(\frac{SI}{SI_b})$  further amplified the estimation anomalies which were suspected to deteriorate the BG prediction. Use of denoised CGM into the KF effectively avoided those large excursions, further confirming their source. In order to examine the impact of CGM defects on BG predictions, we generate a smoothed-out CGM trace applying cubic smoothing spline for each run. The predictions based on raw CGM and treated CGM were compared.

A rudimentary treatment of CGM was a non-causal smoothing. As shown in Table 10, the BG prediction based on non-causal smoothing CGM was significantly better than the one based on raw CGM for PH=30, 45min except “SOGMM-Full model” implementations (p=0.06 and 0.08). Refer to Figure 31 as well. It was expected that the non-causal smoothing would palliate the artifacts.

**Table 10: MARDs of 6 model implementations using non-causal smoothed CGM**

	PH = 30min			PH = 45min		
	Raw CGM	Non-causal	P	Raw CGM	Non-causal	P
SOGMM-Full model	6.98%	5.80%	0.06	9.33%	8.02%	0.08
SOGMM-Core model+ $\Delta$	6.18%	3.59%	<0.01	8.72%	5.23%	<0.01
SOGMM-Core model with SI	5.68%	3.45%	<0.01	8.21%	5.38%	<0.01
LOG-Full model	6.88%	5.06%	<0.01	10.17%	8.18%	<0.01
LOG-Core model+ $\Delta$	6.07%	3.36%	<0.01	8.82%	5.44%	<0.01
LOG-Core model with SI	6.15%	3.05%	<0.01	9.25%	5.68%	<0.01

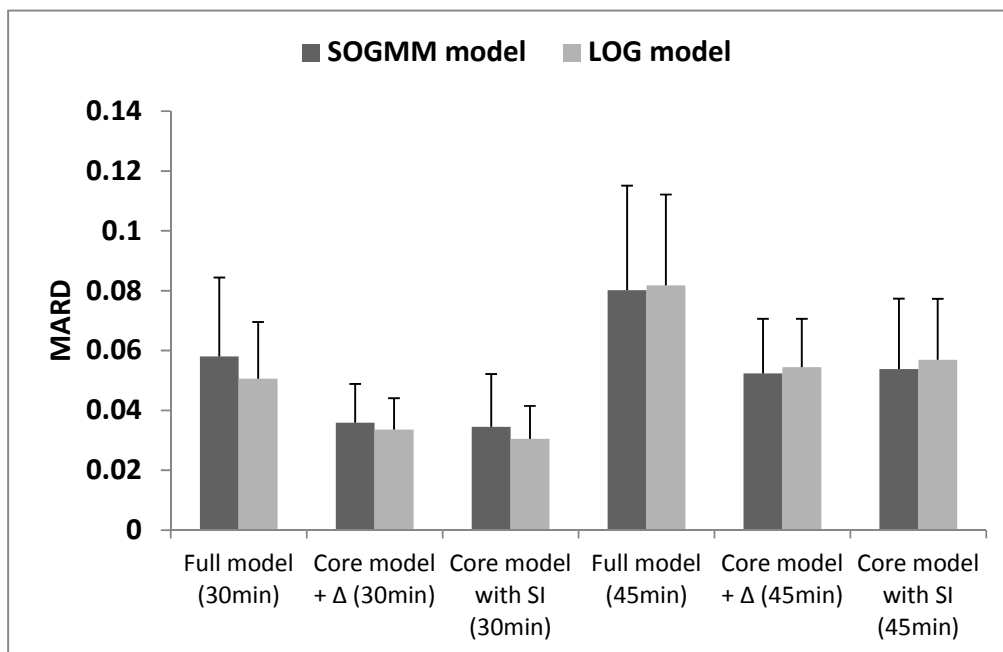


**Figure 31: BG Prediction MARDs (Mean±SE) by 6 implementations for PH=30, 45min. SOGMM and LOG models were compared for each implementation. Non-causal smoothed CGM was used for measurement input.**

A more authentic treatment of CGM was a causal smoothing that where we only adjusted the CGM time series prior to the decision time. As shown in Table 11, the BG prediction based on causal smoothing CGM was significantly outperformed by the one based on raw CGM for PH=30, 45min (Figure 32). This was due to the introduced latency of CGM signals.

**Table 11: MARDs of 6 model implementations using causal smoothed CGM**

	PH = 30min			PH = 45min		
	Raw CGM	Causal	P	Raw CGM	Causal	P
SOGMM-Full model	6.98%	8.42%	<0.01	9.33%	10.67%	<0.05
SOGMM-Core model+ $\Delta$	6.18%	7.76%	<0.01	8.72%	9.95%	<0.01
SOGMM-Core model with SI	5.68%	9.27%	<0.01	8.21%	11.76%	<0.01
LOG-Full model	6.88%	8.85%	<0.01	10.17%	11.88%	<0.01
LOG-Core model+ $\Delta$	6.07%	8.26%	<0.01	8.82%	10.76%	<0.01
LOG-Core model with SI	6.15%	8.36%	<0.01	9.25%	11.11%	<0.01

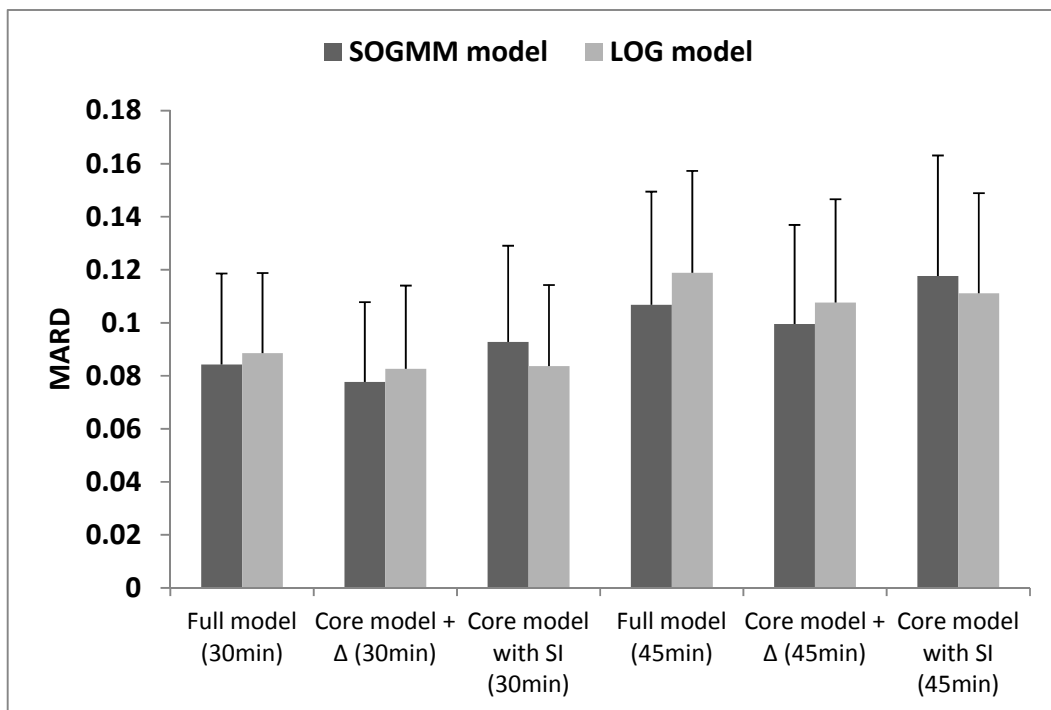


**Figure 32: BG Prediction MARDs (Mean $\pm$ SE) by 6 implementations for PH=30, 45min. SOGMM and LOG models were compared for each implementation. Causal smoothed CGM was used for measurement input.**

In the SOGMM model implementation, negative SI estimation was occasionally obtained by KF, leading to possible illogical relationship between insulin increase and glucose concentration. While short term prediction can remain good under these conditions, use of such model structure for optimization of insulin dosing would be inappropriate. In the LOG model implementation, the risk space form guarantees that SI estimation will remain positive.

In addition to the suitability of the LOG form for SI tracking, one may also consider additional desirable properties in constructing the glucose control objective function in risk space (34). As described in Patek et al. 2014 paper <sup>114</sup>, objective function in risk space allows for appropriate balance between hypo and hyperglycemic risk. Further research may demonstrate that sacrificing some amount of prediction power (see Table 9) can lead to substantial gain in accounting for the intrinsically imbalance glucose scale.

For physiological model-driven methods, the short term BG prediction power gets improved by extracting the meal and insulin transportation as feed-forward compartments. The “LOG-Core model with SI” implementation enables online estimation of SI while maintaining physiologically reasonable values meanwhile provides a relatively accurate way to carry out the BG prediction. Moreover, LOG model expresses the BG in risk space reflecting that the hypoglycemia presents more immediate risk than hyperglycemia. These results place the use of logarithm transform and reduced state Kalman Filtering as a good candidate to construct automated glucose control objective functions.

### 5.3 Validation by Simulation: SI or $\Delta$

The “SOGMM-Full model” implementation presented in this manuscript had been deployed in the “Safety Service Module” in DiAs (Artificial Pancreas developed in University of Virginia). Since the “SOGMM-Core model with SI” implementation as well as the “SOGMM-Core model+ $\Delta$ ” implementation outperformed the “SOGMM-Full model” implementation in PH=30min BG prediction, one of them would be chosen as a good candidate for the next generation of SSM. The first step was to test the algorithm in-silico for different scenarios. The Virginia/Padova Type 1 Simulator was equipped with a cohort of in-silico patients (100 adults, 100 adolescents and 100 children) that spanned the observed variability of metabolic parameters of general population. The latest version of the simulator implemented the intraday glucose variations and dawn phenomena. This offered an ideal environment for our testing.

Five testing scenarios and results are listed as follows:

1) Single meal (open-loop)

The simulation started at 9 AM. Lunch was provided at 12 PM with 0.5 gram/kg of carbohydrates. The corresponding bolus insulin was injected upon the meal arrival time. Figure 33 shows an example of the simulation (adult #005). True BG concentration, predicted BG by “SOGMM-Core model+ $\Delta$ ” and “SOGMM-Core model with SI” were recorded for the following 6 hours. The prediction error (MARD) was averaged across the 5-hour window starting at the beginning of the meal. We ran the test on the entire cohort of in-silico adults. The “SOGMM-Core model with SI” implementation outperformed the “SOGMM-Core model+  $\Delta$  ” implementation (MARD: 4.5% $\pm$ 2.6 vs. 5.5% $\pm$ 4.1,  $p < 0.01$ ).

2) 27 hour simulation without intraday variation and dawn phenomenon (closed-loop)

Simulation started at 6 AM and ended at 9 AM the next day. Breakfast, lunch and dinner were served at 8 AM, 12 PM and 19 PM with carbohydrates 0.5, 0.7 and 0.7 gram/kg. Meal boluses were calculated by meal controllers and Basal Rate Modifier (BRM) was active during the entire simulation. Again we compared the prediction MARD of those two implementations. The “SOGMM-Core model with SI” implementation outperformed the “SOGMM-Core model+ $\Delta$ ” implementation (MARD:  $3.9\% \pm 2.4$  vs.  $4.8\% \pm 2.6$ ,  $p < 0.01$ ).

3) 27 hour simulation with dawn phenomenon (closed-loop)

People with diabetes usually don't have a normal insulin response to compensate the elevated fasting blood glucose thanks to the surge of glucagon between 4 AM to 5 AM. This effect is known as “dawn phenomenon”<sup>118</sup>. In this simulation, “dawn phenomenon” was introduced to the in-silico patients. Simulation started at 6 AM and ended at 9 AM the next day. Breakfast, lunch and dinner were served at 8 AM, 12 PM and 19 PM with 0.5, 0.7 and 0.7 gram/kg of carbohydrates respectively. Meal boluses were calculated by meal controllers and Basal Rate Modifier (BRM) was active during the entire simulation. For the entire simulation period, the “SOGMM-Core model with SI” implementation outperformed the “SOGMM-Core model+ $\Delta$ ” implementation (MARD:  $4.3\% \pm 2.1$  vs.  $5.4\% \pm 2.2$ ,  $p < 0.01$ ); for the dawn period (4 AM to 9 AM), the “SOGMM-Core model with SI” implementation still outperformed the “SOGMM-Core model+ $\Delta$ ” implementation (MARD:  $4.4\% \pm 5.1$  vs.  $5.3\% \pm 5.6$ ,  $p < 0.01$ )

4) 27 hour simulation with intra-day variations (closed-loop)

The scenario was identical to that described in the last session except that we introduced the intra- day variations instead of dawn phenomenon. The “SOGMM-Core model with SI” implementation outperformed the “SOGMM-Core model+ $\Delta$ ” implementation (MARD:  $4.4\% \pm 2.3$  vs.  $5.5\% \pm 2.4$ ,  $p < 0.01$ ).

5) 27 hour simulation with intra-day variations and dawn phenomenon (closed-loop)

The scenario was identical to that described in the last session except that we introduced the intra-day variations as well as the dawn phenomenon. Figure 34 shows an example of the closed-loop simulation (adult #005). The “SOGMM-Core model with SI” implementation outperformed the “SOGMM-Core model+ $\Delta$ ” implementation (MARD: 4.7% $\pm$ 1.9 vs. 5.9% $\pm$ 2.1,  $p < 0.01$ ).

**Table 12: Prediction MARDs by two implementations using five simulation scenarios**

MARD	SOGMM-Core model+ $\Delta$ (Mean $\pm$ SE)	SOGMM-Core model with SI (Mean $\pm$ SE)	t-Test
Scenario 1	5.5% $\pm$ 4.1	4.5% $\pm$ 2.6	P<0.01
Scenario 2	4.8% $\pm$ 2.6	3.9% $\pm$ 2.4	P<0.01
Scenario 3	5.3% $\pm$ 5.6	4.4% $\pm$ 5.1	P<0.01
Scenario 4	5.5% $\pm$ 2.4	4.4% $\pm$ 2.3	P<0.01
Scenario 5	5.9% $\pm$ 2.1	4.7% $\pm$ 1.9	P<0.01

The simulation results showed the “SOGMM-Core model with SI” consistently outperformed the “SOGMM-Core model+ $\Delta$ ” for 30-minute BG prediction. Thus, we proved “SOGMM-Core model with SI” an optimized structure for short-term blood glucose forecasting in-vivo (posteriorly) as well as in-silico. Future work is to incorporate such a structure to the DiAs.

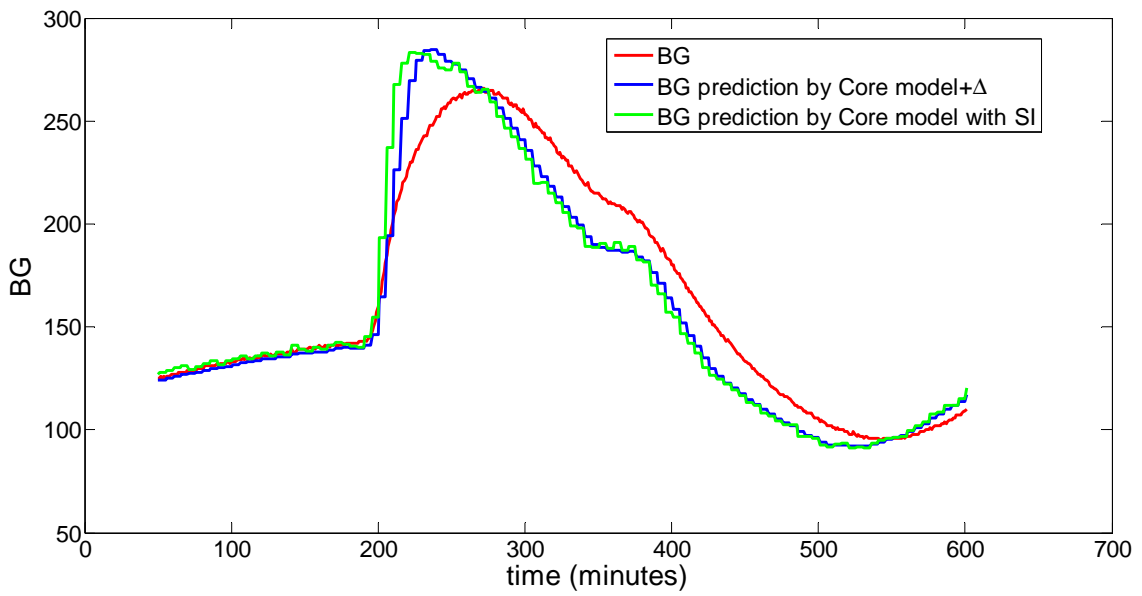


Figure 33: Simulation of one meal in open loop (adult #005).

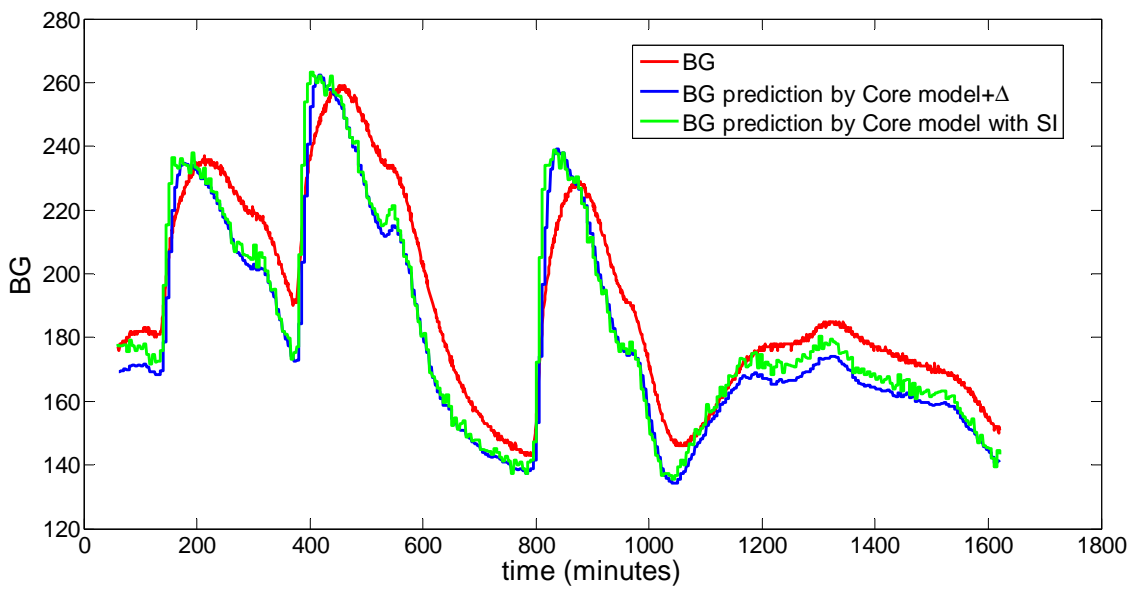


Figure 34: 27-hour closed-loop simulation with intra-day variations and dawn phenomenon (adult #005).

# Chapter 6. Enhancing Model-Based Long Term Glycemic Prediction in T1DM – Application in Semi-Auto Control

Recent years have witnessed the development of sc-to-sc closed loop control systems (Artificial Pancreas) <sup>119,120</sup>. The modular glucose control architecture proposed by Kovatchev et al. in 2009 has been widely accepted <sup>121</sup>. Characterized by the time-scale, the AP controller is composed of multiple layers: the safety supervision layer usually resides at the bottom of the system executing the last override of commands from above, one layer above is embedded with real time controllers using typical algorithms (Latest achievements in Model Predictive Control, Proportional Integral Derivative, and Fuzzy Logic Control can be found in <sup>122–126</sup>) and the top layer is responsible for tuning the controller parameters using clinical parameters and historical inputs into the system <sup>127</sup>.

Every type 1 diabetic is haunted by an optimization problem: how much insulin do I need to compensate the blood sugar without invoking adverse hyperglycemia and fatal hypoglycemia? The ultimate goal of AP is to dispense them completely from the cognitive burden on a daily basis. The system is expected to have the capacity to automatically cope with not only the regular insulin-glucose fluctuations, but also with the vast disturbances, such as meal

consumption and physical exercise <sup>128,129</sup>. In the journey to the emergence of legitimate closed-loop system, intermediate semi-auto systems are worthwhile to be exploited <sup>130</sup>.

Patek et al. presented a Semi-Automated Insulin Advisor (SAIA), which was composed of two main modules: On-Demand Bolus Advisor and Meal-Informed Power Brakes (Figure 35) <sup>114</sup>. Both modules take historical CGM, insulin treatment and meals as the inputs. The former is triggered, sending correction bolus advice episodically subject to user’s request. The advisory bolus is calculated using MPC by penalizing the control cost (BG in target) subject to constraints. The latter serves as the safety supervise layer, constraining basal insulin. This chapter is focused on how to provide a robust and predictive model for the On-Demand Bolus Advisor. The design and test of SAIA was conducted in the UVA/Padova T1DM simulation environment.

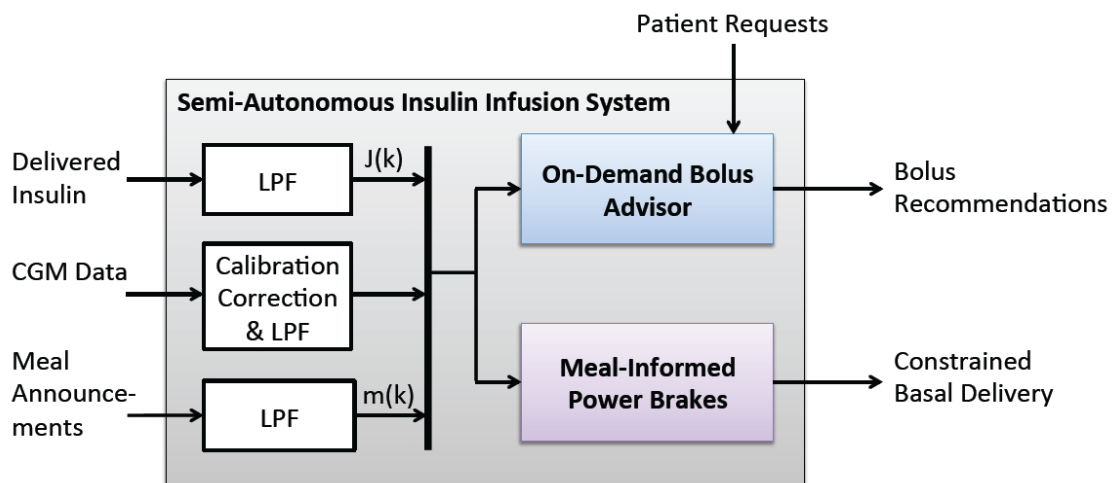


Figure 35: The two-layer architecture of SAIA <sup>114</sup>.

## 6.1 Parameter Uncertainties Characterization In-silico

According to Rahaghi et al. <sup>62</sup>, the time scales of blood glucose dynamics for “Pulsatile secretion of insulin”, “Intrinsic oscillatory phenomena”, “Meals, insulin injection, external schedules” and “Circadian rhythm” are 5-15 minutes, 60-120 minutes, 150-500 minutes and >700 minutes. The

episodic bolus suggested by Semi-Automated Insulin Advisor therefore inevitably enters the third zone, namely 150-500 minutes. Considering the substantial system uncertainty due to the inter-individual or intra-individual variability in this time scale, the stake of the robustness of our predictive model has to be raised. The be-all and end-all solution to account for the problem is to identify the complete set of parameters for each subject, which seems unrealistic at this stage. A compromised approach is to identify a subset of the parameters and tie them to clinical parameters and historical data collection.

Therefore, to ensure optimal, prediction-based, bolus calculations within the On-Demand Bolus Advisor, the model (Table 13) was first tuned using the Virginia/Padova Type 1 Simulator. The population used was composed of one hundred T1D in-silico adults. A subset of the parameters of the model was chosen to be tuned to maximize the average prediction accuracy for each subject while the rest of the parameters were fixed as the population average. The adjustable subset of parameters, namely the subject specific parameters were stratified into 4 groups. Each group of parameters was accounted for by a multiplier (shown in Table 13 and Table 14):  $[p_2] \rightarrow \alpha$ , accounting for insulin action;  $[p_6] \rightarrow \beta$  accounting for misestimated glucose appearance in plasma;  $[k_d] \rightarrow \gamma$  accounting for the speed of dynamics of subcutaneous insulin and  $[a_1 \ a_2 \ a_d] \rightarrow \mu$  accounting for the glucose kinetics in the gastrointestinal tract. BW was measured and  $I_b$  corresponded to the subject's basal rate.

**Table 13: The model in On-Demand Bolus Advisor is composed of LOG core, feed-forward insulin and meal compartments. Four multipliers are chosen to adjust the corresponding parameters**

<b>Core LOG</b>	$\log\left(\frac{\dot{G}(t)}{G_b}\right) = -p_1 \cdot \log\left(\frac{G(t)}{G_b}\right) - \alpha \cdot p_2 \cdot \log\left(\frac{X(t)}{X_b}\right) + \beta \cdot p_6 \cdot Ra(t)/BW$	(6.1)
	$\log\left(\frac{\dot{X}(t)}{X_b}\right) = -p_4 \cdot \log\left(\frac{X(t)}{X_b}\right) + p_4 \cdot \left(\frac{I_p(t)}{VI \cdot BW} - I_b\right)$	(6.2)
<b>Feed-forward Model</b>	Insulin Compartment	
	$\dot{I}_{SC1}(t) = -\gamma \cdot k_d \cdot I_{SC1}(t) + J(t)$	(6.3)
	$\dot{I}_{SC2}(t) = -\gamma \cdot k_d \cdot I_{SC2}(t) + \gamma \cdot k_d \cdot I_{SC1}(t)$	(6.4)
	$\dot{I}_p(t) = -k_{cl} \cdot I_p(t) + \gamma \cdot k_d \cdot I_{SC2}(t)$	(6.5)
	Meal Compartment	
	$\dot{Q}_1(t) = -\mu \cdot a_1 \cdot Q_1(t) - \mu \cdot a_d \cdot Q_1(t) + M(t)$	(6.6)
	$\dot{Q}_2(t) = -\mu \cdot a_2 \cdot Q_2(t) + \mu \cdot a_d \cdot Q_1(t)$	(6.7)
	$Ra(t) = \mu \cdot a_1 \cdot Q_1(t) + \mu \cdot a_2 \cdot Q_2(t)$	(6.8)

**Table 14: Population averaged parameters and tuning multipliers**

measured		tuned			
$BW$	$I_b$	$\alpha$	$\beta$	$\gamma$	$\mu$
fixed					
$p_1$	$p_2$	$p_4$	$p_6$	$VI$	$k_d$
6.9e-3	4.8e-4	1.6e-2	2.2e-3	6.0e-2	2.0e-2
$k_{cl}$	$a_1$	$a_2$	$a_d$	$X_b$	$G_b$
2.5e-1	1.0e-2	1.0e-2	2.0e-2	1	112.5

The framework was originated from the “LOG-Core model+ $\Delta$ ” implementation (Figure 29) introduced in chapter 5 (Figure 36). For a long-term (4 hours) prediction, the filtered insulin and carb was also fed into the system.

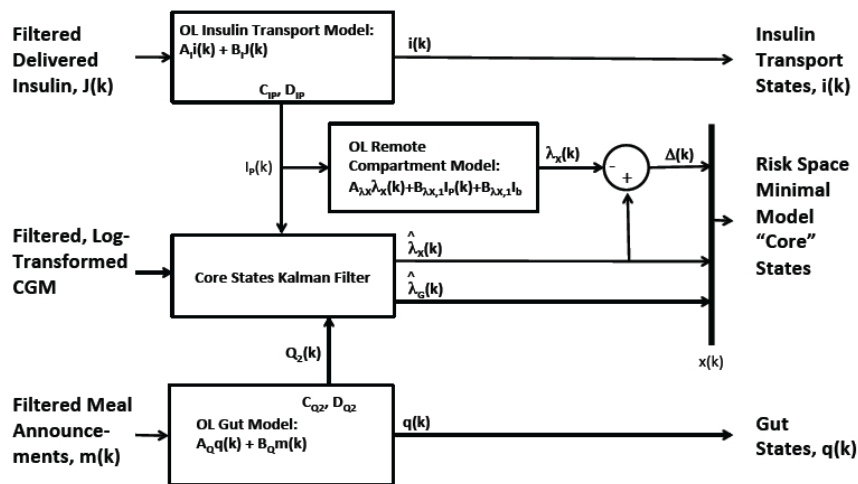


Figure 36: “LOG-Core model+ $\Delta$ ” structure for state estimation and prediction <sup>114</sup>.

The tuning procedure used the forcing function methodology by a 2x2 design (Figure 37): i) two prediction windows (first between 1 and 5 hours following a meal, and second, 4 and 8 hours following the meal), ii) two meal scenarios (first, a meal with a corresponding bolus, and second, the same meal/bolus plus a correction bolus one hour following the meal). The design of two prediction windows was to take into account the prediction performance in the horizon close to a meal as well as the horizon away from the meal. The design of two meal scenarios was to ensure that the model maintained its prediction performance after a correction bolus.

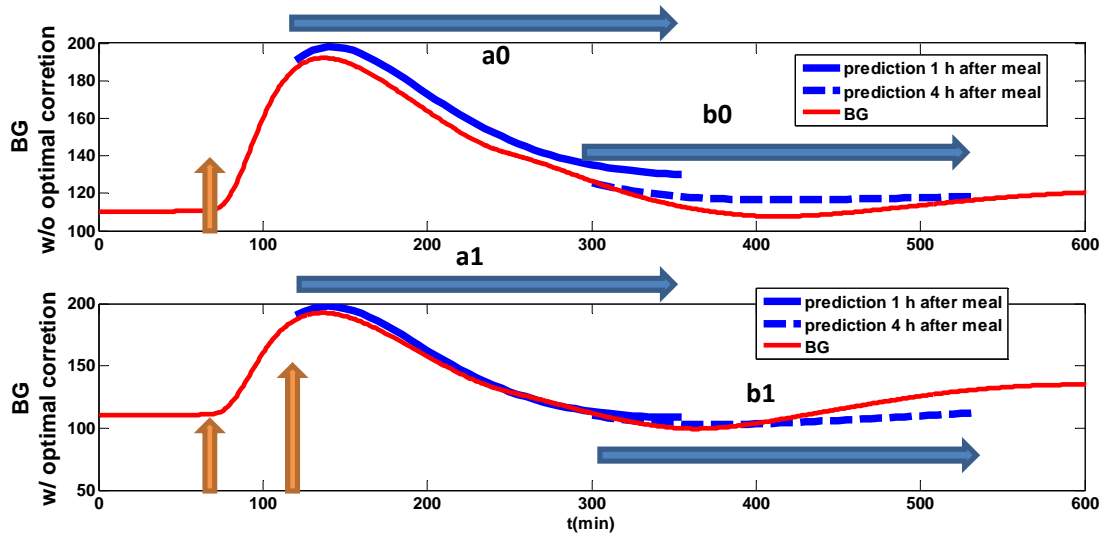


Figure 37: 2x2 tuning design: (top) a meal and bolus served without optimal correction 1 hour afterwards, (bottom) a meal and bolus served with optimal correction 1 hour afterwards. Four prediction windows a0, b0, a1, b1 were chosen.

For each in-silico subject, the 2x2 design generated 4 pairs of BG traces. The differences of BG value were stored in vectors  $\Delta a_0$ ,  $\Delta b_0$ ,  $\Delta a_1$ ,  $\Delta b_1$  respectively .

$$\Delta a_0 = G_{pred\_a0} - G_{a0}$$

$$\Delta b_0 = G_{pred\_b0} - G_{b0}$$

$$\Delta a_1 = G_{pred\_a1} - G_{a1} \tag{6.9}$$

$$\Delta b_1 = G_{pred\_b1} - G_{b1}$$

For window a, a linear piece-wise weight  $\omega_a$  was applied to the prediction errors  $\Delta a_0$  and  $\Delta a_1$ ; for window b, a different weight  $\omega_b$  was applied to  $\Delta b_0$  and  $\Delta b_1$ . The weighed prediction errors for each meal scenario were concatenated (equation 6.10).

$$temp_0 = [\Delta a_0 \cdot \omega_a : \Delta b_0 \cdot \omega_b] \quad (6.10)$$

$$temp_1 = [\Delta a_1 \cdot \omega_a : \Delta b_1 \cdot \omega_b]$$

The introduction of  $\omega_a$  and  $\omega_b$  was to inform the MPC of different penalties for the two windows: the further away from a meal event, the more time in target we wanted. Therefore  $L(q)$  in equation 2.4 was constructed as:

$$w_a = \begin{cases} \frac{1}{3}t, & 0 \leq t \leq 3 \\ 1, & 3 < t \leq 4 \end{cases}, \quad w_b = \begin{cases} t, & 0 \leq t \leq 1 \\ 1, & 1 < t \leq 4 \end{cases} \quad (6.11)$$

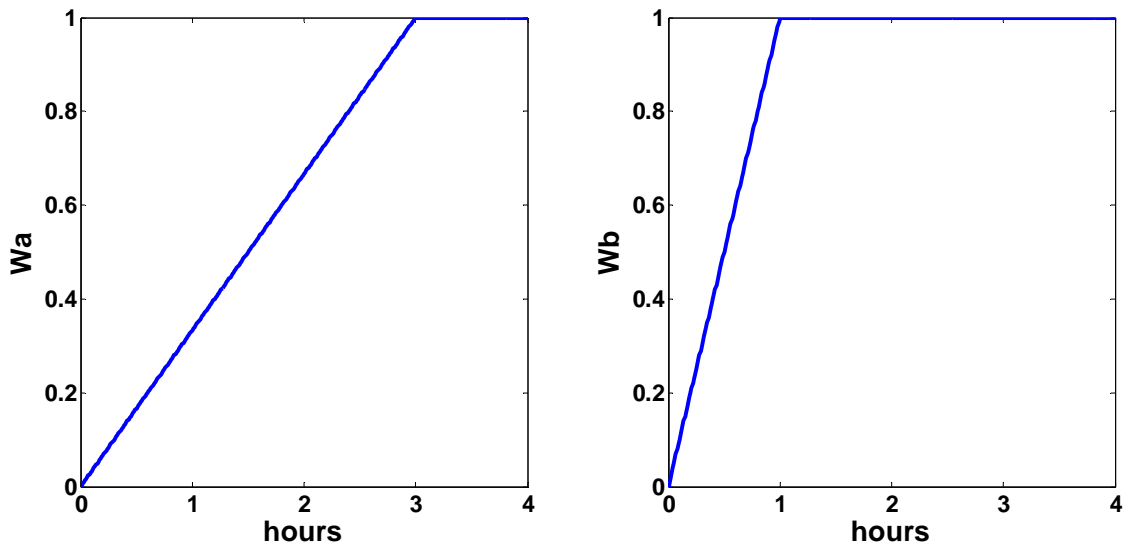


Figure 38: Linear piece-wise cost weights for two different prediction windows:  $W_a$  starts at 1 hour after the meal,  $W_b$  starts at 4 hour after the meal.

The overall prediction accuracy was computed and imbalanced accuracy between scenarios or windows was additionally penalized. A penalty term for parameter variations ( $\sum p^2$ ) was also

added to the ultimate cost function  $J$  (equation 6.12). The multipliers were derived by taking the exponential form of  $p$  (equation 6.13).

$$J = \sum temp_0^2 + \sum temp_1^2 + \sum |temp_0 * temp_1| + \sum p^2 \quad (6.12)$$

$$\alpha = e^{p(1)} \quad \beta = e^{p(2)} \quad \gamma = e^{p(3)} \quad \mu = e^{p(4)} \quad (6.13)$$

The cost  $J$  in equation 6.12 is a classic unconstrained optimization problem. We applied the “fminsearch(@costfun, x0)” method in Matlab to search for the optimal solution for this problem. “fminsearch” starts at the designated initial point  $x_0$  and utilizes the algorithm of “Nelder-Mead simplex direct search” to find the minimum of the cost function<sup>131</sup>. In our case, the initial point  $p_0$  was set to [0 0 0 0] (started from the population averaged parameters).

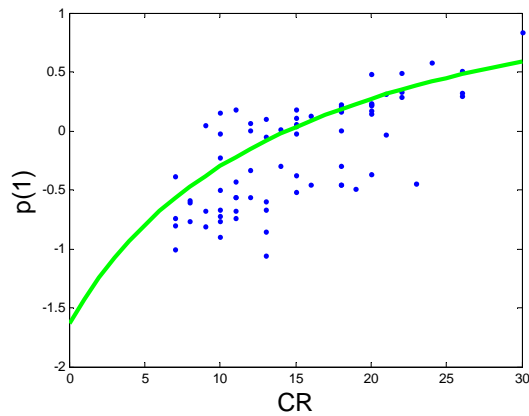
After obtaining the optimized parameter set for each subject, we tried to link the physiological parameters to the tuned parameters. Backwards-stepwise model selection was applied herein. The candidate predictors were CHO:I (CR), correction factor (CF) and basal insulin. The selected models are shown in Table 15.

*Backwards-Stepwise Selection:*

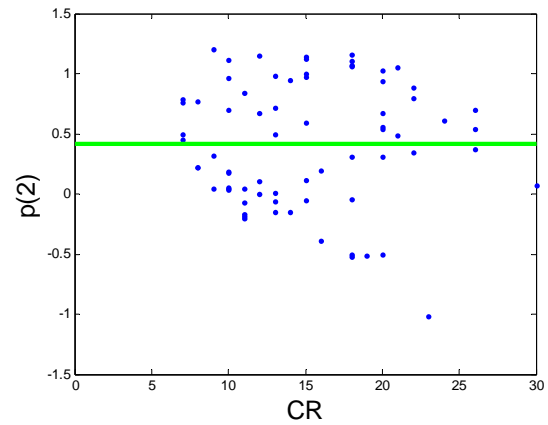
Rather than search through all combinations of predictors, backwards-stepwise selection starts with the full model (intercept + all candidate predictors) and sequentially deletes the predictor that imposes least impact on the regression fit or improves the model the most. Ultimately, the process stops if no improvements can be made.

Table 15: Step-wise selection of regression model

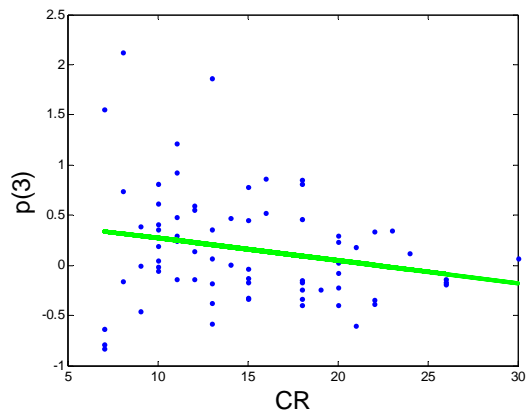
<b>p(1)</b>			
	coefficient	95% interval	
b0 (int)	-2.208	-4.141	-0.276
b1 (CR)	0.052	0.024	0.081
R2	F*	p-value	error variance
0.533	25.907	0.000	0.097
<b>p(2)</b>			
	coefficient	95% interval	
b0 (int)	0.235	-3.023	3.493
b1 (CR)	0.008	-0.041	0.056
R2	F*	p-value	error variance
0.018	0.414	0.744	0.274
<b>p(3)</b>			
	coefficient	95% interval	
b0 (int)	1.239	-2.143	4.620
b1 (CR)	-0.033	-0.083	0.018
R2	F*	p-value	error variance
0.101	2.553	0.063	0.296
<b>p(4)</b>			
	coefficient	95% interval	
b0 (int)	-0.178	-2.702	2.347
b1 (CR)	-0.034	-0.071	0.004
R2	F*	p-value	error variance
0.151	4.018	0.011	0.165



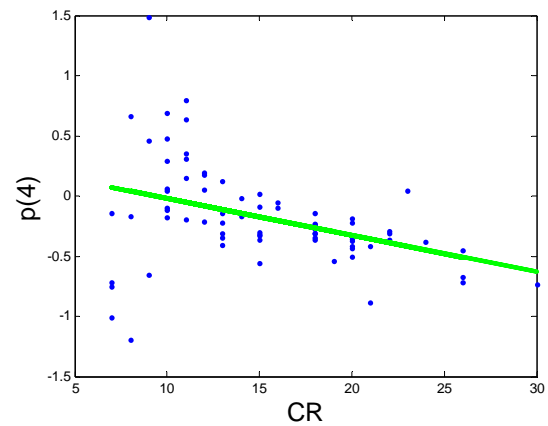
$$P = -0.8 + 2.5 \cdot \frac{CR - 5}{CR + 15}$$



$$P(2) = 0.43$$



$$P(3) = -0.02 \cdot CR + 0.49$$



$$P(4) = -0.03 \cdot CR + 0.28$$

Figure 39: Regressions of parameter multipliers to CR.

### Performance Evaluation In-silico

The impact of the new model was assessed in-silico using a predictive optimal (LQR) bolus advice system. The test consisted of three underinsulinized meals (50% of the CR-optimal bolus) over 24h, each with a bolus advice 1h afterwards; LQR tuning was done to avoid hypoglycemia in both cases.

The risk based optimal advice system significantly improved in-silico time in target range [70-180 mg/dl] compared to conventional therapy ( $79\pm 1.5\%$  vs.  $61\pm 2\%$ ,  $p < 0.01$ ) with no hypoglycemia in either case. Refer to Figure 40.

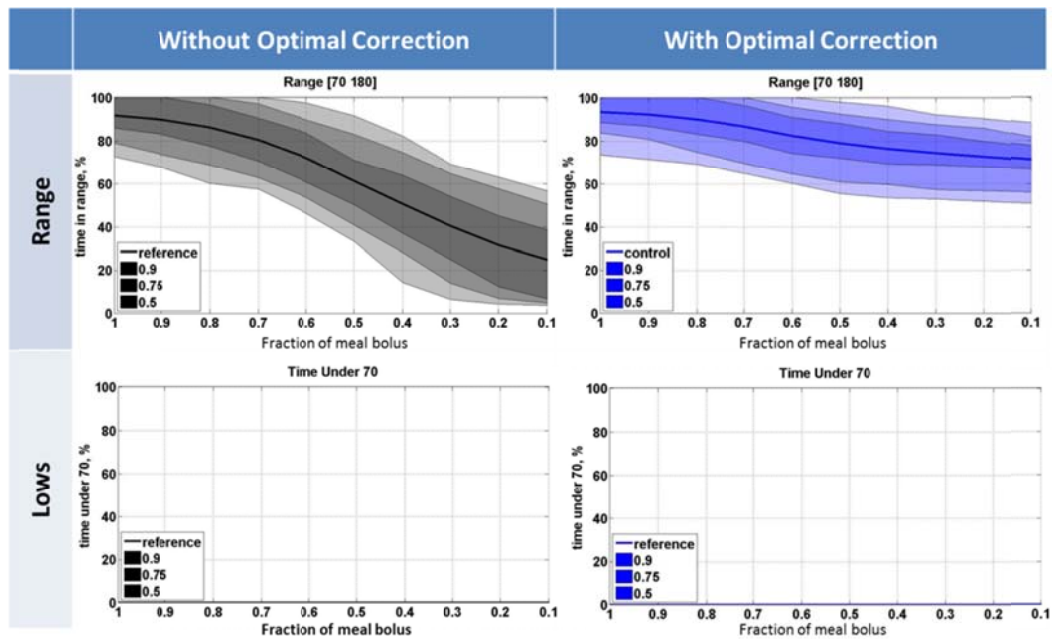


Figure 40: Time in range: conventional therapy vs. advisory system.

## 6.2 In-vivo Clinical Study – Application in Semi-Auto Control

The in-silico success of the system encouraged us to move forward to a clinical study: “Early feasibility study of adaptive advisory/automated (AAA) control of type 1 diabetes” conducted in UVA health system. The purpose of the study was to evaluate the system’s performance of controlling blood glucose levels in an outpatient setting.

In an experimental session, subjects were admitted to guesthouse at 1800 PM and were discharged 40 hours later at 0900 AM on day 3 of admission (Figure 41). Breakfast, lunch and dinner were served around 0700 AM, 1200 PM and 1900 PM respectively. A 45-minute physical exercise session was required starting at 1400 PM. After the initialization of AAA control, Safety

Supervision Module (SSM) and Basal Rate Modifier (BRM) were kept active throughout the entire admission period while Advisory Module was only active during the day time (0700 AM - 2300 PM). SMBG readings, CGM data (DexCom® Gen4), meal serve and insulin administration were collected.

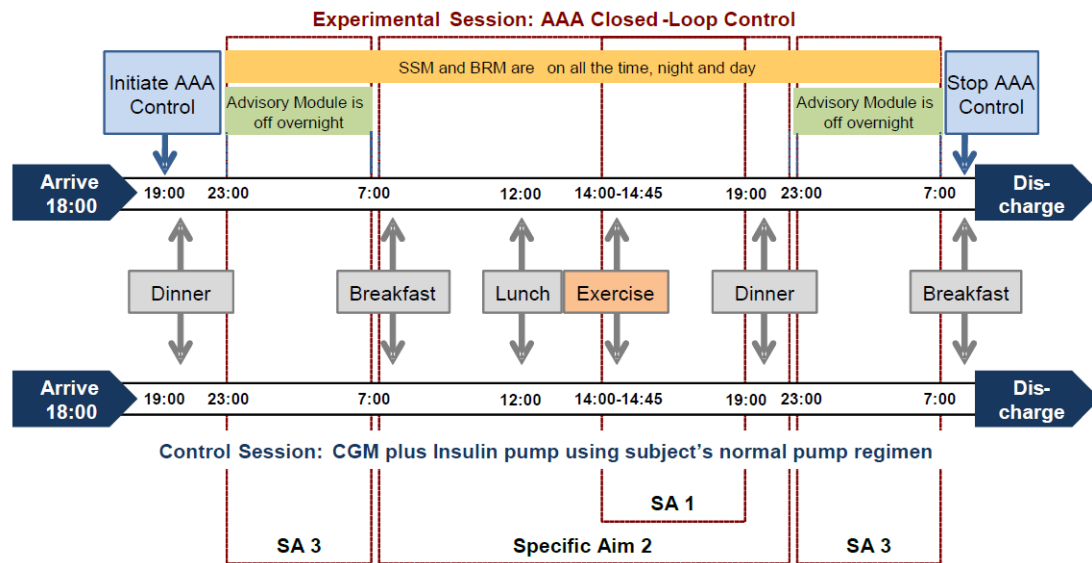


Figure 41: Experimental and control sessions of a test day.

### Pilot Study

Two subjects were recruited to participate in the pilot experimental session. The procedure was in accordance with what has been described above. Multiple correction bolus advices with or without overriding by patients had been taken. The advisory bolus did not meet the expectation. A suspension of Advisory Module was called for the rest of the study. The causes of the failure were complex and entangled. A posterior analysis based on reconstruction of BG predictions in the simulator had given us some insights of the defect residing in our system:

### 1) Under-correction

Figure 43 (top) shows a snapshot of the BG trace of one of the pilot subject, 28101. A mixed meal containing 52 grams of carbohydrate was served at 1900 PM. The patient reported 2.25 U of historical insulin injection within 2 hours and delivered 5.4 U of meal bolus insulin. The blood glucose stayed flattened for almost 3 hours and started to climb up. A 0.7 U advisory correction bolus was accepted by the patient when BG was reaching 180 mg/dl. For next one hour and a half, BRM sent frequent elevated basal insulin to compensate the projected BG that implied the amount of advisory correction was underestimated. We confirmed that implication with the reconstructed BG prediction in the simulator (Figure 43 bottom). The inaccuracy of BG prediction was probably due to the lacking capacity of characterizing delayed meal absorption by our model. It has been proven that the meal composition has a massive impact on the post-prandial glucose response. For example, co-ingestion of fat resulted in a significant fluttering of the post-prandial BG<sup>132</sup>. Since the framework in which we conducted the model tuning did not incorporate this effect, a failure in the in-vivo application occurred.

### 2) Over-correction

Figure 44 (top) shows a snapshot of the BG trace of one of the pilot subject, 28102. A 1.9 U correction was accepted and injected at 1015 AM. One and a half hours later, the BG went low and SSM was triggered to suspend basal delivery for more than one hour. It implied that the system had given the overestimated correction bolus. By reconstructing the BG prediction in-silico (Figure 44 bottom), we found that the model failed to catch the insulin-glucose kinetic and made an inaccurate prediction. The capacity of our model to account for the inter-individual variability needed an iterative design.

### 3) Carb-miscounting

One design of AAA was to ask the subjects to assess their meal (carbohydrate) size and post-prandial glucose response based on their perception. They were provided a user interface (Figure 42) to input their decision. The instruction was as follows:

“There are two aspects of how food raises the blood sugar- how high the blood sugar goes up and how quickly the blood sugar goes up. For instance, some foods may raise the blood sugar quickly, but not increase the blood sugar very much. Other foods may increase the blood sugar slowly but will eventually increase the blood sugar to a high final level. We want you to rate both how high you think the blood sugar will increase, and how quickly it will increase after you eat each meal and snack.”

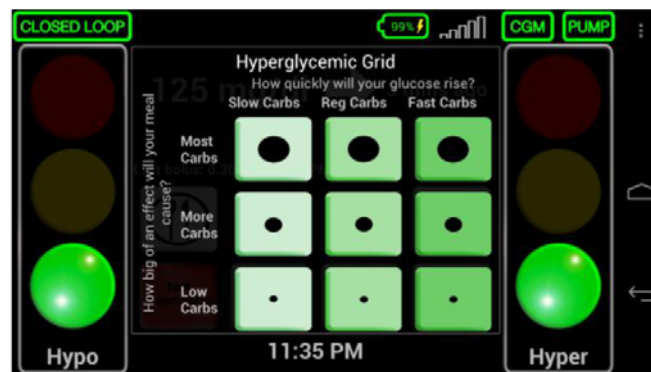


Figure 42: Hyperglycemic Grid

Without a systematic training, the perception of the carbohydrate content would be inaccurate. An extreme case in this study was that one meal with about 90 grams of carbohydrates was estimated as 30 grams (three folds underestimated). The miscounting amounts of carbohydrates added more complexity to the prediction performance.

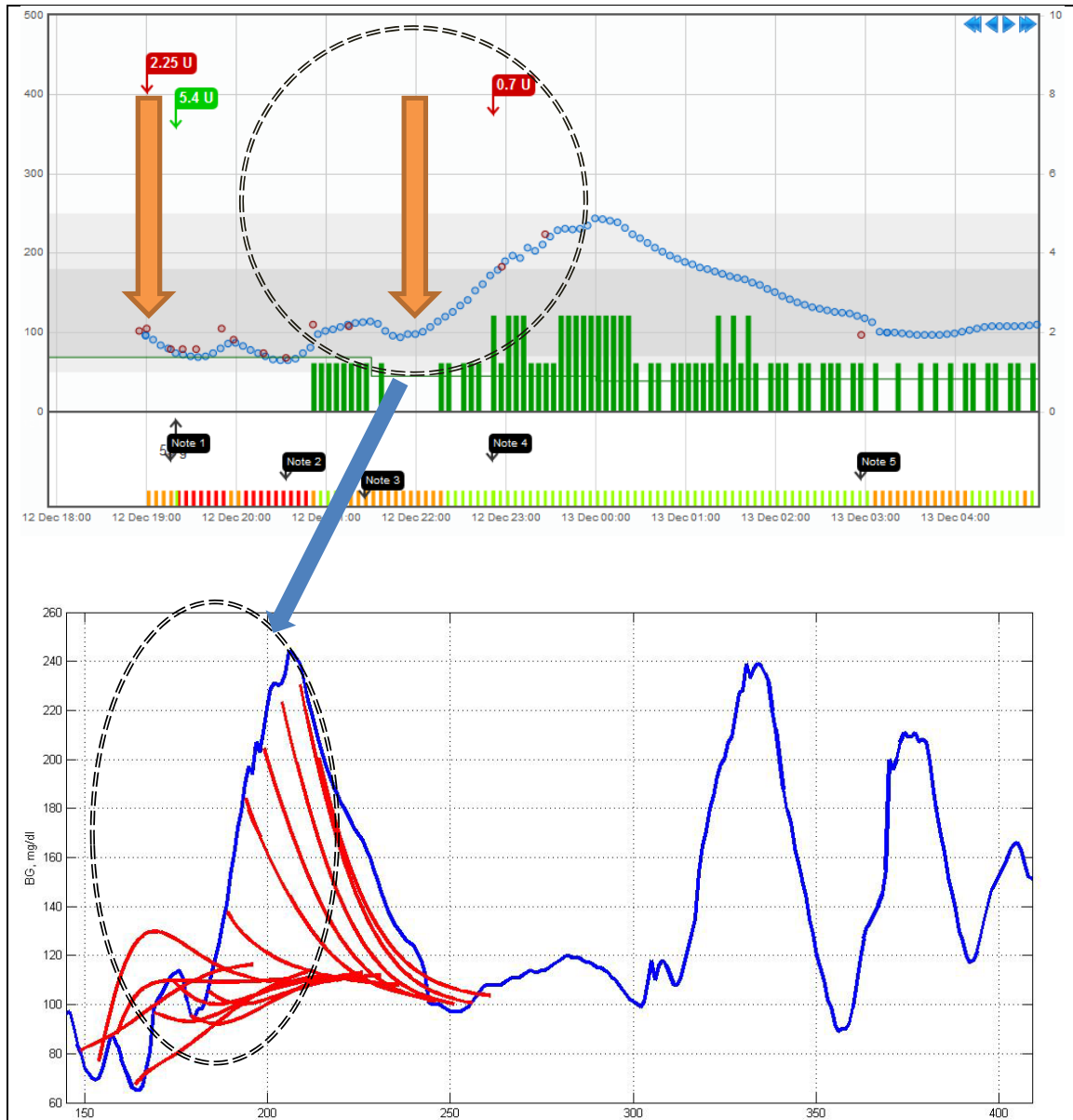


Figure 43: Clinical study (top) and reconstruction of BG prediction around the first meal in the simulator (bottom) of sub28101.

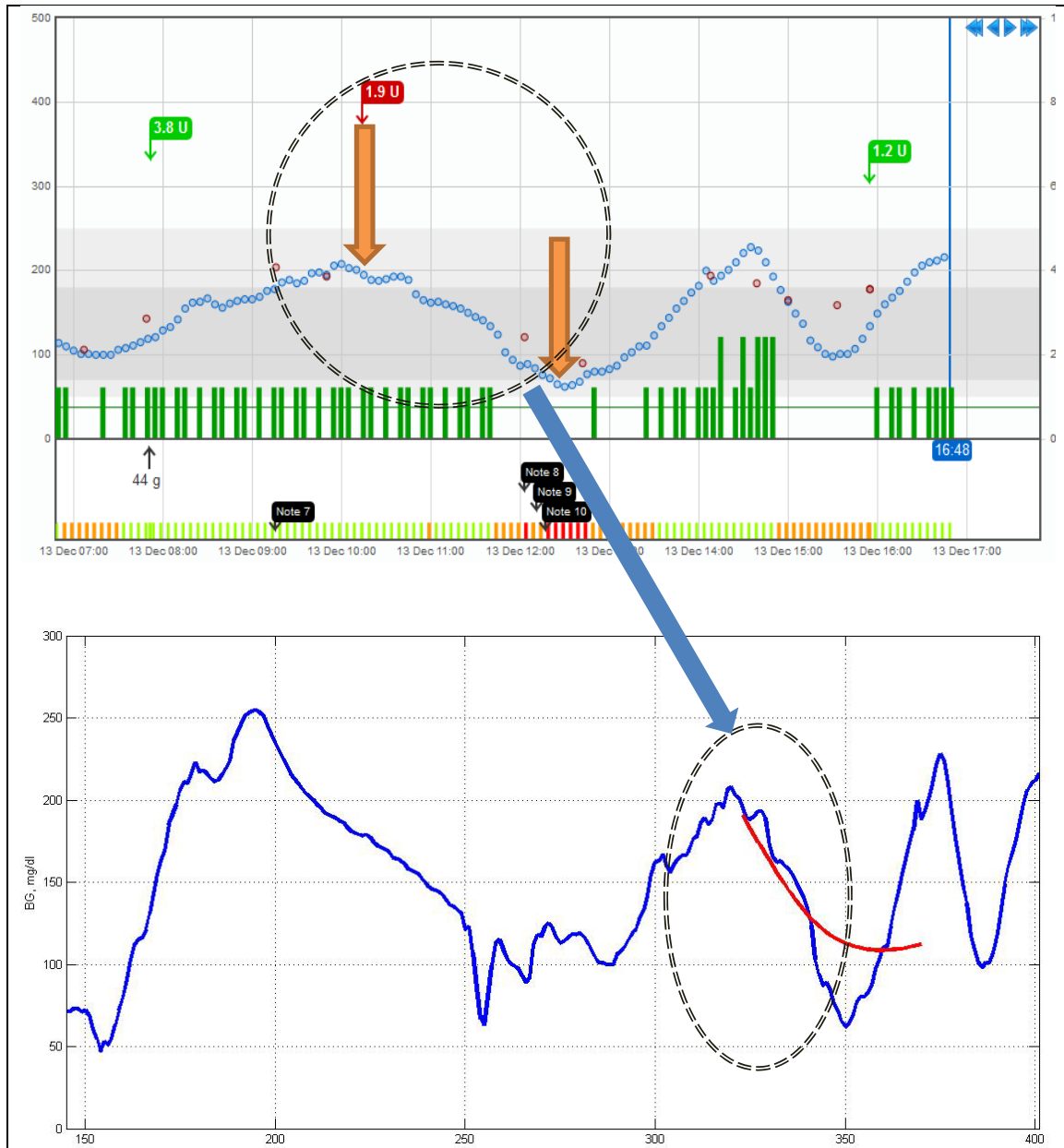


Figure 44: Clinical study (top) and reconstruction of BG prediction at decision time in the simulator (bottom) of sub28102.

4) LOG model: parameter  $p_1$

A simulation starting at BG=200 mg/dl with basal delivery was conducted. Figure 45 shows the BG traces of subject adult #025. The blue line was the BG predicted by the population-averaged

LOG model and the red line is the simulated BG trace. The vast difference of BG the dropping rate implied that the actual  $p_1$  (glucose effectiveness) for this in-silico subject was different from the population averaged value. Figure 46 shows the simulated BG envelop (light blue) and predicted BG envelop (blue) of 100 in-silico adults. Therefore, treating  $p_1$  as a population average value of glucose effectiveness ( $p_1$ ), which had already been underestimated, was inappropriate.

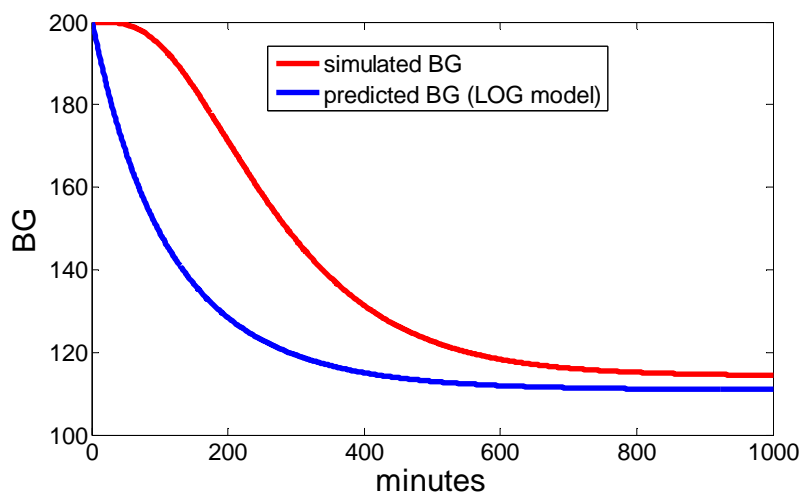


Figure 45: Predicted (blue) and simulated (red) BG traces starting from 200 mg/dl with basal insulin delivered (subject adult #025).

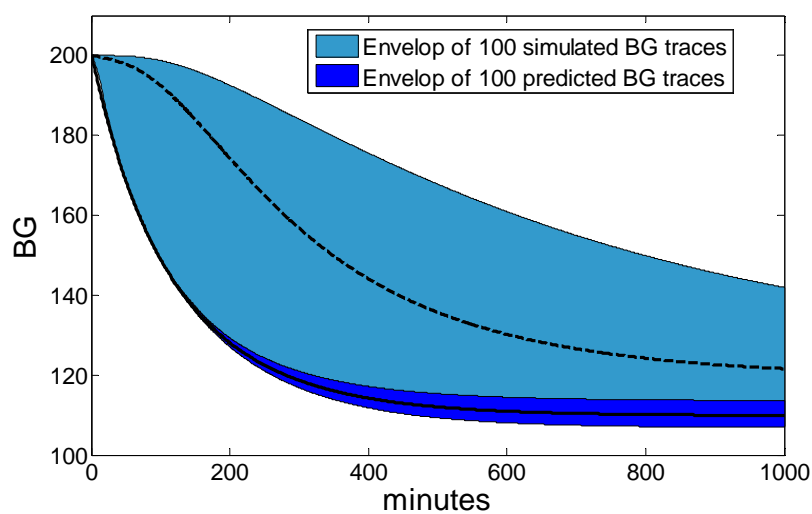


Figure 46: Simulation of 100 subjects starting from 200 mg/dl with basal insulin delivered: light blue) simulated BG envelop with mean, blue) predicted BG envelop with mean by LOG model.

The examinations listed above implied that despite the parameters of the in-silico patients spanned the observed variety of metabolic parameters of general population, the characteristics of the meal input had not been well accounted for considering that the meal composition had a substantial impact on the post-prandial glucose response. This encouraged us match the model to the in-vivo data which possessed more variability than the simulator. We reconsidered the selective model and proposed that more predictors should be added to the candidates, such as body weight, total daily insulin and meal size. Also, the tuning parameter set should be expanded by adding  $p_1$  which had a vast influence on the BG tolerance.

### **6.3 Parameter Uncertainties Characterization “In-vivo”**

The “in vivo” simulator or net effect simulator was essentially a framework combining in-silico experiments and collected clinical data to reconstruct the treatment scenarios <sup>46</sup>. The framework contained 56 pump users with type 1 diabetes and the data for each subject was “chopped” into a collection of 11h-length segments yielding a total of 2082 BG segments. Based on the SMBG readings, CGM, bolus administration, basal insulin delivery, and meal treatment, a signal called “net effect” was extracted for each subject by a deconvolution method using an established model of insulin-glucose metabolism. By doing this, the BG variability is accounted for: meal perturbation, insulin resistance by a positive net effect and elevated insulin sensitivity by a negative net effect.

By feeding the net effect in return, along with the complete set of historical data, the original CGM can be recovered. It also made possible the simulation of the effect of modified insulin delivery. Additionally, the source data that was collected from the real world users spanned a

vast variability of meal composition which was lacking in the T1D simulator. Therefore, the net effect simulator was a sound tool for parameter tuning of our model.

Out of the 2082 segments, a subset was selected as the training data. The criteria were: 1) Two meals must be separated at least 6 hours, 2) The carbohydrate of the meal was greater than 40 grams, 3) No hypoglycemic incidences were present during the prediction window. The subset contained 46 subjects with 245 BG segments.

The tuning design was similar to what has been described in section 6.1. Several modifications had been made due to the structural limitation of the Net Effect Simulator (Figure 47): a) we changed the 2X2 design to a 1X2 design by taking out the 2-prediction-window dimension for the very low frequency of meals separated by 8 hours, b) the optimal correction bolus was computed by the correction factor (CF) subject to an upper bound: 1U (equation 6.14). As discussed in section 6.2, we added  $[p_1] \rightarrow \theta$  to the tuning set.

$$bolus = \text{minimum}(1, (\text{minimum}(CGM) - 70)/CF) \quad (6.14)$$

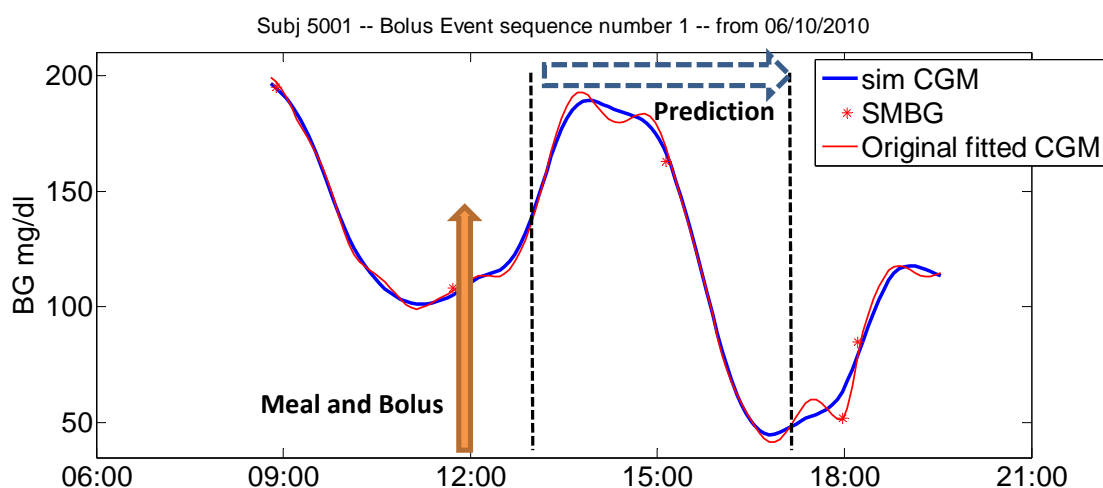


Figure 47: Prediction started from 1 hour after the meal and lasted 4 hours.

### Tuning Procedure

#### a) Global Search

The cost function became equation 6.17.

$$\Delta a_0 = G_{pred\_a0} - G_{a0} \quad (6.15)$$

$$\Delta b_0 = G_{pred\_b0} - G_{b0}$$

$$temp_0 = \Delta a_0 * \omega_a \quad (6.16)$$

$$temp_0 = \Delta a_0 * \omega_a$$

$$J = \sum temp_0^2 + \sum temp_1^2 + \sum |temp_0 * temp_1| + \sum p^2 \quad (6.17)$$

$$\alpha = e^{p(1)} \quad \beta = e^{p(2)} \quad \gamma = e^{p(3)} \quad \mu = e^{p(4)} \quad \theta = e^{p(5)} \quad (6.18)$$

Similar to what had been tried in in-silico tuning, we conducted backward step-wise linear regressions on the subject's clinical parameters as well the historical data collection (body weight (BW), basal insulin delivery (basal), total daily insulin (TDI), correction factor (CF), carb ratio (CR), meal (M) and SI (TDI/BW)). The model selection hardly showed significant candidate predictors. This was probably due to the intra-individual variability; i.e., for the same subject, different BG segments might present quite different insulin-glucose dynamic (appendix C.1). A rudimentary solution was to lump the segments for each subjects.

If we combined the set for optimized multipliers by taking the average for each subject, the model selection yielded significant results:

$$P(1) \sim \frac{TDI}{BW} \quad (p < 0.05)$$

$$P(2) \sim M + \frac{TDI}{BW} \quad (p < 0.05 \quad \& \quad p < 0.05)$$

$$P(3) \sim M + CF \quad (p = 0.12 \quad \& \quad p < 0.05)$$

$$P(4) \sim TDI/BW \quad (p < 0.05)$$

$$P(5) \sim CF + basal \quad (p < 0.05 \quad \& \quad p < 0.05)$$

Appendix C.2 listed the pair plot of each multiplier against the selected predictors.

#### b) In-depth Search

Even though the averaged tuning set showed its merit in model selection, it was still coarse. A more convincing solution was combining the cost from all BG segments for each subject and using the averaged parameter obtained from a) as the starting point for search. The Bayesian cost for each parameter was still included in the cost function, with mean  $\bar{p}$  and standard error  $\Delta p$  computed from a) except  $p(4)$ . The unconstrained parameter  $[a_1 \ a_2 \ a_d]$  governed by  $p(4)$  was thereby accounting for the intra-individual variability.

$$J = \sum_{n=1}^{n \text{ segments}} \sum temp_0^2 + \sum_{n=1}^{n \text{ segments}} \sum temp_1^2 + \sum_{n=1}^{n \text{ segments}} \sum |temp_0 * temp_1| + \sum_{n=1}^{n \text{ segments}} \sum_{p \neq p(4)} \left( \frac{p - \bar{p}}{\Delta p} \right)^2 \quad (6.19)$$

The backwards-stepwise model selection for each parameter was listed as follows:

$$P(1) = -0.2622 - 0.4564 * \frac{TDI}{BW}$$

( $p < 0.05$  )

$$P(2) = 1.0006 - 0.0043 * M - 0.0343 * CR - 0.0033 * basal$$

( $p < 0.05$  &  $p < 0.05$  &  $p < 0.05$ )

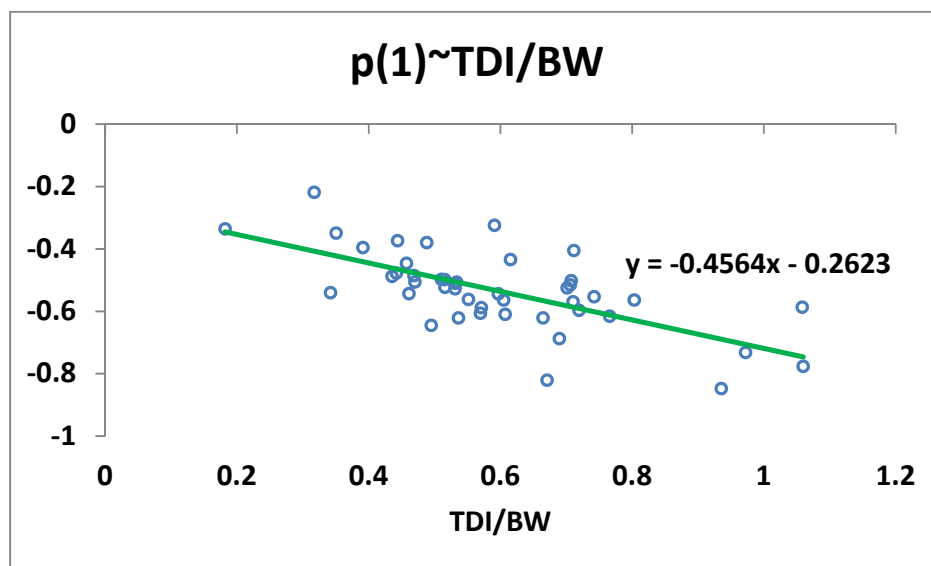
$$P(3) = -0.5454 + 0.0155 * CF$$

( $p < 0.05$ )

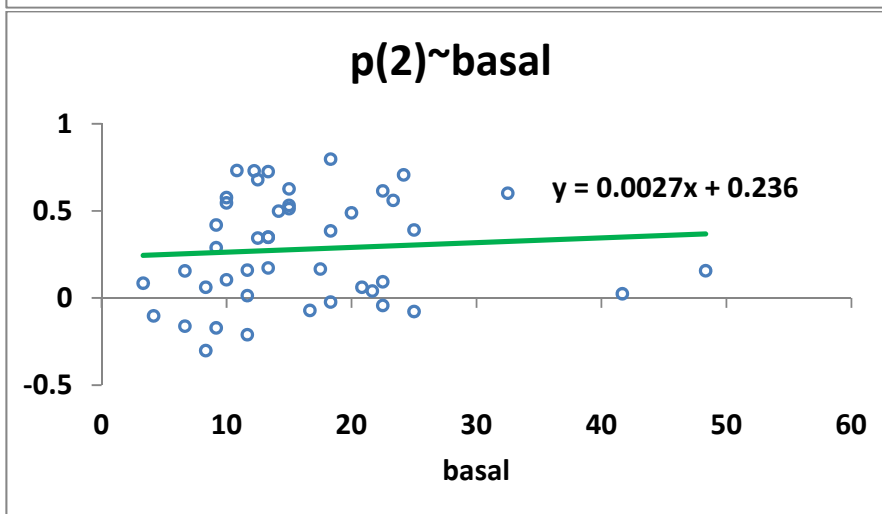
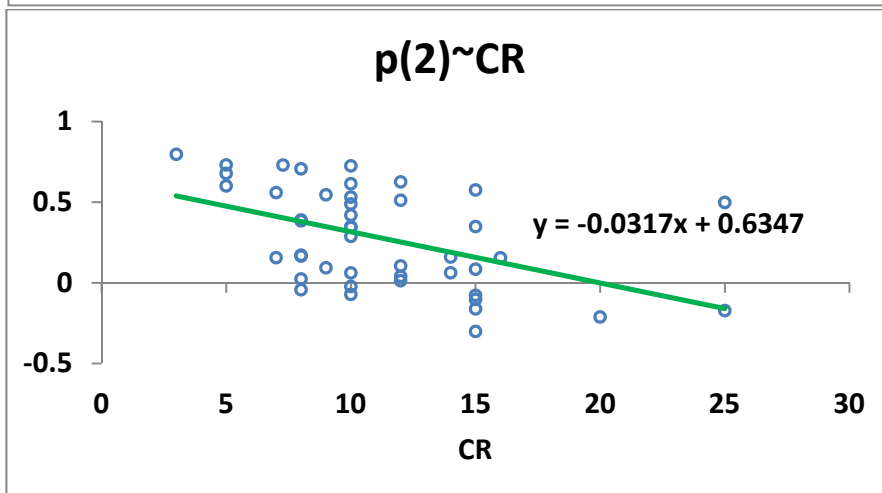
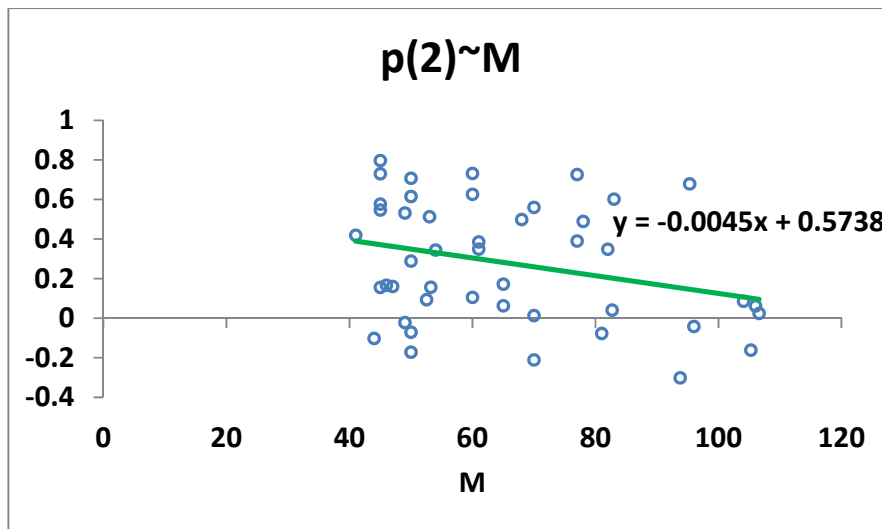
$$P(5) = 0.6319 - 0.01253 * CF - 0.0289 * basal$$

( $p < 0.05$  &  $p < 0.05$ )

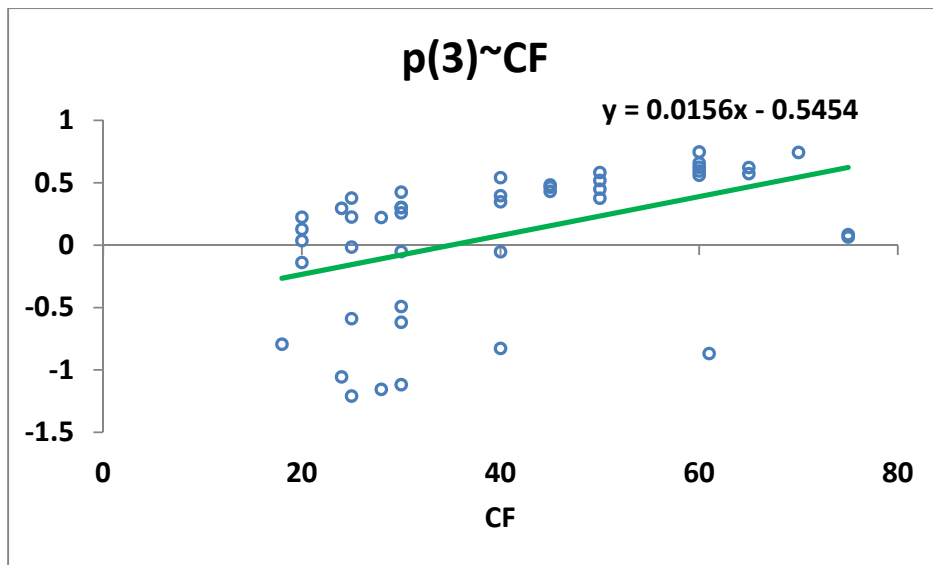
Figure 48 lists the pair plot of each multiplier against the selected predictors. The MARD and MAD of fitted prediction were  $18.8\% \pm 6.9$  and  $30.2 \pm 13.9$  mg/dl.



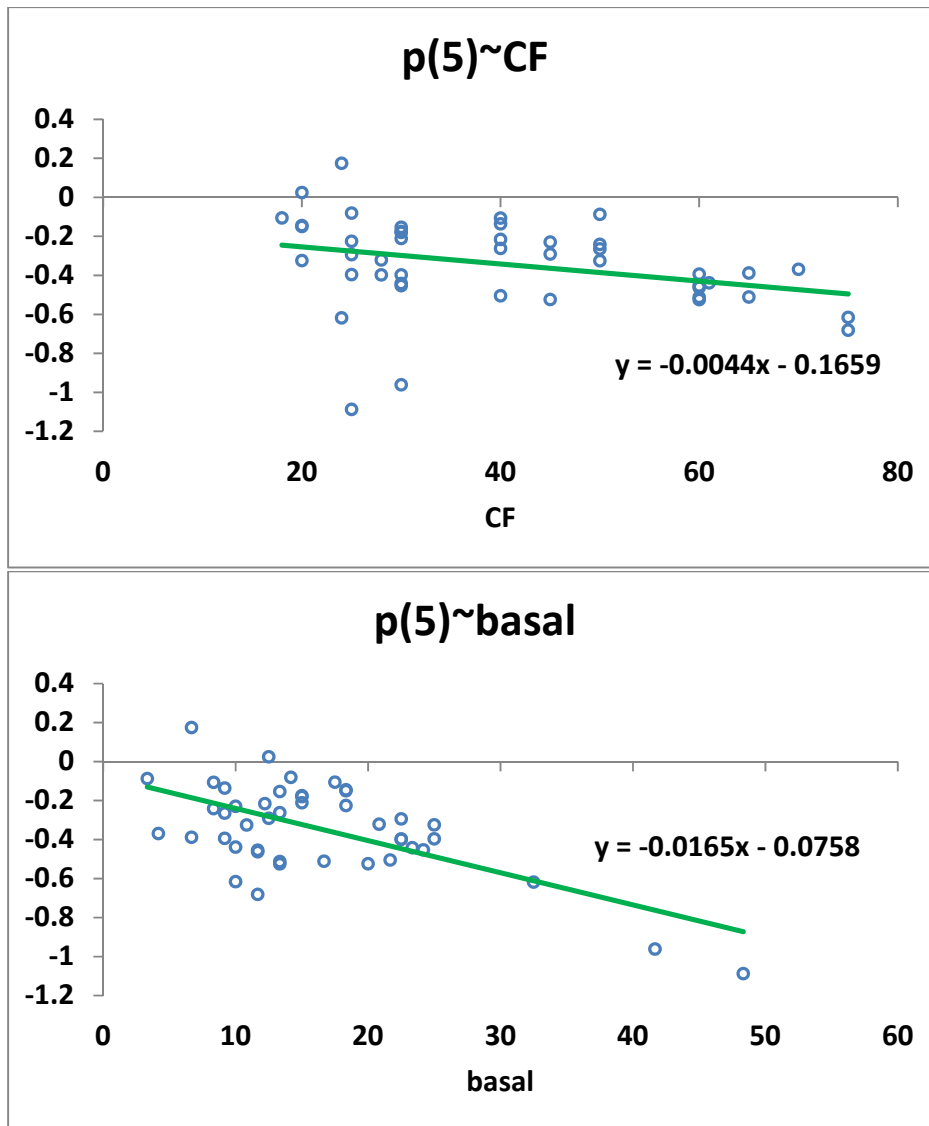
(A)



(B)



(C)



(D)

Figure 48: Tuned multipliers against the selected predictors.

### Test

The model tested in the remaining simulated segments included 2763 meals and 270774 BG points. For each segment, the multiple prediction simulations were conducted and we took the mean of the prediction error. The averaged MARD and MAD of BG prediction were  $26.9\% \pm 5.5$  and  $38.9 \pm 11.8$  mg/dl. Figure 49 shows the average MARD for each time horizon of prediction

(0-1hour, 1-2hour, 2-3hour and 3-4hour): 8.3%, 22.7%, 37.5% and 42.1%. The standard errors for each were 15.6%, 24.5%, 35.2% and 33.9%.

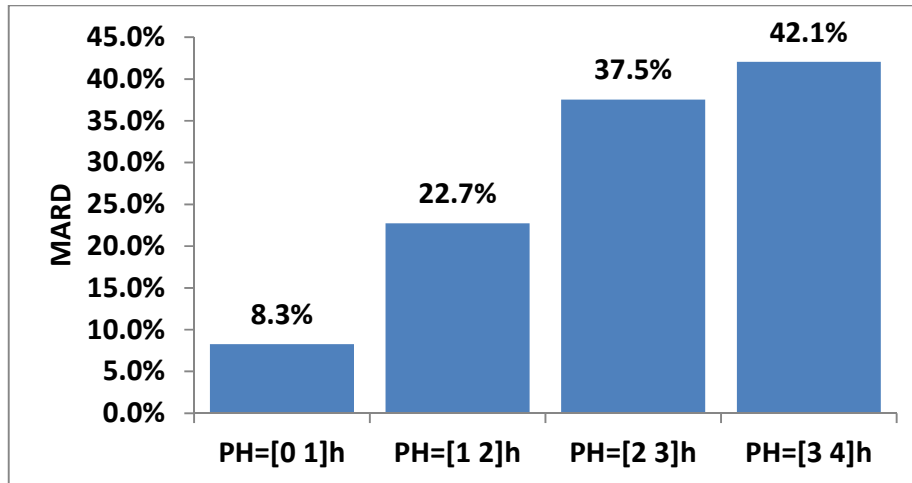


Figure 49: Distribution of MARD in 4 prediction horizon across all subjects.

We also computed the mean relative difference (MRD, referring equation 6.20) and the interquartile range for each prediction horizon was plotted in Figure 50.

$$MRD = \frac{1}{n} \sum_{i=1}^n \frac{G_{pred}(i) - G(i)}{G(i)} \quad (6.20)$$

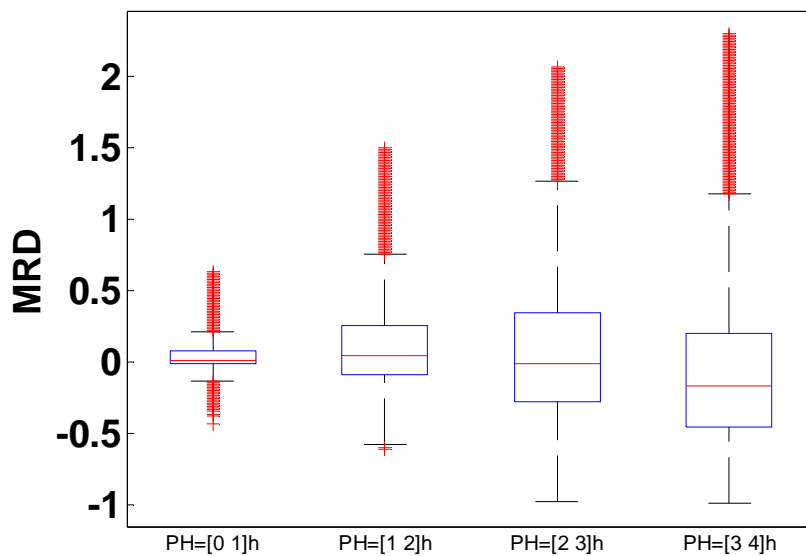


Figure 50: Interquartile range of MRD for each prediction horizon.

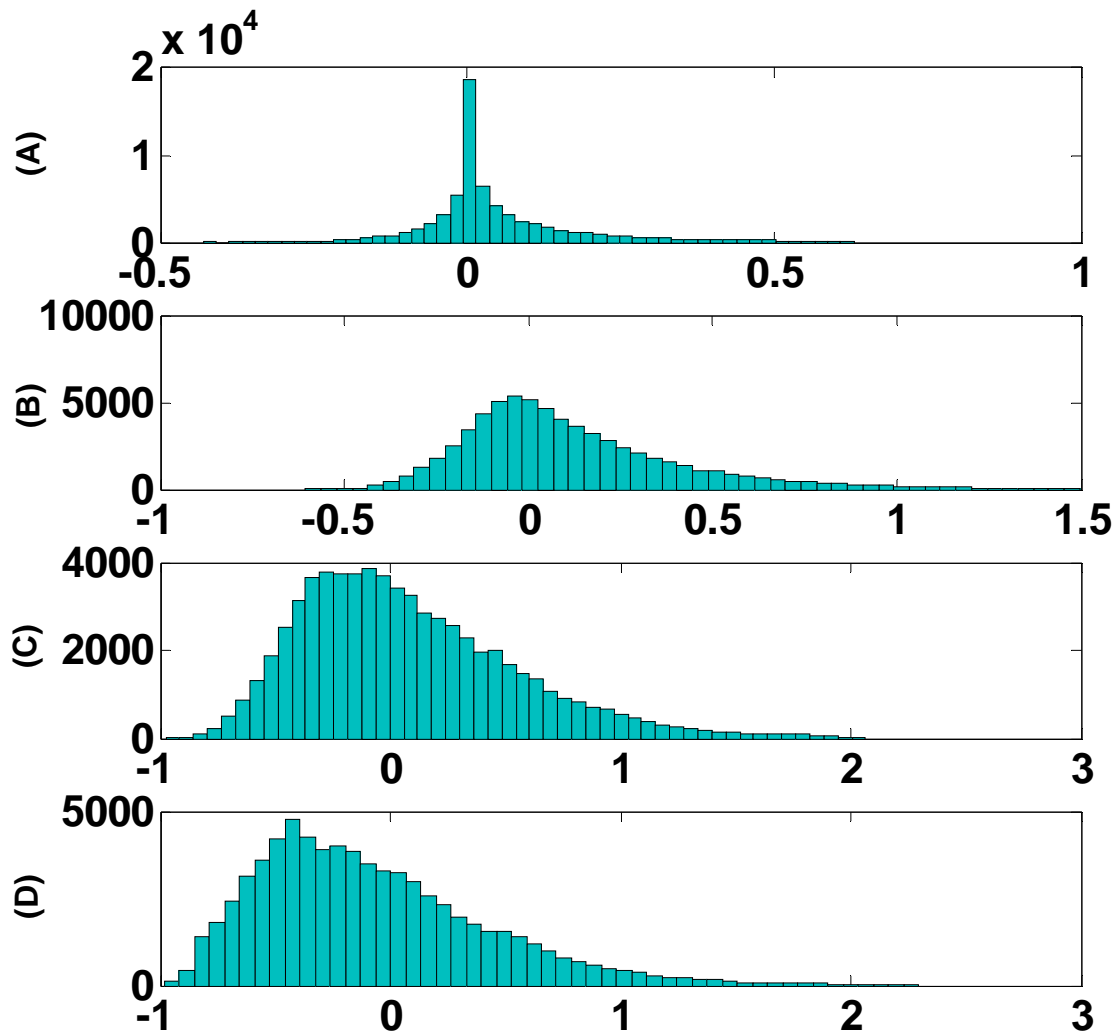


Figure 51: Distribution of MRD of different prediction horizon: (A)PH=[0 1]h, (B)PH=[1 2]h, (C)PH=[2 3]h, (D)PH=[3 4]h using the new regression model.

Compared to the training data, the prediction MARD and MAD of test data was increased by 43% and 28% respectively. The decomposition of MARD into separate prediction horizons (Figure 49) showed that the prediction error increased monotonically: the further away from the starting point, the larger the error was. Despite the satisfying accuracy in PH=[0 1]h, the average performance of BG prediction got mitigated by the error in PH=[2 3]h and PH=[3 4]h.

**Table 16: Interquartile range of MRD for each prediction horizon**

MRD	PH=[0 1]h	PH=[1 2]h	PH=[2 3]h	PH=[3 4]h
Minimum	-42.97%	-60.43%	-97.59%	-98.33%
25th Percentile	-0.58%	-8.52%	-27.13%	-44.83%
Median	1.01%	4.91%	-0.49%	-16.92%
75th Percentile	8.18%	25.15%	34.31%	20.20%
Maximum	62.96%	149.65%	206.50%	229.60%

We also applied the previous regression model (refer to Figure 39) to repeat the test. The averaged MARD and MAD of BG prediction were 29.9%±8.0 and 47.8 ±15.6 mg/dl. Figure 52 shows the average MARD for each time horizon of prediction (0-1hour, 1-2hour, 2-3hour and 3-4hour): 7.3%, 19.3%, 38.5% and 50.6%. The standard errors for each were 12.4%, 20.6%, 37.3% and 49.9%. For comparison, the result of using the old regression model is plotted as red bar.

**Table 17: Comparison of MARD using two different regression models**

	MARD	MARD [0 1]h	MARD [1 2]h	MARD [2 3]h	MARD [3 4]h
Old regression	29.9%	7.3%	19.3%	38.5%	50.6%
New regression	26.9%	8.3%	22.7%	37.5%	42.1%
t-test	p<0.05	p<0.05	p<0.05	p<0.05	p<0.05

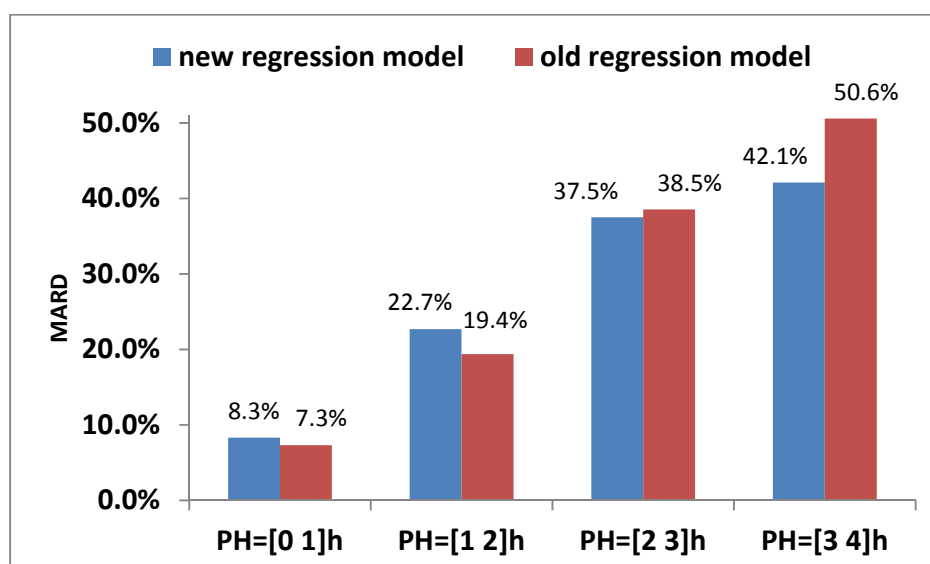


**Figure 52: Distribution of MARD in 4 prediction horizon across all subjects. Blue uses the new regression model and red uses the old regression model.**

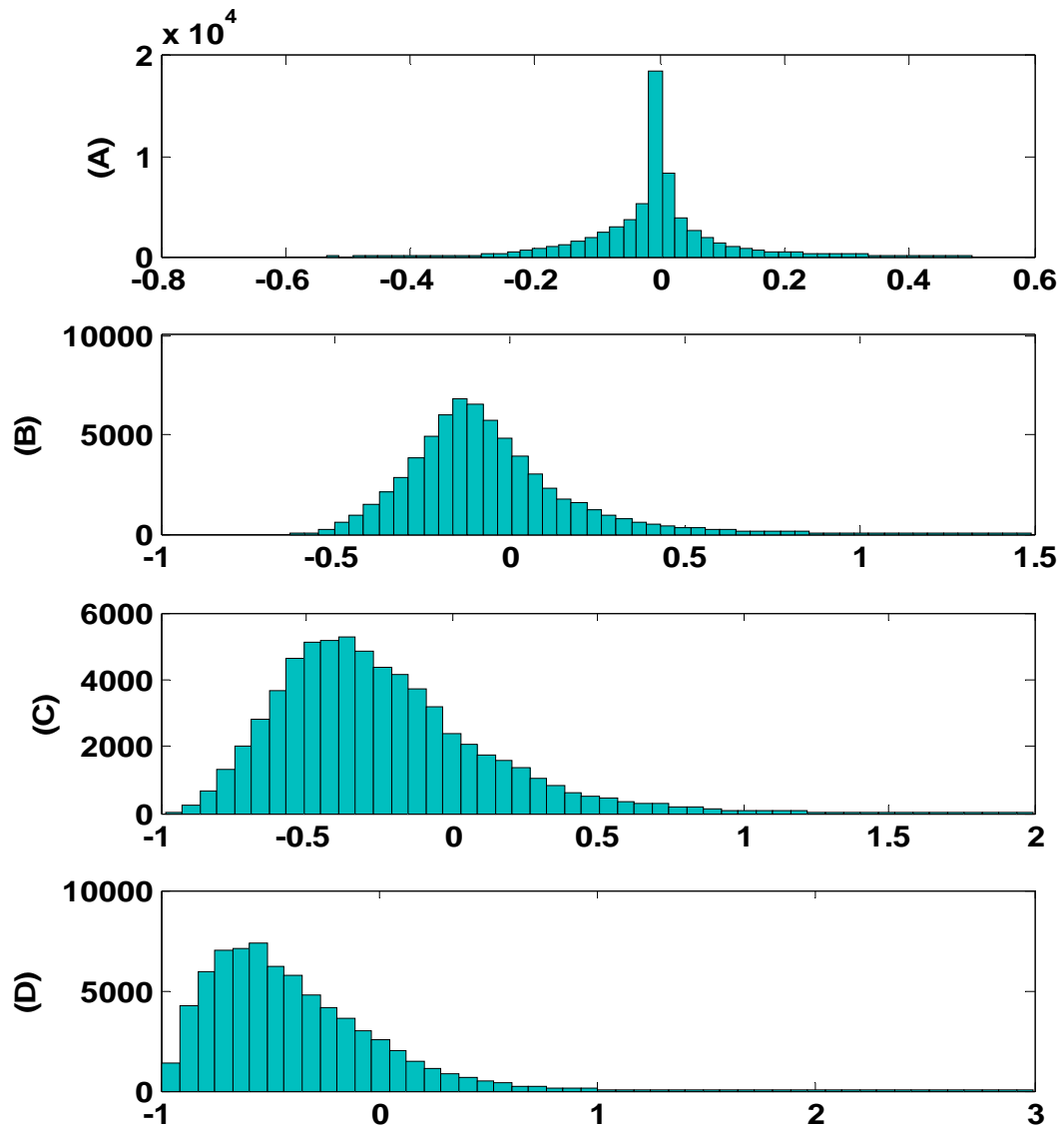


Figure 53: Distribution of MRD of different prediction horizon: (A)PH=[0 1]h, (B)PH=[1 2]h, (C)PH=[2 3]h, (D)PH=[3 4]h using old regression model.

Figure 51 shows the histogram of MRD decomposed into separate prediction horizons. The negative bias in PH=[2 3]h and PH=[3 4]h indicated BG was under predicted on average in the second half of the forecasting window. While the positive bias in PH=[0 1]h and PH=[1 2]h

implied that BG was over predicted on average in the first half of the forecasting window. This could be explained partially by the effect of delayed meal absorption, which was in line with one of the cases in pilot study (section 6.1).

Despite the negative bias, multiple outliers were located on the positive side of the MRD box plot (Figure 50). It was due to the over-corrected  $p(5)$  and  $p(2)$  that governed the glucose effectiveness ( $p_1$ ) and rate of glucose appearance ( $p_6$ ) respectively. Refer to Figure 48 (B), on the bottom left of the regression line  $P(2) \sim M$ , the predicted  $p(2)$  values were larger than the measured values. This informed an elevated rate of glucose appearance. In addition to that, the predicted  $p(5)$  values were smaller than the measured values for data points located on the right top of the regression line  $P(5) \sim CF$  in Figure 48 (D). As a result, the glucose effectiveness was underestimated for those subjects. The mixture of the two effects led to the over forecasting of BG.

Meals are a major perturbation to glucose variability. Accompanied by changes of rates of gastric emptying, as well as diurnal patterns of postprandial insulin sensitivity, they bring massive challenges to the robustness of physiological models. Regression models that linked the tuned parameters to the physiological parameters seemed mitigating the robustness of the insulin-glucose model. This increased the burdens of the gastrointestinal parameter,  $[a_1 \ a_2 \ a_d]$ , which was expected to account for the model discrepancies brought by the approximations of the regression line. Applying adaptive methodology is a way to resolve this problem. Meanwhile, a comprehensive assessment of the effect of meal composition on the post-prandial glucose excursion is anticipated.

The confounding factors underlying the inter-variability and intra-variability yanked the chain when we tried to account for the prolonged physiological changes in human body. A simple

physiological model which was designed to possess the ability to adapt to various subjects encountered a vast challenge in the realistic environment (in-vivo test). Such a traditional analytic tool alone has its limitations. With increasing number of diabetes management devices getting connected to the “cloud”, we will be exposed unprecedentedly to an enormous size of data. The solutions of diabetes management must be rethought in a bigger picture in which diabetes management devices, traditional analytics, informatics, leadership technologies, cognitive computing are married with big data. Once this field finds its position in “Web 3.0”, a game-changing breakthrough will be not far.

# Chapter 7. Conclusions and Future Work

“Essentially, all models are wrong, but some are useful” [George E. P. Box] reveals two basic facts in the context of physiological modeling: it is impossible to estimate every single parameter of the system based on in-vivo data and even if one is capable of doing that at an instant, and it is impossible to keep that capability for the next instant. Therefore, some sacrifices have to be made when modeling physiological systems. Combining subsystems into one simpler representation is one of such. The consequential reduction of the parameter set then brings more difficulty to match the model to the in-vivo data, especially when substantial inter-individual and intra-individual variability is present. To compensate for this phenomenon, one can keep track of the characteristics of the system parameters and take corresponding remedial actions. Considering the complexity of the physiology surrounding the insulin-glucose system, any closed loop system dosing insulin needs to at least be robust to these variations, and at best account for them.

Traditional methods of insulin sensitivity quantification usually require frequent blood sampling to measure the plasma insulin and glucose concentration. In this dissertation, we proposed an innovative technique, which enables online SI tracking ( $SI_{KF}$ ) using CGM and pump data. The validation of KF-generated SI against minimal-model fitted SI showed a significantly

high correlation. We believe this technique can push the boundaries of fast and easy access to SI as an auxiliary to the treatment of Type 1 diabetics in their daily lives.

Compared to the traditional SI indexing, the dynamic  $SI_{KF}$  provides a more granular insight into patient's insulin-glucose kinetics. An interesting application of  $SI_{KF}$  could be a hypoglycemia/hyperglycemia warning system. For example, if an elevated  $SI_{KF}$  (above a certain threshold) is detected, a hypo-alarm indicator will be turned on and the patient can adjust their insulin infusion rate accordingly.  $SI_{KF}$  can also be integrated into the "Safety Service Module" <sup>110</sup> to facilitate the traffic light decision. Last but not least, since  $SI_{KF}$  is more tolerant of the data structure than the traditional SI indexing (for example,  $SI_{mm}$  needs OGTT data), the vast majority of modern T1D clinical data can be analyzed by using this technique.

As an application of  $SI_{KF}$ , we analyzed a set of clinical data collected surrounding the menstrual cycle and substantiated the hypothesis that a subset of premenopausal women with T1DM would experience a decrease in insulin sensitivity during the second half of the menstrual cycle (luteal phase). Our ultimate goal was to develop an advisory system aimed at improving the diabetes control in younger women experiencing BG variation related to menstrual cycle. The future work includes: 1) develop detection algorithms to inform the patients of abnormal BG fluctuations related to menstrual cycle; 2) train a model to project the BG based on the historical data and the menstrual cycle parameters (date of menses, average length of cycle and timing of ovulation); 3) design a user-friendly interface for patients to better interact with the device.

By using traditional SI extraction technique, we confirmed that after moderate intensity exercise and high intensity exercise, whole-body insulin sensitivity derived by the oral minimal model was improved. OGTT is a pragmatic tool for measuring insulin sensitivity in early phase of

exercise effect, however,  $SI_{KF}$  is considered a more appropriate tool for measuring SI in both early and late phase of exercise effect. Possible future work on this project would involve extracting SI from clinical data involving physical activity and identify patterns that can be exploited to help improving glycemic control.

We studied the short-term (up to 45 minutes) BG prediction performance based on physiological modeling and explored the impact of different structural designs (full model, feed-forward, with and without SI tracking) on BG prediction. We found that the short-term BG prediction power got improved by extracting the meal and insulin transportation as feed-forward compartments. The “LOG-Core model with SI” implementation enabled online estimation of SI maintaining physiologically reasonable values meanwhile provided a relatively accurate way to carry out the BG prediction.

Finally, as a robust long-term prediction of BG is indispensable in designing a MPC based bolus advisory system (Patek <sup>114</sup>), we have tied, in part, the inter-individual and intra-individual variability to the patient’s physiological parameters, leaving the unaccounted uncertainties to the gastrointestinal models. Future work aims at identifying (tuning) the gastrointestinal parameters in an adaptive way. One approach is run-to-run (R2R) control, namely, adjusting the parameter based on the outcome from the last run. The choice of time window for each run and the aggressiveness for the tuning are subject to study. A more intensive approach can be online tuning: the parameter is tuned at decision time considering the historical meal announcement and the computed glucose changing rate.

The invention of the LOG model was originated in the SI tracking research. We found later its desirable properties in constructing the glucose control objective function in risk space as described in Patek et al. 2014 paper <sup>114</sup> that the objective function in risk space allowed for

appropriate balance between hypo and hyperglycemic risk. Kovatchev<sup>133</sup> published a BG risk function that has set standards for a variety of aspects such as BG risk analysis and prediction of extreme BG variations. We are interested in comparing the performance of MPC control by using the LOG model-based control objective function to that using the BG risk function.

The main contribution of this dissertation was the formalization of a series of techniques developed to characterize parameter uncertainties of the insulin-glucose physiological system, for the purpose of enhancing model based insulin dosing strategies in diabetes. Through this project, we have strived to intertwine knowledge and techniques from multiple disciplines (physiology, system engineering, automatic control and medicine to cite but a few) and constantly applied newly developed techniques to the design and testing of medical devices. This interface, often referred to as translational research, is where the proverbial rubber meets the road. It has been my great privilege and honor being a scientist and engineer of diabetes technology. I look forward to continuing my dedications to this field.

# References

1. Trautner, C., Icks, A., Haastert, B., Plum, F. & Berger, M. Incidence of Blindness in Relation to Diabetes: A population-based study. *Diabetes Care* **20**, 1147–1153 (1997).
2. Buse, J. B. *et al.* Primary Prevention of Cardiovascular Diseases in People With Diabetes Mellitus A scientific statement from the American Heart Association and the American Diabetes Association. *Diabetes Care* **30**, 162–172 (2007).
3. Dyck, P. J. *et al.* The prevalence by staged severity of various types of diabetic neuropathy, retinopathy, and nephropathy in a population-based cohort The Rochester Diabetic Neuropathy Study. *Neurology* **43**, 817–817 (1993).
4. Mogensen, C. E., Christensen, C. K. & Vittinghus, E. The Stages in Diabetic Renal Disease: With Emphasis on the Stage of Incipient Diabetic Nephropathy. *Diabetes* **32**, 64–78 (1983).
5. Pecoraro, R. E., Reiber, G. E. & Burgess, E. M. Pathways to Diabetic Limb Amputation: Basis for Prevention. *Diabetes Care* **13**, 513–521 (1990).
6. Zoungas, S. *et al.* Severe Hypoglycemia and Risks of Vascular Events and Death. *N. Engl. J. Med.* **363**, 1410–1418 (2010).
7. Cox, D. J. *et al.* Frequency of severe hypoglycemia in insulin-dependent diabetes mellitus can be predicted from self-monitoring blood glucose data. *J. Clin. Endocrinol. Metab.* **79**, 1659–1662 (1994).
8. Rovet, J. F. & Ehrlich, R. M. The effect of hypoglycemic seizures on cognitive function in children with diabetes: A 7-year prospective study. *J. Pediatr.* **134**, 503–506 (1999).

9. Schultes, B. *et al.* Modulation of Hunger by Plasma Glucose and Metformin. *J. Clin. Endocrinol. Metab.* **88**, 1133–1141 (2003).
10. Exercise and Type 2 Diabetes: *Med. Sci. Sports Exerc.* **32**, 1345–1360 (2000).
11. Hu, F. B. *et al.* Diet, Lifestyle, and the Risk of Type 2 Diabetes Mellitus in Women. *N. Engl. J. Med.* **345**, 790–797 (2001).
12. Buchwald, H. *et al.* Weight and Type 2 Diabetes after Bariatric Surgery: Systematic Review and Meta-analysis. *Am. J. Med.* **122**, 248–256.e5 (2009).
13. Harris, M. I. Frequency of Blood Glucose Monitoring in Relation to Glycemic Control in Patients With Type 2 Diabetes. *Diabetes Care* **24**, 979–982 (2001).
14. Bock, G. *et al.* Pathogenesis of Pre-Diabetes Mechanisms of Fasting and Postprandial Hyperglycemia in People With Impaired Fasting Glucose and/or Impaired Glucose Tolerance. *Diabetes* **55**, 3536–3549 (2006).
15. Williams, D. E. *et al.* Prevalence of Impaired Fasting Glucose and Its Relationship With Cardiovascular Disease Risk Factors in US Adolescents, 1999–2000. *Pediatrics* **116**, 1122–1126 (2005).
16. DeFronzo, R. A. & Abdul-Ghani, M. Assessment and Treatment of Cardiovascular Risk in Prediabetes: Impaired Glucose Tolerance and Impaired Fasting Glucose. *Am. J. Cardiol.* **108**, 3B–24B (2011).
17. Boney, C. M., Verma, A., Tucker, R. & Vohr, B. R. Metabolic Syndrome in Childhood: Association With Birth Weight, Maternal Obesity, and Gestational Diabetes Mellitus. *Pediatrics* **115**, e290–e296 (2005).
18. Dall, T. M. *et al.* The Economic Burden of Elevated Blood Glucose Levels in 2012: Diagnosed and Undiagnosed Diabetes, Gestational Diabetes Mellitus, and Prediabetes. *Diabetes Care* **37**, 3172–3179 (2014).

19. Association, A. D. Economic Costs of Diabetes in the U.S. in 2007. *Diabetes Care* **31**, 596–615 (2008).
20. Association, A. D. Economic Costs of Diabetes in the U.S. in 2012. *Diabetes Care* DC\_122625 (2013). doi:10.2337/dc12-2625
21. Alex, A. D. A. 1701 N. B. S., ria & 1-800-Diabetes, V. 22311. Type 1 Diabetes. *American Diabetes Association* at <<http://www.diabetes.org/diabetes-basics/type-1/>>
22. Type 2 Diabetes Statistics and Facts. *Healthline* at <<http://www.healthline.com/health/type-2-diabetes/statistics>>
23. DeSisto, C. L., Kim, S. Y. & Sharma, A. J. Prevalence Estimates of Gestational Diabetes Mellitus in the United States, Pregnancy Risk Assessment Monitoring System (PRAMS), 2007–2010. *Prev. Chronic. Dis.* **11**, (2014).
24. MD, R. M. B. By Robert M. Berne MD *Physiology*, 4e. (Mosby, 1997).
25. admin. Introduction to Modeling in Physiology and Medicine | Medical Books. at <<http://medicalibooks.blogspot.com/2011/07/introduction-to-modeling-in-physiology.html>>
26. Krewski, D., Withey, J. R., Ku, L. F. & Andersen, M. E. Applications of physiologic pharmacokinetic modeling in carcinogenic risk assessment. *Environ. Health Perspect.* **102**, 37–50 (1994).
27. Zhang, Z. & Kleinstreuer, C. Transient airflow structures and particle transport in a sequentially branching lung airway model. *Phys. Fluids 1994-Present* **14**, 862–880 (2002).
28. Ljung, L. in *Signal Analysis and Prediction* (eds. Procházka, A., Uhlíř, J., Rayner, P. W. J. & Kingsbury, N. G.) 163–173 (Birkhäuser Boston, 1998). at <[http://link.springer.com/chapter/10.1007/978-1-4612-1768-8\\_11](http://link.springer.com/chapter/10.1007/978-1-4612-1768-8_11)>
29. Quandt, R. E. The Estimation of the Parameters of a Linear Regression System Obeying Two Separate Regimes. *J. Am. Stat. Assoc.* **53**, 873–880 (1958).

30. Toda, T., Black, A. W. & Tokuda, K. Voice Conversion Based on Maximum-Likelihood Estimation of Spectral Parameter Trajectory. *IEEE Trans. Audio Speech Lang. Process.* **15**, 2222–2235 (2007).
31. Young, P. C. An instrumental variable method for real-time identification of a noisy process. *Automatica* **6**, 271–287 (1970).
32. Zhu, X., Wang, S., Li, P. & Wozny, G. Parameter estimation for nonlinear dynamic systems from a feedback control viewpoint. in *International Conference on Control and Automation, 2005. ICCA '05* **1**, 119–124 Vol. 1 (2005).
33. Zhang, C. P., Liu, J. Z., Sharkh, S. M. & Zhang, C. N. Identification of dynamic model parameters for lithium-ion batteries used in hybrid electric vehicles. (2010). at <http://eprints.soton.ac.uk/73265/>
34. Rizza, R. A., Cryer, P. E. & Gerich, J. E. Role of Glucagon, Catecholamines, and Growth Hormone in Human Glucose Counterregulation. *J. Clin. Invest.* **64**, 62–71 (1979).
35. Feo, P. D. *et al.* Contribution of cortisol to glucose counterregulation in humans. *Am. J. Physiol. - Endocrinol. Metab.* **257**, E35–E42 (1989).
36. Bolli, G. *et al.* Abnormal Glucose Counterregulation in Insulin-dependent Diabetes Mellitus: Interaction of Anti-Insulin Antibodies and Impaired Glucagon and Epinephrine Secretion. *Diabetes* **32**, 134–141 (1983).
37. Nauck, M. A. *et al.* Effects of glucagon-like peptide 1 on counterregulatory hormone responses, cognitive functions, and insulin secretion during hyperinsulinemic, stepped hypoglycemic clamp experiments in healthy volunteers. *J. Clin. Endocrinol. Metab.* **87**, 1239–1246 (2002).

38. Manicardi, V., Camellini, L., Bellodi, G., Coscelli, C. & Ferrannini, E. Evidence for an Association of High Blood Pressure and Hyperinsulinemia in Obese Man. *J. Clin. Endocrinol. Metab.* **62**, 1302–1304 (1986).
39. Weyer, C. *et al.* Hypoadiponectinemia in Obesity and Type 2 Diabetes: Close Association with Insulin Resistance and Hyperinsulinemia. *J. Clin. Endocrinol. Metab.* **86**, 1930–1935 (2001).
40. Eom, C.-S. *et al.* Metabolic Syndrome and Accompanying Hyperinsulinemia have Favorable Effects on Lower Urinary Tract Symptoms in a Generally Healthy Screened Population. *J. Urol.* **186**, 175–179 (2011).
41. DeFronzo, R. A., Tobin, J. D. & Andres, R. Glucose clamp technique: a method for quantifying insulin secretion and resistance. *Am. J. Physiol.* **237**, E214–223 (1979).
42. Bergman, R. N., Ider, Y. Z., Bowden, C. R. & Cobelli, C. Quantitative estimation of insulin sensitivity. *Am. J. Physiol. - Endocrinol. Metab.* **236**, E667 (1979).
43. Man, C. D. *et al.* Minimal model estimation of glucose absorption and insulin sensitivity from oral test: validation with a tracer method. *Am. J. Physiol. - Endocrinol. Metab.* **287**, E637–E643 (2004).
44. Harashima, S. *et al.* Self-monitoring of blood glucose (SMBG) improves glycaemic control in oral hypoglycaemic agent (OHA)-treated type 2 diabetes (SMBG-OHA study). *Diabetes Metab. Res. Rev.* **29**, 77–84 (2013).
45. Benjamin, E. M. Self-Monitoring of Blood Glucose: The Basics. *Clin. Diabetes* **20**, 45–47 (2002).
46. Kovatchev, B. P., Patek, S. D., Ortiz, E. A. & Breton, M. D. Assessing Sensor Accuracy for Non-Adjunct Use of Continuous Glucose Monitoring. *Diabetes Technol. Ther.* **17**, 177–186 (2014).

47. Facchinetti, A., Sparacino, G. & Cobelli, C. Reconstruction of glucose in plasma from interstitial fluid continuous glucose monitoring data: role of sensor calibration. *J. Diabetes Sci. Technol.* **1**, 617–623 (2007).
48. Ludwig, V., Heinemann, L. & Glucose Monitoring Study Group. Continuous glucose monitoring with glucose sensors: calibration and assessment criteria. *Diabetes Technol. Ther.* **5**, 572–586 (2003).
49. Rossetti, P., Bondia, J., Vehí, J. & Fanelli, C. G. Estimating Plasma Glucose from Interstitial Glucose: The Issue of Calibration Algorithms in Commercial Continuous Glucose Monitoring Devices. *Sensors* **10**, 10936–10952 (2010).
50. Nielsen, J. K. *et al.* Continuous Glucose Monitoring in Interstitial Subcutaneous Adipose Tissue and Skeletal Muscle Reflects Excursions in Cerebral Cortex. *Diabetes* **54**, 1635–1639 (2005).
51. Basu, A. *et al.* Time Lag of Glucose From Intravascular to Interstitial Compartment in Type 1 Diabetes. *J. Diabetes Sci. Technol.* **9**, 63–68 (2015).
52. Barry Keenan, D., Mastrototaro, J. J., Weinzimer, S. A. & Steil, G. M. Interstitial fluid glucose time-lag correction for real-time continuous glucose monitoring. *Biomed. Signal Process. Control* **8**, 81–89 (2013).
53. Breton, M. & Kovatchev, B. Analysis, Modeling, and Simulation of the Accuracy of Continuous Glucose Sensors. *J. Diabetes Sci. Technol.* **2**, 853–862 (2008).
54. Facchinetti, A., Sparacino, G. & Cobelli, C. An Online Self-Tunable Method to Denoise CGM Sensor Data. *IEEE Trans. Biomed. Eng.* **57**, 634–641 (2010).
55. Chase, J. G. *et al.* Integral-based filtering of continuous glucose sensor measurements for glycaemic control in critical care. *Comput. Methods Programs Biomed.* **82**, 238–247 (2006).

56. Knobbe, E. J. & Buckingham, B. The extended Kalman filter for continuous glucose monitoring. *Diabetes Technol. Ther.* **7**, 15–27 (2005).
57. Tamborlane, W. V., Sherwin, R. S., Genel, M. & Felig, P. Reduction to Normal of Plasma Glucose in Juvenile Diabetes by Subcutaneous Administration of Insulin with a Portable Infusion Pump. *N. Engl. J. Med.* **300**, 573–578 (1979).
58. Chait, J. Insulin Pumps. *Diabetes Self-Management* at <http://www.diabetesselfmanagement.com/diabetes-resources/tools-tech/insulin-pumps/>
59. Wainstein, J. *et al.* Insulin pump therapy vs. multiple daily injections in obese Type 2 diabetic patients. *Diabet. Med. J. Br. Diabet. Assoc.* **22**, 1037–1046 (2005).
60. Karagianni, P. *et al.* Continuous subcutaneous insulin infusion versus multiple daily injections. *Hippokratia* **13**, 93–96 (2009).
61. Bolli, G. B. *et al.* Comparison of a Multiple Daily Insulin Injection Regimen (Basal Once-Daily Glargine Plus Mealtime Lispro) and Continuous Subcutaneous Insulin Infusion (Lispro) in Type 1 Diabetes A randomized open parallel multicenter study. *Diabetes Care* **32**, 1170–1176 (2009).
62. Rahaghi, F. N. & Gough, D. A. Blood glucose dynamics. *Diabetes Technol. Ther.* **10**, 81–94 (2008).
63. Clearinghouse, T. N. N. D. I. What I Need to Know about Diabetes medicines- Types of Insulin- Insert C. at [http://diabetes.niddk.nih.gov/dm/pubs/medicines\\_ez/insert\\_C.aspx](http://diabetes.niddk.nih.gov/dm/pubs/medicines_ez/insert_C.aspx)
64. Kovatchev, B. P., Breton, M. D., Cobelli, C. & Man, C. D. Method, System and Computer Simulation Environment for Testing of Monitoring and Control Strategies in Diabetes. (2010). at <http://www.google.com/patents/US20100179768>
65. Man, C. D., Rizza, R. A. & Cobelli, C. Meal Simulation Model of the Glucose-Insulin System. *IEEE Trans. Biomed. Eng.* **54**, 1740–1749 (2007).

66. Man, C. D. *et al.* The UVA/PADOVA Type 1 Diabetes Simulator New Features. *J. Diabetes Sci. Technol.* **8**, 26–34 (2014).
67. Avanzolini, G., Barbini, P., Cappello, A., Cevenini, G. & Chiari, L. A new approach for tracking respiratory mechanical parameters in real-time. *Ann. Biomed. Eng.* **25**, 154–163 (1997).
68. Caumo, A., Bergman, R. N. & Cobelli, C. Insulin Sensitivity from Meal Tolerance Tests in Normal Subjects: A Minimal Model Index. *J. Clin. Endocrinol. Metab.* **85**, 4396–4402 (2000).
69. Man, C. D., Caumo, A. & Cobelli, C. The oral glucose minimal model: Estimation of insulin sensitivity from a meal test. *IEEE Trans. Biomed. Eng.* **49**, 419–429 (2002).
70. Man, C. D. *et al.* Insulin sensitivity by oral glucose minimal models: validation against clamp. *Am. J. Physiol. - Endocrinol. Metab.* **289**, E954–E959 (2005).
71. Schiavon, M., Man, C. D., Kudva, Y. C., Basu, A. & Cobelli, C. Quantitative Estimation of Insulin Sensitivity in Type 1 Diabetic Subjects Wearing a Sensor-Augmented Insulin Pump. *Diabetes Care* **37**, 1216–1223 (2014).
72. Boden, G., Chen, X. & Urbain, J. L. Evidence for a Circadian Rhythm of Insulin Sensitivity in Patients With NIDDM Caused by Cyclic Changes in Hepatic Glucose Production. *Diabetes* **45**, 1044–1050 (1996).
73. Pate, R. R. *et al.* Physical activity and public health. A recommendation from the Centers for Disease Control and Prevention and the American College of Sports Medicine. *JAMA* **273**, 402–407 (1995).
74. Pereira, M. A. *et al.* Fast-food habits, weight gain, and insulin resistance (the CARDIA study): 15-year prospective analysis. *The Lancet* **365**, 36–42 (2005).
75. Pilonetto, G., Caumo, A. & Cobelli, C. Dynamic insulin sensitivity index: importance in diabetes. *Am. J. Physiol. - Endocrinol. Metab.* **298**, E440–E448 (2010).

76. Lin, J. *et al.* Stochastic modelling of insulin sensitivity and adaptive glycemic control for critical care. *Comput. Methods Programs Biomed.* **89**, 141–152 (2008).
77. Man, C. D., Camilleri, M. & Cobelli, C. A System Model of Oral Glucose Absorption: Validation on Gold Standard Data. *IEEE Trans. Biomed. Eng.* **53**, 2472–2478 (2006).
78. Grosman, B., Dassau, E., Zisser, H. C., Jovanovic, L. & Doyle, F. J., 3rd. Zone model predictive control: a strategy to minimize hyper- and hypoglycemic events. *J. Diabetes Sci. Technol.* **4**, 961–975 (2010).
79. Continuous Glucose Monitoring and Intensive Treatment of Type 1 Diabetes. *N. Engl. J. Med.* **359**, 1464–1476 (2008).
80. Kovatchev, B. P., Breton, M., Man, C. D. & Cobelli, C. In silico preclinical trials: a proof of concept in closed-loop control of type 1 diabetes. *J. Diabetes Sci. Technol.* **3**, 44–55 (2009).
81. Clarke, W. L. *et al.* Closed-loop artificial pancreas using subcutaneous glucose sensing and insulin delivery and a model predictive control algorithm: the Virginia experience. *J. Diabetes Sci. Technol.* **3**, 1031–1038 (2009).
82. Voskanyan, G., Keenan, D. B., Mastrototaro, J. J. & Steil, G. M. Putative Delays in Interstitial Fluid (ISF) Glucose Kinetics Can Be Attributed to the Glucose Sensing Systems Used to Measure Them Rather than the Delay in ISF Glucose Itself. *J. Diabetes Sci. Technol.* **1**, 639–644 (2007).
83. Kamath, A., Mahalingam, A. & Brauker, J. Analysis of Time Lags and Other Sources of Error of the DexCom SEVEN Continuous Glucose Monitor. *Diabetes Technol. Ther.* **11**, 689–695 (2009).
84. Steil, G. M., Rebrin, K., Mastrototaro, J., Bernaba, B. & Saad, M. F. Determination of Plasma Glucose During Rapid Glucose Excursions with a Subcutaneous Glucose Sensor. *Diabetes Technol. Ther.* **5**, 27–31 (2003).

85. Kovatchev, B. P., Cox, D. J., Gonder-Frederick, L. A. & Clarke, W. Symmetrization of the Blood Glucose Measurement Scale and Its Applications. *Diabetes Care* **20**, 1655–1658 (1997).
86. Borghouts, L. B. & Keizer, H. A. Exercise and insulin sensitivity: a review. *Int. J. Sports Med.* **21**, 1–12 (2000).
87. Goodyear, L. J., PhD & Kahn, B. B., MD. Exercise, Glucose Transport, and Insulin Sensitivity. *Annu. Rev. Med.* **49**, 235–261 (1998).
88. McMahon, S. K. *et al.* Glucose Requirements to Maintain Euglycemia after Moderate-Intensity Afternoon Exercise in Adolescents with Type 1 Diabetes Are Increased in a Biphasic Manner. *J. Clin. Endocrinol. Metab.* **92**, 963–968 (2007).
89. Widmaier, E., Raff, H. & Strang, K. *Vander's Human Physiology: The Mechanisms of Body Function.* (McGraw-Hill Science/Engineering/Math, 2013).
90. Impact of Gender, Menstrual Cycle Phase, and Oral Contracept... : Psychosomatic Medicine. *LWW* at  
<[http://journals.lww.com/psychosomaticmedicine/Fulltext/1999/03000/Impact\\_of\\_Gender,\\_Menstrual\\_Cycle\\_Phase,\\_and\\_Oral.6.aspx](http://journals.lww.com/psychosomaticmedicine/Fulltext/1999/03000/Impact_of_Gender,_Menstrual_Cycle_Phase,_and_Oral.6.aspx)>
91. Goldner, W. S., Kraus, V. L., Sivitz, W. I., Hunter, S. K. & Dillon, J. S. Cyclic changes in glycemia assessed by continuous glucose monitoring system during multiple complete menstrual cycles in women with type 1 diabetes. *Diabetes Technol. Ther.* **6**, 473–480 (2004).
92. Trout, K. K. *et al.* Menstrual cycle effects on insulin sensitivity in women with type 1 diabetes: a pilot study. *Diabetes Technol. Ther.* **9**, 176–182 (2007).
93. Pulido, J. M. E. & Salazar, M. A. Changes in Insulin Sensitivity, Secretion and Glucose Effectiveness During Menstrual Cycle. *Arch. Med. Res.* **30**, 19–22 (1999).

94. Bertoli, A., Fusco, A., Greco, A. V. & Lauro, R. Differences in Insulin Receptors between Men and Menstruating Women and Influence of Sex Hormones on Insulin Binding during the Menstrual Cycle. *J. Clin. Endocrinol. Metab.* **50**, 246–250 (1980).
95. Moore, P., Kolterman, O., Weyant, J. & Olefsky, J. M. Insulin binding in human pregnancy: comparisons to the postpartum, luteal, and follicular states. *J. Clin. Endocrinol. Metab.* **52**, 937–941 (1981).
96. Marsden, P. J., Murdoch, A. & Taylor, R. Adipocyte insulin action during the normal menstrual cycle. *Hum. Reprod.* **11**, 968–974 (1996).
97. Menstruation. *Simple English Wikipedia, the free encyclopedia* (2015). at <http://simple.wikipedia.org/w/index.php?title=Menstruation&oldid=5034150>
98. Seals, D. R. *et al.* Glucose tolerance in young and older athletes and sedentary men. *J. Appl. Physiol.* **56**, 1521–1525 (1984).
99. Hardin, D. S. *et al.* Mechanisms of enhanced insulin sensitivity in endurance-trained athletes: effects on blood flow and differential expression of GLUT 4 in skeletal muscles. *J. Clin. Endocrinol. Metab.* **80**, 2437–2446 (1995).
100. Devlin, J. T., Hirshman, M., Horton, E. D. & Horton, E. S. Enhanced Peripheral and Splanchnic Insulin Sensitivity in NIDDM Men After Single Bout of Exercise. *Diabetes* **36**, 434–439 (1987).
101. Rynders, C. A. *et al.* Effects of exercise intensity on postprandial improvement in glucose disposal and insulin sensitivity in prediabetic adults. *J. Clin. Endocrinol. Metab.* **99**, 220–228 (2014).
102. Rose, A. J., Howlett, K., King, D. S. & Hargreaves, M. Effect of prior exercise on glucose metabolism in trained men. *Am. J. Physiol. - Endocrinol. Metab.* **281**, E766–E771 (2001).

103. Holtz, K. A., Stephens, B. R., Sharoff, C. G., Chipkin, S. R. & Braun, B. The effect of carbohydrate availability following exercise on whole-body insulin action. *Appl. Physiol. Nutr. Metab. Physiol. Appliquée Nutr. Métabolisme* **33**, 946–956 (2008).
104. Cameron, F., Niemeyer, G., Gundy-Burlet, K. & Buckingham, B. Statistical Hypoglycemia Prediction. *J. Diabetes Sci. Technol. Online* **2**, 612–621 (2008).
105. Sparacino, G. *et al.* Glucose Concentration can be Predicted Ahead in Time From Continuous Glucose Monitoring Sensor Time-Series. *IEEE Trans. Biomed. Eng.* **54**, 931–937 (2007).
106. Pappada, S. M., Cameron, B. D. & Rosman, P. M. Development of a Neural Network for Prediction of Glucose Concentration in Type 1 Diabetes Patients. *J. Diabetes Sci. Technol. Online* **2**, 792–801 (2008).
107. Pérez-Gandía, C. *et al.* Artificial neural network algorithm for online glucose prediction from continuous glucose monitoring. *Diabetes Technol. Ther.* **12**, 81–88 (2010).
108. Kuure-Kinsey, M., Palerm, C. C. & Bequette, B. W. A dual-rate Kalman filter for continuous glucose monitoring. *Conf. Proc. Annu. Int. Conf. IEEE Eng. Med. Biol. Soc. IEEE Eng. Med. Biol. Soc. Conf.* **1**, 63–66 (2006).
109. Palerm, C. C., Willis, J. P., Desemone, J. & Bequette, B. W. Hypoglycemia prediction and detection using optimal estimation. *Diabetes Technol. Ther.* **7**, 3–14 (2005).
110. Hughes, C. S., Patek, S. D., Breton, M. D. & Kovatchev, B. P. Hypoglycemia prevention via pump attenuation and red-yellow-green ‘traffic’ lights using continuous glucose monitoring and insulin pump data. *J. Diabetes Sci. Technol.* **4**, 1146–1155 (2010).
111. Chase, J. G. *et al.* Physiological modeling, tight glycemic control, and the ICU clinician: what are models and how can they affect practice? *Ann. Intensive Care* **1**, 1–8 (2011).

112. Pillonetto, G., Sparacino, G. & Cobelli, C. Numerical non-identifiability regions of the minimal model of glucose kinetics: superiority of Bayesian estimation. *Math. Biosci.* **184**, 53–67 (2003).
113. Hann, C. E. *et al.* Integral-based parameter identification for long-term dynamic verification of a glucose–insulin system model. *Comput. Methods Programs Biomed.* **77**, 259–270 (2005).
114. Stephen, P. Model-Based Control of Type I Diabetes in Risk Space. in (ed. Edward, B.) 237–242 (2014). doi:10.3182/20140824-6-ZA-1003.02105
115. Breton, M. D. Physical Activity—The Major Unaccounted Impediment to Closed Loop Control. *J. Diabetes Sci. Technol. Online* **2**, 169–174 (2008).
116. Stengel, R. F. *Optimal Control and Estimation*. (Courier Corporation, 2012).
117. Youqing Wang, X. W. A Novel Adaptive-Weighted-Average Framework for Blood Glucose Prediction. *Diabetes Technol. Amp Ther.* (2013). doi:10.1089/dia.2013.0104
118. Bolli, G. B. & Gerich, J. E. The Dawn Phenomenon — A Common Occurrence in Both Non-Insulin-Dependent and Insulin-Dependent Diabetes Mellitus. *N. Engl. J. Med.* **310**, 746–750 (1984).
119. Cobelli, C., Renard, E. & Kovatchev, B. Artificial Pancreas: Past, Present, Future. *Diabetes* **60**, 2672–2682 (2011).
120. Peyser, T., Dassau, E., Breton, M. & Skyler, J. S. The artificial pancreas: current status and future prospects in the management of diabetes. *Ann. N. Y. Acad. Sci.* **1311**, 102–123 (2014).
121. Kovatchev, B. *et al.* Control to Range for Diabetes: Functionality and Modular Architecture. *J. Diabetes Sci. Technol.* **3**, 1058–1065 (2009).
122. Ruiz, J. L. *et al.* Effect of Insulin Feedback on Closed-Loop Glucose Control: A Crossover Study. *J. Diabetes Sci. Technol.* **6**, 1123–1130 (2012).

123. Cobelli, C. *et al.* Pilot Studies of Wearable Outpatient Artificial Pancreas in Type 1 Diabetes. *Diabetes Care* **35**, e65–e67 (2012).
124. Breton, M. *et al.* Fully Integrated Artificial Pancreas in Type 1 Diabetes Modular Closed-Loop Glucose Control Maintains Near Normoglycemia. *Diabetes* **61**, 2230–2237 (2012).
125. Phillip, M. *et al.* Nocturnal Glucose Control with an Artificial Pancreas at a Diabetes Camp. *N. Engl. J. Med.* **368**, 824–833 (2013).
126. Mauseth, R. *et al.* Use of a ‘fuzzy logic’ controller in a closed-loop artificial pancreas. *Diabetes Technol. Ther.* **15**, 628–633 (2013).
127. Cobelli, C. *et al.* Diabetes: Models, Signals, and Control. *Biomed. Eng. IEEE Rev. In* **2**, 54–96 (2009).
128. Riddell, M. & Perkins, B. A. Exercise and Glucose Metabolism in Persons with Diabetes Mellitus: Perspectives on the Role for Continuous Glucose Monitoring. *J. Diabetes Sci. Technol. Online* **3**, 914–923 (2009).
129. Roy, A. & Parker, R. S. Mixed meal modeling and disturbance rejection in type I diabetic patients. *Conf. Proc. Annu. Int. Conf. IEEE Eng. Med. Biol. Soc. IEEE Eng. Med. Biol. Soc. Annu. Conf.* **1**, 323–326 (2006).
130. Artificial Pancreas Project Research. *JDRF: Improving Lives. Curing Type 1 Diabetes* at <http://jdrf.org/research/treat/artificial-pancreas-project/>
131. Nelder, J. A. & Mead, R. A Simplex Method for Function Minimization. *Comput. J.* **7**, 308–313 (1965).
132. Collier, G., McLean, A. & O’Dea, K. Effect of co-ingestion of fat on the metabolic responses to slowly and rapidly absorbed carbohydrates. *Diabetologia* **26**, 50–54 (1984).

133. Kovatchev, B. P., Straume, M., Cox, D. J. & Farhy, L. S. Risk Analysis of Blood Glucose Data: A Quantitative Approach to Optimizing the Control of Insulin Dependent Diabetes. *Comput. Math. Methods Med.* **3**, 1–10 (2000).

# Appendix

## A. Terms in integral SI formula

Refer to <sup>71</sup>:

- i) AoC: amount of carbohydrates

$$\text{AoC}(\text{meal}^i) = D(t_{\text{meal}}^i) \cdot f(t_{\text{end}}^i) + \text{COB}(t_{\text{end}}^{i-1}) \cdot D(t_{\text{meal}}^{i-1})$$

The amount of CHO ingested of i-th meal includes the current meal constrained by the meal rate of appearance  $f(t)$  and the last meal (i-1) evaluated by the carbohydrates on board  $\text{COB}(t)$ .

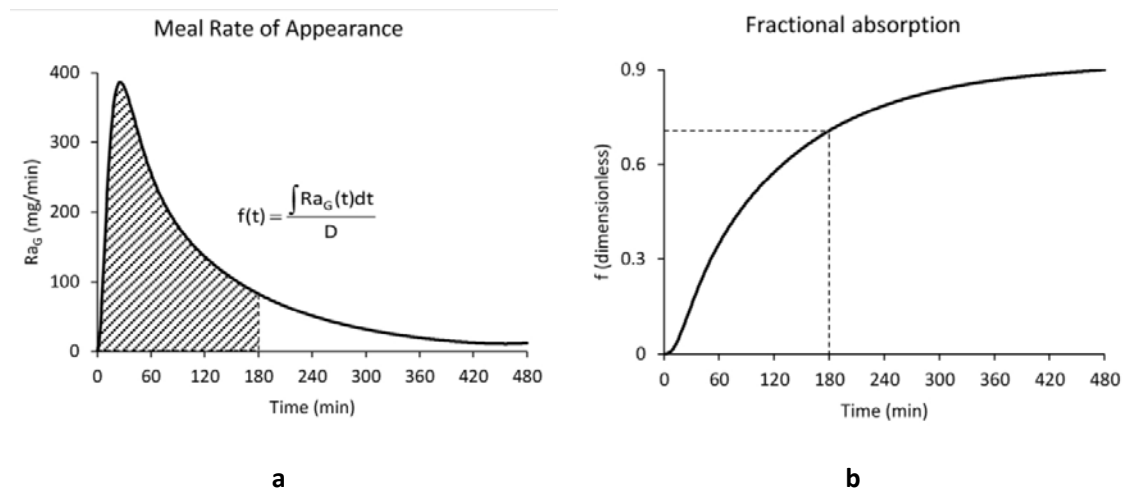


Figure 54: a. Meal rate of appearance  $f(t)$  and b. carbohydrates on board  $\text{COB}(t)$ .

- ii) IOB: Insulin on Board

Insulin on board curves (Figure 55) was adopted to compute the residual active insulin from the bolus administered before the meal.

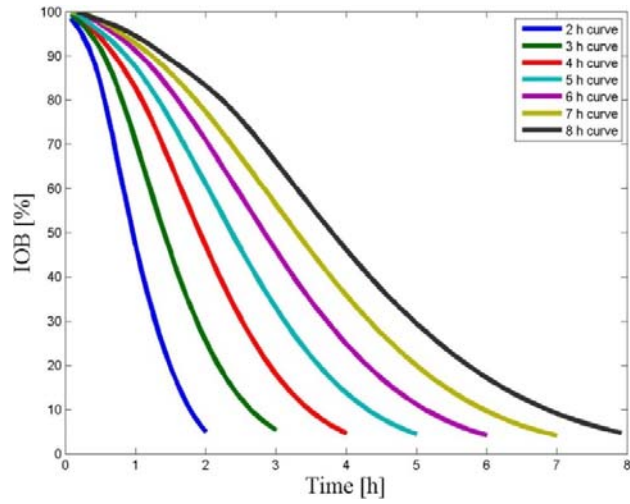


Figure 55: Insulin on board as function of time.

## B.1 KF matrices and noise covariance

Table 18: KF states and noise settings

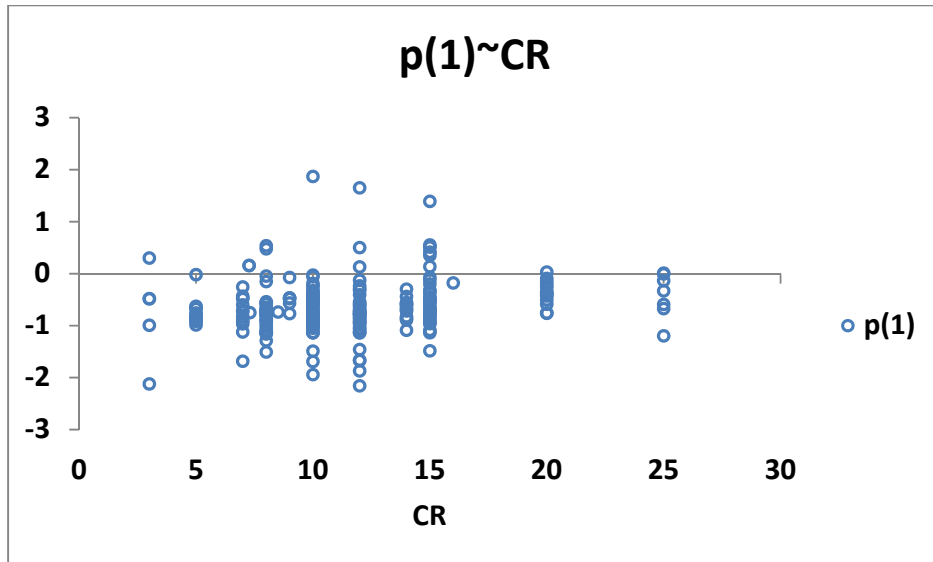
KF setting	<b>SOGMM-Full</b>	<b>SOGMM Core+<math>\Delta</math></b>	<b>SOGMM Core with <math>SI</math></b>
States	$[G X I_{sc1} I_{sc2} I_p Q_1 Q_2]$	$[G X]$	$[G X SI]$
G	$[0 0 1 0 0 1 1]'$	$\begin{bmatrix} 1 & 0 \\ 0 & 1e-2 \end{bmatrix}$	$\begin{bmatrix} 1 & 0 & 0 \\ 0 & 0 & 0 \\ 0 & 0 & 1e-5 \end{bmatrix}$
H	0	$[0 0]$	$[0 0 0]$
Q	1	$\begin{bmatrix} 1e-3 & 0 \\ 0 & 1e-3 \end{bmatrix}$	$\begin{bmatrix} 1 & 0 & 0 \\ 0 & 1 & 0 \\ 0 & 0 & 1 \end{bmatrix}$
R	$5e-4$	$e-1$	1
N	0	$[0 0]'$	$[0 0 0]'$
KF setting	<b>LOG-Full</b>	<b>LOG Core+<math>\Delta</math></b>	<b>LOG Core with <math>SI</math></b>
States	$[\ln(\frac{G}{G_b}) \ln(\frac{X}{X_b}) I_{sc1} I_{sc2} I_p Q_1 Q_2]$	$[\ln(\frac{G}{G_b}) \ln(\frac{X}{X_b})]$	$[\ln(\frac{G}{G_b}) \ln(\frac{X}{X_b}) \ln(\frac{SI}{SI_b})]$
G	$[0.05 10 0 0 0 0 0]'$	$\begin{bmatrix} 5e-2 & 0 \\ 0 & 5 \end{bmatrix}$	$\begin{bmatrix} 5e-2 & 0 & 0 \\ 0 & 0 & 0 \\ 0 & 0 & 1 \end{bmatrix}$
H	0	$[0 0]$	$[0 0 0]$
Q	1	$\begin{bmatrix} 1 & 1 \\ 1 & 1 \end{bmatrix}$	$\begin{bmatrix} 1 & 1 & 1 \\ 1 & 1 & 1 \\ 1 & 1 & 1 \end{bmatrix}$
R	$5e-6$	$5e-3$	$5e-4$
N	0	$[0 0]'$	$[0 0 0]'$

## B.2 Prediction matrices

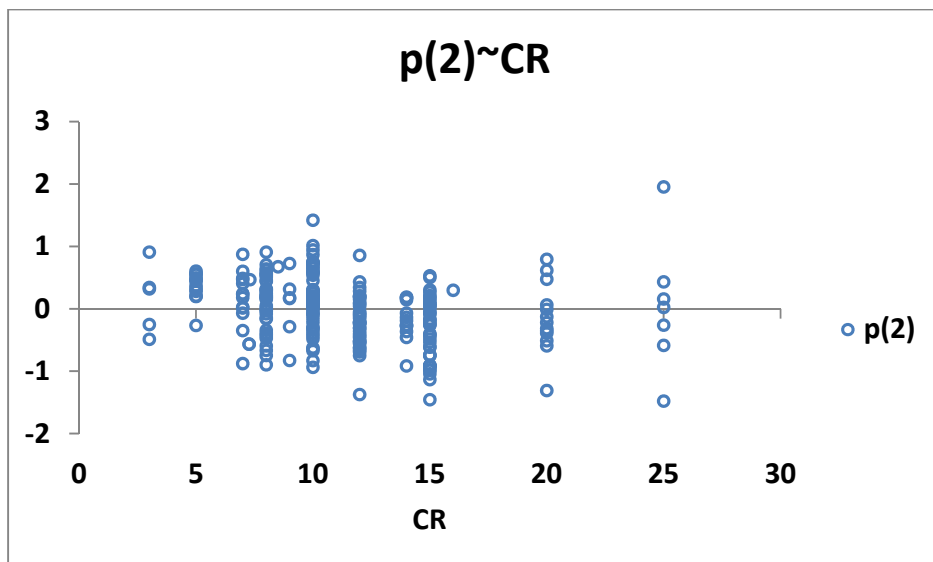
Table 19: Prediction states and matrices

	$A_p$	$B_p$	$C_p$
SOGMM-Full	$\begin{bmatrix} 9.1e-1 & -5.7e+2 & -9.3e-6 & -3.4e-4 & -8.6e-3 & 5.1e-5 & 2.5e-4 \\ 0 & 5.1e-1 & 4.1e-8 & 1.1e^{-5} & 1.5e^{-5} & 0 & 0 \\ 0 & 0 & 9.0e-1 & 0 & 0 & 0 & 0 \\ 0 & 0 & 9.0e-2 & 9.0e-1 & 0 & 0 & 0 \\ 0 & 0 & 3.3e-3 & 5.4e-2 & 2.8e-1 & 0 & 0 \\ 0 & 0 & 0 & 0 & 0 & 6.3e-1 & 0 \\ 0 & 0 & 0 & 0 & 0 & 3.6e-1 & 9.4e-1 \end{bmatrix}$	$\begin{bmatrix} -1.0e-5 & 8.9e-5 \\ 5.8e-8 & 0 \\ 4.8 & 0 \\ 2.3e-1 & 0 \\ 6.2e-3 & 0 \\ 0 & 4.0 \\ 0 & 9.9e-1 \end{bmatrix}$	$\begin{bmatrix} 1 \\ 0 \\ 0 \\ 0 \\ 0 \\ 0 \\ 0 \end{bmatrix}$
SOGMM Core+ $\Delta$	$\begin{bmatrix} 9.1e-1 & -7.8e+2 & -5.7e+2 & -9.3e-6 & -3.4e-4 & -8.6e-3 & 5.1e-5 & 2.5e-4 \\ 0 & 1.0 & 0 & 0 & 0 & 0 & 0 & 0 \\ 0 & 0 & 5.1e-1 & 4.1e-8 & 1.1e-6 & 1.5e-5 & 0 & 0 \\ 0 & 0 & 0 & 9.0e-1 & 0 & 0 & 0 & 0 \\ 0 & 0 & 0 & 9.2e-2 & 9.0e-1 & 0 & 0 & 0 \\ 0 & 0 & 0 & 3.3e-3 & 5.4e-2 & 2.8e-1 & 0 & 0 \\ 0 & 0 & 0 & 0 & 0 & 0 & 6.3e-1 & 0 \\ 0 & 0 & 0 & 0 & 0 & 0 & 3.6e-1 & 9.4e-1 \end{bmatrix}$	$\begin{bmatrix} -1.0e-5 & 8.9e-5 \\ 0 & 0 \\ 5.8e-8 & 0 \\ 4.8 & 0 \\ 2.3e-1 & 0 \\ 6.2e-3 & 0 \\ 0 & 4.0 \\ 0 & 9.9e-1 \end{bmatrix}$	$\begin{bmatrix} 1 \\ 0 \\ 0 \\ 0 \\ 0 \\ 0 \\ 0 \\ 0 \end{bmatrix}$
SOGMM Core with $SI$	$\begin{bmatrix} 8.8e-1 & -3.8e+2 & -6.3e-6 & -2.3e-4 & -5.8e-3 & 5.0e-5 & 2.4e-4 & -7.9e+3 \\ 0 & 5.1e-1 & 4.2e-8 & 1.1e-6 & 1.5e-5 & 0 & 0 & 2.6e+1 \\ 0 & 0 & 9.0e-1 & 0 & 0 & 0 & 0 & 0 \\ 0 & 0 & 9.2e-2 & 9.0e-1 & 0 & 0 & 0 & 0 \\ 0 & 0 & 3.3e-3 & 5.4e-2 & 2.8e-1 & 0 & 0 & 0 \\ 0 & 0 & 0 & 0 & 0 & 6.3e-1 & 0 & 0 \\ 0 & 0 & 0 & 0 & 0 & 3.6e-1 & 9.4e-1 & 0 \\ 0 & 0 & 0 & 0 & 0 & 0 & 0 & 9.2e-1 \end{bmatrix}$	$\begin{bmatrix} -6.8e-6 & 8.8e-5 \\ 5.8e-8 & 0 \\ 4.8 & 0 \\ 2.4e-1 & 0 \\ 6.2e-3 & 0 \\ 0 & 4.0 \\ 0 & 9.9e-1 \\ 0 & 0 \end{bmatrix}$	$\begin{bmatrix} 1 \\ 0 \\ 0 \\ 0 \\ 0 \\ 0 \\ 0 \\ 0 \end{bmatrix}$
LOG-Full	$\begin{bmatrix} 9.7e-1 & -2.3e-3 & -1.3e-8 & -4.9e-7 & -1.3e-5 & 1.4e-6 & 2.6e-6 \\ 0 & 9.3e-1 & 2.0e-5 & 5.5e-4 & 9.2e-3 & 0 & 0 \\ 0 & 0 & 9.0e-1 & 0 & 0 & 0 & 0 \\ 0 & 0 & 9.2e-2 & 9.0e-1 & 0 & 0 & 0 \\ 0 & 0 & 3.3e-3 & 5.4e-2 & 2.8e-1 & 0 & 0 \\ 0 & 0 & 0 & 0 & 0 & 9.0e-1 & 0 \\ 0 & 0 & 0 & 0 & 0 & 4.5e-2 & 9.0e-1 \end{bmatrix}$	$\begin{bmatrix} -1.4e-8 & 3.5e-6 \\ 2.7e-5 & 0 \\ 4.8 & 0 \\ 2.3e-1 & 0 \\ 6.2e-3 & 0 \\ 0 & 4.8 \\ 0 & 1.2e-1 \end{bmatrix}$	$\begin{bmatrix} 1 \\ 0 \\ 0 \\ 0 \\ 0 \\ 0 \\ 0 \end{bmatrix}$
LOG Core+ $\Delta$	$\begin{bmatrix} 9.7e-1 & -2.4e-3 & -2.3e-3 & -1.3e-8 & -4.9e-7 & -1.3e-5 & 1.4e-6 & 2.6e-6 \\ 0 & 1.0 & 0 & 0 & 0 & 0 & 0 & 0 \\ 0 & 0 & 9.3e-1 & 2.0e-5 & 5.5e-4 & 9.2e-3 & 0 & 0 \\ 0 & 0 & 0 & 9.0e-1 & 0 & 0 & 0 & 0 \\ 0 & 0 & 0 & 9.2e-2 & 9.0e-1 & 0 & 0 & 0 \\ 0 & 0 & 0 & 3.3e-3 & 5.4e-2 & 2.8e-1 & 0 & 0 \\ 0 & 0 & 0 & 0 & 0 & 0 & 9.0e-1 & 0 \\ 0 & 0 & 0 & 0 & 0 & 0 & 4.5e-2 & 9.0e-1 \end{bmatrix}$	$\begin{bmatrix} -1.4e-8 & 3.5e-6 \\ 0 & 0 \\ 2.7e-5 & 0 \\ 4.8 & 0 \\ 2.3e-1 & 0 \\ 6.2e-3 & 0 \\ 0 & 4.8 \\ 0 & 1.2e-1 \end{bmatrix}$	$\begin{bmatrix} 1 \\ 0 \\ 0 \\ 0 \\ 0 \\ 0 \\ 0 \\ 0 \end{bmatrix}$
LOG Core with $SI$	$\begin{bmatrix} 9.7e-1 & -2.3e-3 & -1.3e-8 & -4.9e-7 & -1.3e-5 & 1.4e-6 & 2.6e-6 & -1e-2 \\ 0 & 9.3e-1 & 2.0e-5 & 5.5e-4 & 9.2e-3 & 0 & 0 & 0 \\ 0 & 0 & 9.0e-1 & 0 & 0 & 0 & 0 & 0 \\ 0 & 0 & 9.2e-2 & 9.0e-1 & 0 & 0 & 0 & 0 \\ 0 & 0 & 3.3e-3 & 5.4e-2 & 2.8e-1 & 0 & 0 & 0 \\ 0 & 0 & 0 & 0 & 0 & 9.0e-1 & 0 & 0 \\ 0 & 0 & 0 & 0 & 0 & 4.5e-2 & 9.0e-1 & 0 \\ 0 & 0 & 0 & 0 & 0 & 0 & 0 & 9.2e-1 \end{bmatrix}$	$\begin{bmatrix} -1.4e-8 & 3.5e-6 \\ 2.7e-5 & 0 \\ 4.8 & 0 \\ 2.4e-1 & 0 \\ 6.2e-3 & 0 \\ 0 & 4.8 \\ 0 & 1.2e-1 \\ 0 & 0 \end{bmatrix}$	$\begin{bmatrix} 1 \\ 0 \\ 0 \\ 0 \\ 0 \\ 0 \\ 0 \\ 0 \end{bmatrix}$

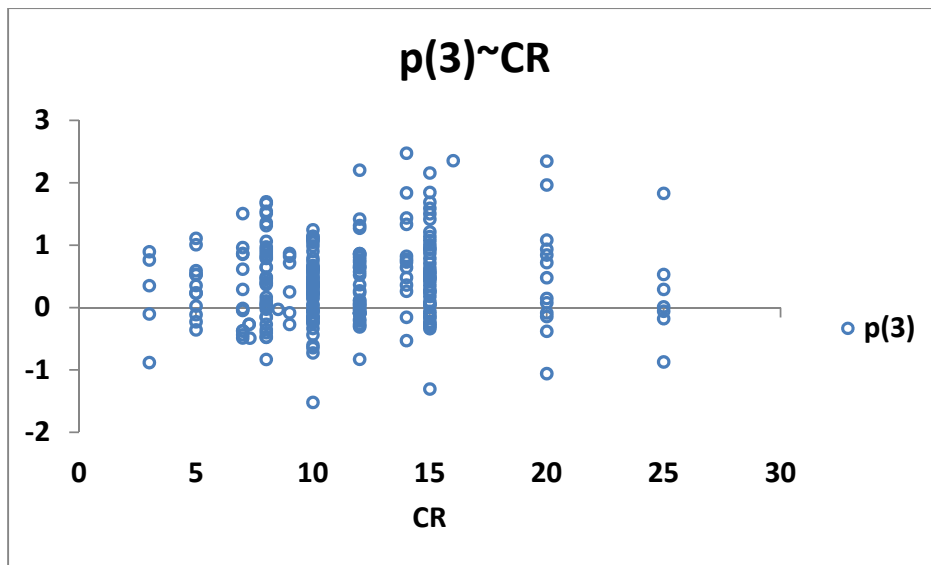
**C. 1 Tuned multipliers against the selected response variable (CR) by global search**



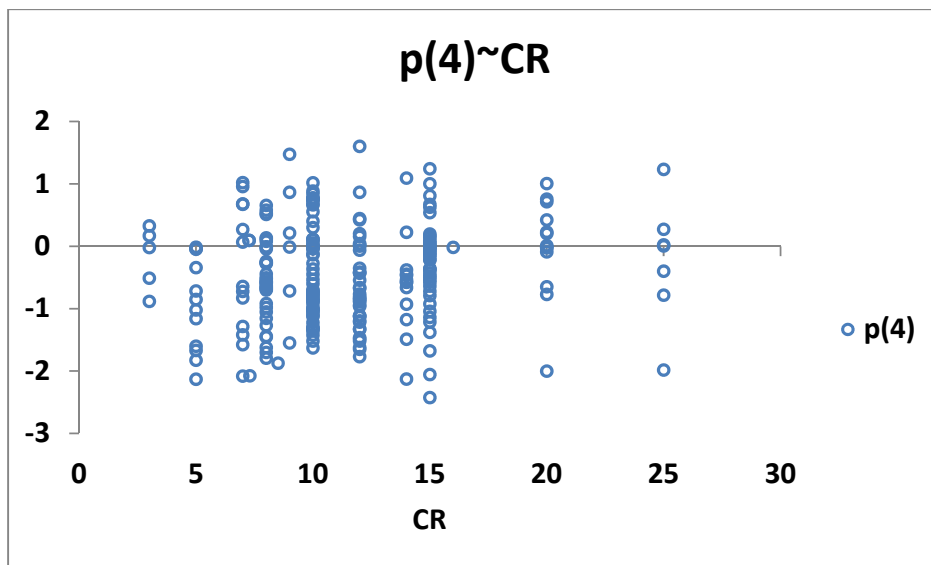
(A)

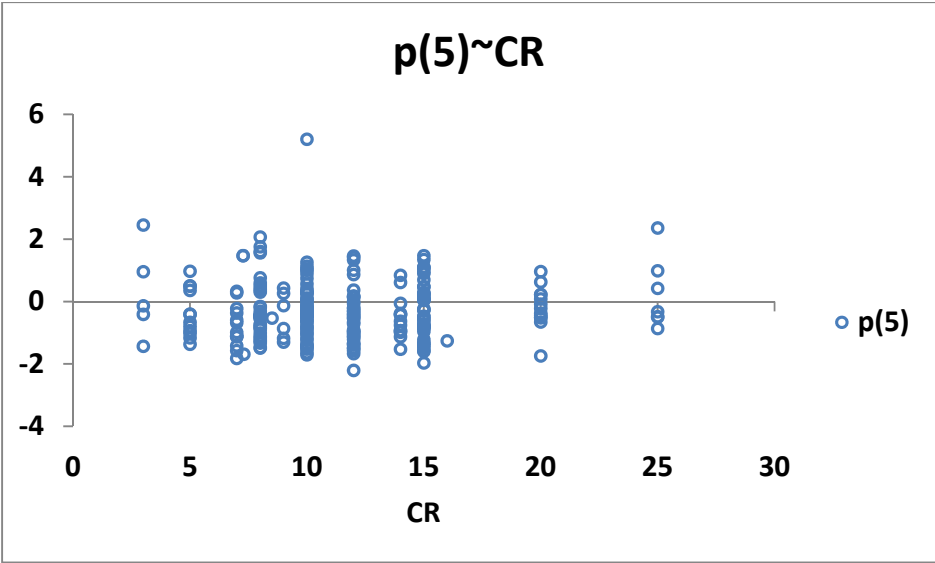


(B)



(C)

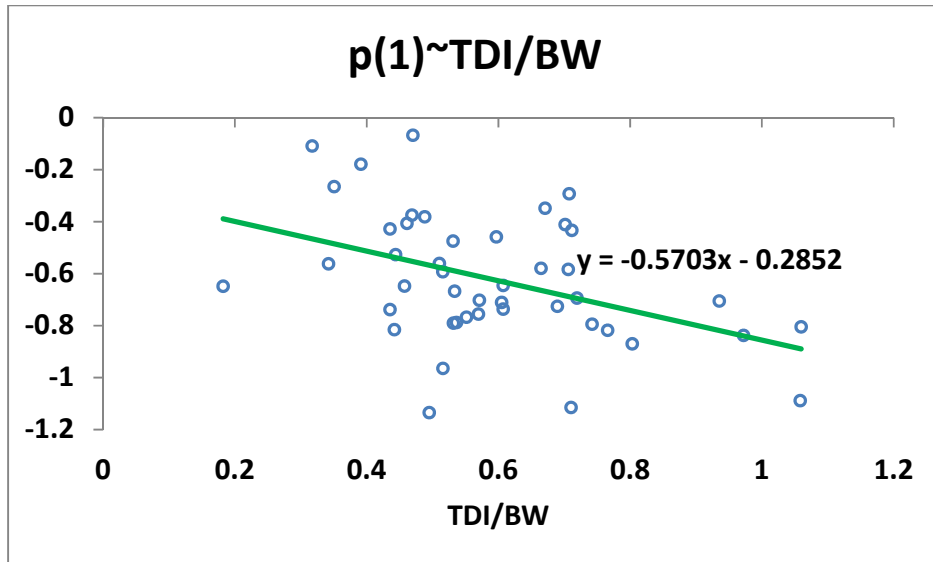




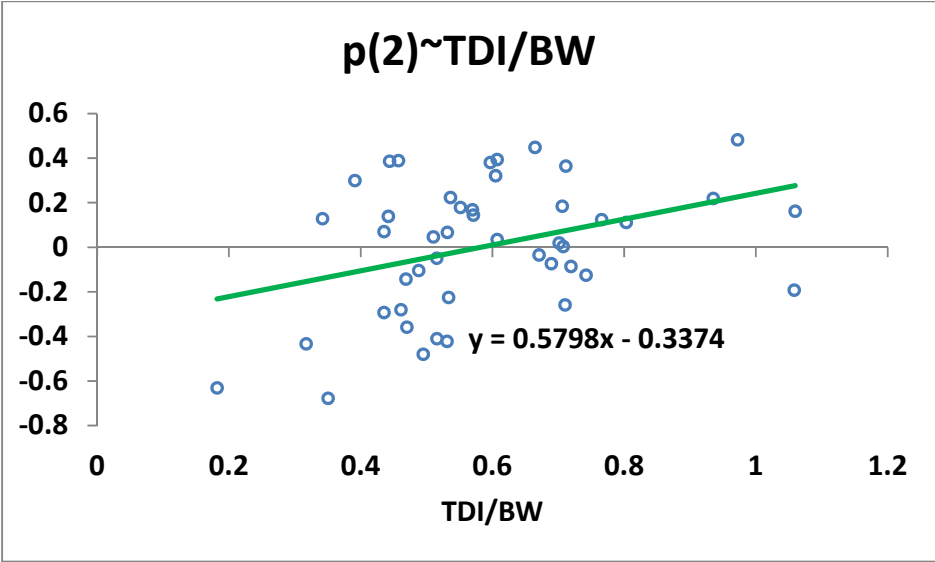
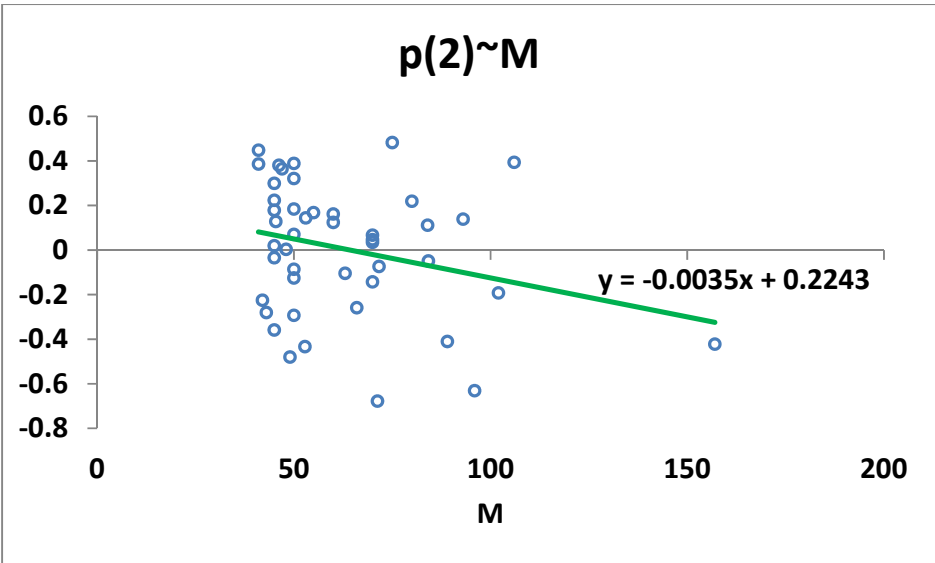
(E)

Figure 56: Tuned multipliers against the selected response variable (CR) by global search.

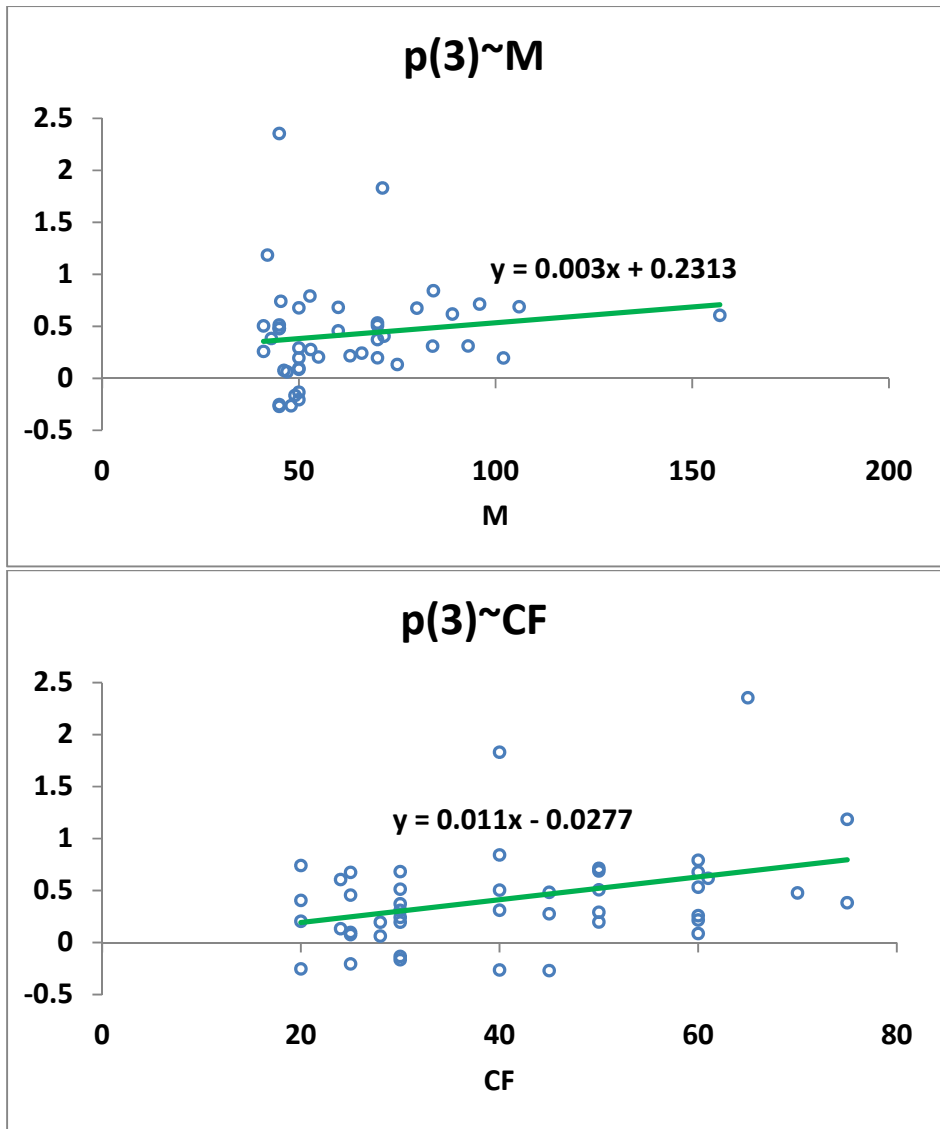
**C. 2 Tuned multipliers against the response variables (segments averaged) based on global search**



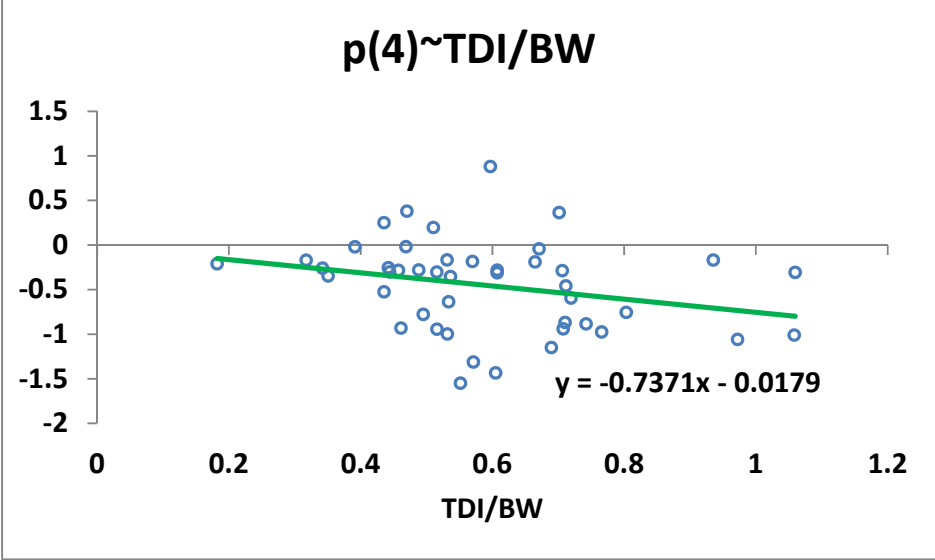
(A)



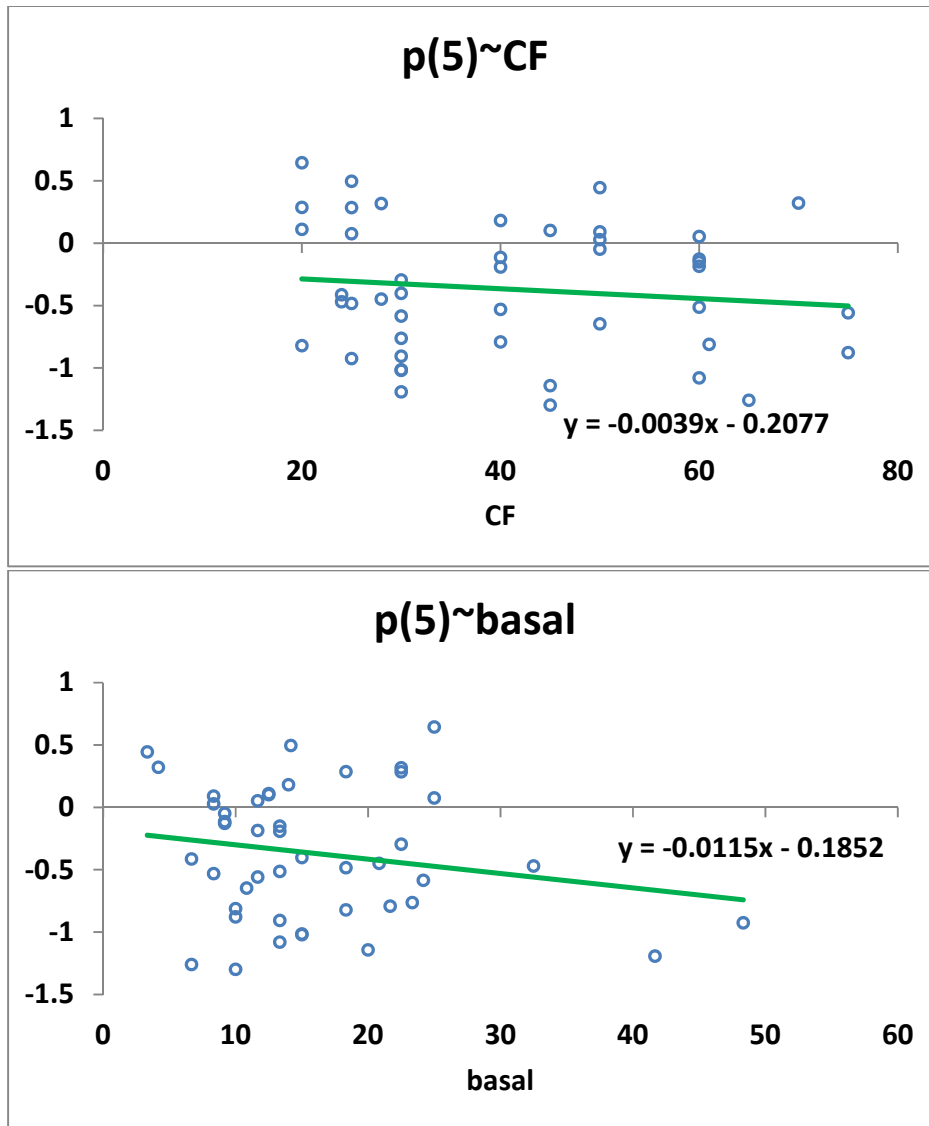
(B)



(C)



(D)



(E)

Figure 57: Tuned multipliers against the response variables (segments averaged) based on global search.